Utilization of Polyaniline as a Solid Antioxidant for Active Packaging Applications

by

Ashveen Vikash Nand
Hybrid Polymers Research Group,
School of Chemical Sciences,
The University of Auckland.

A thesis submitted in fulfillment of the requirements for the degree of
Doctor of Philosophy in Chemistry.

2012

Principal Supervisor:
Assoc. Prof. Paul A. Kilmartin,
School of Chemical Sciences, The University of Auckland.
Co-Supervisor:
Assoc. Prof. Jadranka Travas-Sejdic,
School of Chemical Sciences, The University of Auckland.

ABSTRACT

Polyaniline (PANI) was chemically synthesized by oxidizing aniline with ammonium persulfate (APS) with and without HCl, to produce granular (G-PANI) and nanorod (NR-PANI) forms, respectively. NR-PANI and G-PANI were dedoped with ammonium hydroxide to yield NR-PANIdd and G-PANIdd. SEM images revealed a typical granular morphology for G-PANI and G-PANIdd, while NR-PANI, formed using a 'falling pH method', and NR-PANIdd, consisted of micro/nanorods and flakes. The samples were characterized using FTIR and the level of oxidation was determined by XPS. The surface area of the samples was measured by the BET method. The free radical scavenging activity, using the $DPPH^{\bullet}$ assay, showed the following ranking: NR-PANI > G-PANI ≈ NR-PANIdd > G-PANIdd. The radical scavenging activity of the PANIs did not correlate with conductivity or surface area measurements, but was critically dependent upon the level of oxidation, and higher activity was obtained with the more reduced PANI samples.

The PANI samples were examined before and after dedoping (dd) using thermogravimetric analysis (TGA), which showed small mass losses in the 200 to 300 ºC temperature range, and greater mass losses due to oxidative degradation at higher temperatures. Furthermore, samples were treated thermally at 100, 125, 150, 175, 200, 250 and 300 ºC for 30 min in air. SEM images did not show any pronounced effect on the morphologies of the samples from thermal treatment up to 300 ºC. The ratios of the intensities (*Q/B*) of the predominantly quinoid (*Q*) and benzenoid peaks (*B*) from FTIR spectroscopic analysis revealed that NR-PANI and NR-PANIdd underwent cross-linking upon thermal treatment up to 175 ºC and were oxidized after treatment above 175 ºC. G-

PANI and G-PANIdd also underwent the same chemical changes with oxidation occurring above 200 ºC. The free radical scavenging capacity of the samples was evaluated using the DPPH assay, and was found to be independent of the spin concentrations of the samples. All samples exhibited a rapid decline in free radical scavenging capacity when exposed to temperatures above 200 ºC, indicating that any polymer processing should be undertaken at temperatures less than this value to achieve high antioxidant activity.

NR-PANI/ PET blends were prepared by dispersion in a melt of PET at 265 ºC. Blends with 1, 2 and 3 wt% NR-PANI loading were prepared. Optical microscopy revealed an even distribution of NR-PANI particles within the PET matrix. The blends were characterized using FTIR, XPS, DSC and DMTA. Melt flow index (MFI) values suggested hydrolysis of PET chains to lower molecular weight units when NR-PANI was blended. Some PET hydrolysis was also evident from the increasing O/C ratios with an increased NR-PANI content in the composites. While the PET glass transition temperature remained relatively unaffected, the degree of PET crystallinity was increased with the addition of NR-PANI. The electrical conductivity as well as the free radical scavenging capacity of PET increased with greater NR-PANI loading in the matrix. The mechanical properties of PET, however, declined with NR-PANI loading suggesting a lack of adequate interfacial adhesion between the NR-PANI particles and the PET matrix.

NR-PANI/ LLDPE were prepared by dispersing NR-PANI in the melt of LLDPE at 150 º C. The composites had 5, 10, 15 and 20 wt% loading of NR-PANI. ESEM images revealed an even dispersion of NR-PANI in the LLDPE matix. Coalescence of NR-PANI particles and an increase in electrical conductivity was observed at higher loading of NR-PANI. The composites were characterized further using FTIR, XPS, ESR, XRD and DSC.

The composites exhibited characteristic vibrational bands due to both LLDPE and NR-PANI, but did not show any chemical interaction between the components. With an increased loading of NR-PANI in the composites, the amount of NR-PANI present on the surface of the samples increased, and the crystallinity of LLDPE decreased. The tensile strength and elongation at break of LLDPE also declined suggesting a lack of interfacial adhesion between the NR-PANI particles and the LLDPE matrix. The Young's modulus, however, increased with higher loading of NR-PANI. The composites also demonstrated very good free radical scavenging activity, dependent upon the amount of NR-PANI included in the composites.

The NR-PANI/ LLDPE composites were further evaluated for active packaging applications. The oxygen permeability decreased as the amount of NR-PANI in the composites increased. The composite films also exhibited antimicrobial and antioxidant capabilities. The oxidation of fish oil was delayed in the presence of the NR-PANI/ LLDPE composites, and there was a negative correlation between oxidation and the NR-PANI content in the films. Moreover, the composites films were biocompatible to mammalian cells, meaning that NR-PANI/ LLDPE films can potentially be utilized for a range of active packaging applications.

ACKNOWLEDGEMENTS

First and foremost I would like to acknowledge the support of my academic supervisor, Assoc. Prof. Paul Kilmartin. Paul has rendered to me enormous technical and logistical support during the course of my PhD studies. While he has been fully supportive of my ideas, he was also a source of encouragement and motivation. I am honoured and grateful to have had him as my mentor. Thanks are also due to Assoc. Prof. Jadranka Travas-Sejdic for her continuous support and assistance.

I was fortunate to be awarded a University of Auckland PhD scholarship through the Hybrid Polymers research programme (UOAX812), with additonal support from Frucor Beverages (NZ) Ltd. I would like to thank Prof. Ralph Cooney and late Assoc. Prof. Allan Easteal for having faith in me and giving me financial support through the Hybrid Polymers research program. Moreover, late Assoc. Prof. Allan Easteal was instrumental in getting this study started.

The members of the Hybrid Polymers research group; Dr Sudip Ray, Dr Marija Gizdavic-Nikolaidis, Dr Karnika de Silva, Dr Jianyong Jin, James Wu, Walt Wheelwright, Teresa To, Xiao Wang and Neil Edmonds are thanked for their assistance and companionship during my studies. Walt's help with the Chem Draw software is greatly appreciated. This study would not have been possible without technical assistance by Shane Crump and Dr Sudip Ray.

Jimmy Thomas, Jos Geurts, Callum Turnbull and Stephen Cawley of the Centre of Advanced Composites and Materials are thanked for the assistance in preparing the polymer composites, characterizing the mechanical properties and measuring their conductivities. The

assistance by Dr Colin Doyle and Catherine Hobbis, of the Research Centre for Surface and Materials Science, during SEM and XPS studies is also acknowledged. Dr Simon Swift, Adeline Le Cocq and Benedict Uy were instrumental in the microbiology and biocompatiblity studies on the polymer composites. I am also grateful to Michel Nieuwoudt and Dr Geoff Waterhouse, of the School of Chemical Sciences, for their help in the spectroscopic and surface area charaterizations, respectively, of the polymer samples.

Thanks are also due to Alexsandro Santos Costa, Winai Suthanthagjai, Hande Karaosmanoglu and Marsilea Booth, of the Polymer Electronics Research Centre, for their companionship during my studies. I really enjoyed discussions during the coffee sessions.

Finally, I am thankful to my wife, Ferial Nand, and children, Aaryan and Anaya, for being so understanding and supportive. They inspired and motivated me when the "going got tough". I am looking forward to spending more time with them now.

TABLE OF CONTENTS

LIST OF FIGURES

LIST OF SCHEMES

LIST OF TABLES

ABBREVIATIONS

AAPH	2,2´-azobis-2-methylpropionamidine dihydrochloride
ABTS	2,2-azino-bis(3-ethylbenzothiazoline-6-sulfonic acid)
APS	Ammonium persulfate
AUC	Area under curve
BET	Brunauer-Emmett-Teller
BHA	Butylated hydroxyanisole
BHT	Butylated hydrxoytoluene
BJH	Barrett-Joyner-Halenda
CFU	Colony forming unit
CSA	Camphor sulfonic acid
DBSA	Dodecylbenzenesulfonic acid
DMEM	Dulbecco's Modified Eagle Medium
DMSO	Dimethyl sulfonate oxide
DMTA	Dynamic thermomechanical analysis
DPPH	1,1-diphenyl-2-picrylhydrazyl
DSC	Differential scanning calorimetry
ESEM	Environmental scanning electron microscope
ESR	Electron spin resonance spectroscopy
EVA	Ethylene vinyl acetate
FCS	Foetal calf serum
FTIR	Fourier transform infrared spectroscopy

FWHM	Full width at half maxima
HCl	Hydrochloric acid
LDPE	Low density polyethylene
LLDPE	Linear low density polyethylene
MFI	Melt flow index
NMP	N-methyl-2-pyrrolidone
ORAC	Oxygen radical absorbance capacity
OTR	Oxygen transmission rate
PA	Polyamide
PANI	Polyaniline
PBS	Phosphate buffered saline
PC	Polycarbonate
PCL	Polycaprolactone
PE	Polyethylene
PEO	Polyethylene oxide
PET	Poly(ethylene terephthalate)
PLA	Polylactic acid
PMMA	Poly(methyl methacrylate)
PP	Polypropylene
PS	Polystyrene
PTFE	Poly(tetrafluoroethylenelene)
*p*TSA	*p*-toluenesulfonic acid

PUFA	Polyunsaturated fatty acids
PV	Peroxide value
PVAc	Poly(vinyl acetate)
PVC	Polyvinyl chloride
PVdC	Polyvinylidene chloride
PVDF	Poly(vinylidene fluoride)
PVF	Poly(vinyl formal)
SEM	Scanning electron microscope
TCP	Tissue culture plate
TGA	Thermogravimetric analysis
THF	Tetrahydrofuran
TSA	Trypticase soy agar
TSB	Tryptic soy broth
UV	Ultraviolet
XPS	X-ray photoelectron spectroscopy
XRD	X-ray diffraction

The following papers and conference presentations have emanated from this thesis:

Papers

1. Nand A.V., Ray S., Easteal A.J., Waterhouse G.I.N., Gizdavic-Nikolaidis M., Cooney R.P., Travas-Sejdic J., Kilmartin P.A. (2011) Factors affecting the radical scavenging activity of polyaniline. *Synthetic Metals* 161: 1232-1237.
2. Nand A.V., Ray S., Gizdavic-Nikolaidis M., Travas-Sejdic J., Kilmartin P.A. (2011) The effects of thermal treatment on the antioxidant activity of polyaniline. *Polymer Degradation and Stability* 96: 2159-2166.
3. Nand A.V., Ray S., Easteal A.J., Gizdavic-Nikolaidis M., Cooney R.P., Travas-Sejdic J., Kilmartin P.A. (2012) Evaluation of polyaniline for packaging applications. *Materials Science and Forum* 700: 236-239.
4. Nand A.V., Ray S., Travas-Sejdic J., Kilmartin P.A. (2012) Characterization of polyethylene terephthalate/ polyaniline blends as potential antioxidant materials. *Materials Chemistry and Physics* 134: 443-450.
5. Nand A.V., Ray S., Travas-Sejdic J., Kilmartin P.A. (2012) Characterization of antioxidant low polyethylene/ polyaniline blends prepared via extrusion *Materials Chemistry and Physics* 135: 903-911.
6. Nand A.V., Kilmartin P.A. (2012) Synthetic polymers with antioxidant properties. In: Cirillo G., Iemma F. (Eds.) *Antioxidant polymers: synthesis, properties and applications*, Scrivener Publishing, USA, pp. 333-354.
7. Nand A.V., Swift S., Uy B., Kilmartin P.A. Evaluation of extruded low polyethylene/ polyaniline blends for active packaging applications. *Journal of Food Engineering.* In

press.

Conference Presentations

1. Nand A.V., Jin J., Ray S., Travas-Sejdic J., Kilmartin P.A., Polyaniline containing composites for antioxidant applications, *World Polymer Congress*, Blacksburg, USA, 24th-29th, June 2012.
2. Nand A.V., Travas-Sejdic J., Kilmartin P.A., Antioxidant activity of polyaniline, *The International Conference on Science and Technology of Synthetic Metals (ICSM)*, Atlanta, USA, 8th-13th July, 2012.
3. Nand A.V., Ray S., Travas-Sejdic J., Easteal A.J., Gizdavic-Nikolaidis M., Kilmartin P., Evaluation of polyaniline for antioxidant packaging aplications, *International Conference on Advanced Materials and Nanotechnology (AMN-5)*, Wellington, New Zealand, 7-11 February, 2011.
4. Nand A.V., Ray S., Easteal A.J., Cooney R.P., Gizdavic-Nikolaidis M., Waterhouse G., Travas-Sejdic J., Kilmartin P., Free-radical scavenging capacity of nanotubular and granular polyaniline, *19th International Symposium on Processing and Fabrication of Advanced Materials (PFAM XIX)*, Auckland, New Zealand, 14-17 January, 2011.

CHAPTER ONE

Introduction and Literature Review

This chapter has been partially published as:

Nand A.V., Kilmartin P.A. (2012) Synthetic polymers with antioxidant properties. In: Cirillo G., Iemma F. (Eds.) *Antioxidant polymers: synthesis, properties and applications*, Scrivener Publishing, USA, pp. 333-354.

1.1 Introduction

Packaging is an integral part of the food industry. Food processing and packaging industries spend an estimated 15 % of their total variable costs on packaging materials [1]. The principal role of packaging is preservation and protection of foodstuffs from external contamination. Packaging helps protect foods from environmental influences such as heat, light, moisture, oxygen, microorganisms, dirt and dust particles, which are known to cause food deterioration [2]. It has also contributed to the globalization of the food industry by stabilizing food products so that they can be distributed over long distances [3].

Historically, the ideal packaging material is one which is inert, resistant to hazards and does not allow molecular transfer to and from the packaging [1]. Plastics, in addition to their ease of processibility, low cost and light weight, have emerged as the major food packaging materials. Polymers such as polyethylene (PE), polypropylene (PP), polyethylene terephthalate (PET), polyvinyl chloride (PVC), polycarbonate (PC), polyvinylidene chloride (PVdC) and polystyrene (PS) have long served the food industry as packaging materials [2]. However, the quest for improved packaging systems, usually driven by the demand for extended shelf-life and better quality of food stuffs, has led to remarkable developments in the area of packaging [4]. Active packaging systems are one such innovation that is attracting academic as well as industrial interest [3, 5]. This thesis explores the application of polyaniline (PANI), an intrinsically conducting polymer, as an active additive in antioxidant food packaging materials.

1.2 Active Packaging

Active packaging refers to the incorporation of certain additives into the packaging systems with the aim of maintaining or extending product quality and shelf-life. The active additives can be either incorporated directly into the packaging matrix, attached to the interior of the packaging material or contained in separate containers such as sachets within the packaging system [6, 7], as demonstrated in Figure 1.1.

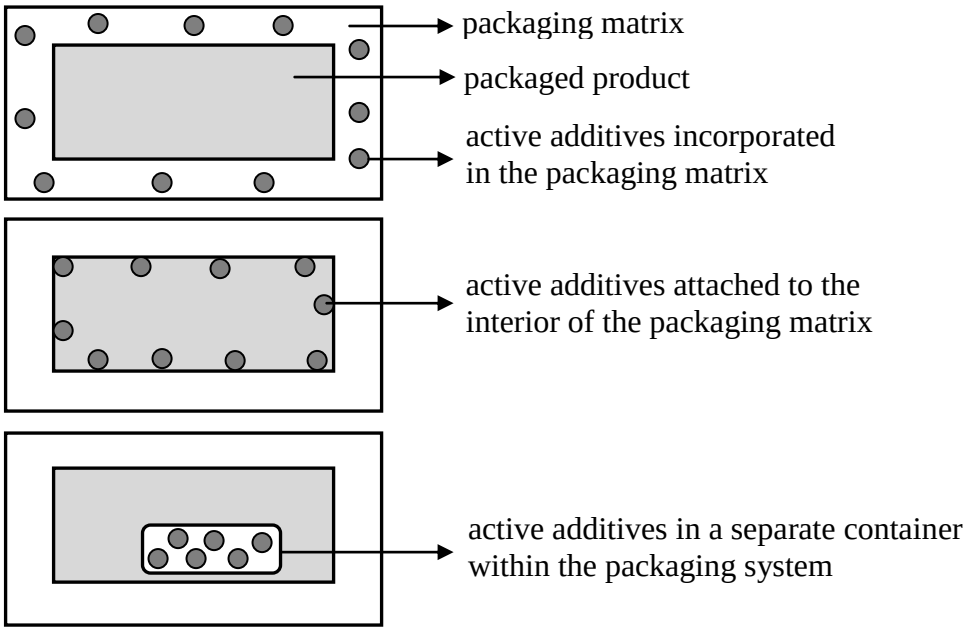

Figure 1.1. Active packaging models.

Active packaging provides dynamic, rather than the conventional passive, protection to the food it contains. It performs some desired role in food preservation other than just providing an inert barrier from external conditions [3, 6]. The additives incorporated in the

active packaging system release or absorb substances into or from the packaged food and the surrounding environment [4, 8, 9], thus promoting food preservation. Various active packaging systems, with attributes such as oxygen and carbon dioxide scavenging, antimicrobiology and antioxidant activity, have been developed.

1.2.1 Oxygen scavengers

Scavenging of oxygen from packaged foods is important as oxygen is deleterious to most food products. The presence of oxygen can trigger oxidative rancidity, discoloration, nutrient degradation and growth of aerobic bacteria, yeast and molds which cause food spoilage [3, 6, 10]. Most of the oxygen scavengers used commercially are based on the principal of iron oxidation [11, 12], as follows:

$$Fe \rightarrow Fe^{2+} + 2e^{-}$$

$$\frac{1}{2}O_2 + H_2O + 2e^{-} \rightarrow 2OH^{-}$$

$$Fe^{2+} + 2OH^{-} \rightarrow Fe(OH)_2$$

$$Fe(OH)_2 + \frac{1}{4}O_2 + \frac{1}{2}H_2O \rightarrow Fe(OH)_3$$

Byun *et al*. (2012) have developed an oxygen scavenging system by incorporating α-tocopherol and iron (II) chloride in fish gelatin films. Moisture played an important role in triggering the oxygen scavenging reaction of the films [13]. Similary, an ascrobyl palmitate-

β-cyclodextrin complex containing iron (II) chloride was developed for oxygen scavenging applications [14]. Moreover, a biological based system consisting of heat resistant *Bacillus amyloquetaciens* spores in poly(ethylene terephthalate, 1,4-cyclohexane dimethanol) plates has been proposed as an oxygen scavenger for PET bottles [15].

1.2.2 Carbon dioxide scavengers

Carbon dioxide, formed in some foods due to respiration reactions, also needs to be removed from the package to prevent it from bursting. Carbon dioxide absorbent sachets containing either calcium hydroxide, or calcium oxide and a dehydrating agent such as silica gel are commonly used for carbon dioxide removal [6, 16]. The scavenging of carbon dioxide occurs as follows:

$$CaO + H_2O \rightarrow Ca(OH)_2$$

$$Ca(OH)_2 + CO_2 \rightarrow CaCO_3 + H_2O$$

1.2.3 Antimicrobials

Antimicrobial active packaging materials help extend shelf-life and maintain product quality and safety by extending the lag phase and reducing the growth phase of microorganisms responsible for product spoilage [17]. The antimicrobial agents can be coated, incorporated or surface immobilized on the packaging materials to confer antimicrobial activity [18]. The antimicrobial effect is achieved by migration of active

compounds from the active surface to the packaged product, as demonstrated in Figure 1.2.

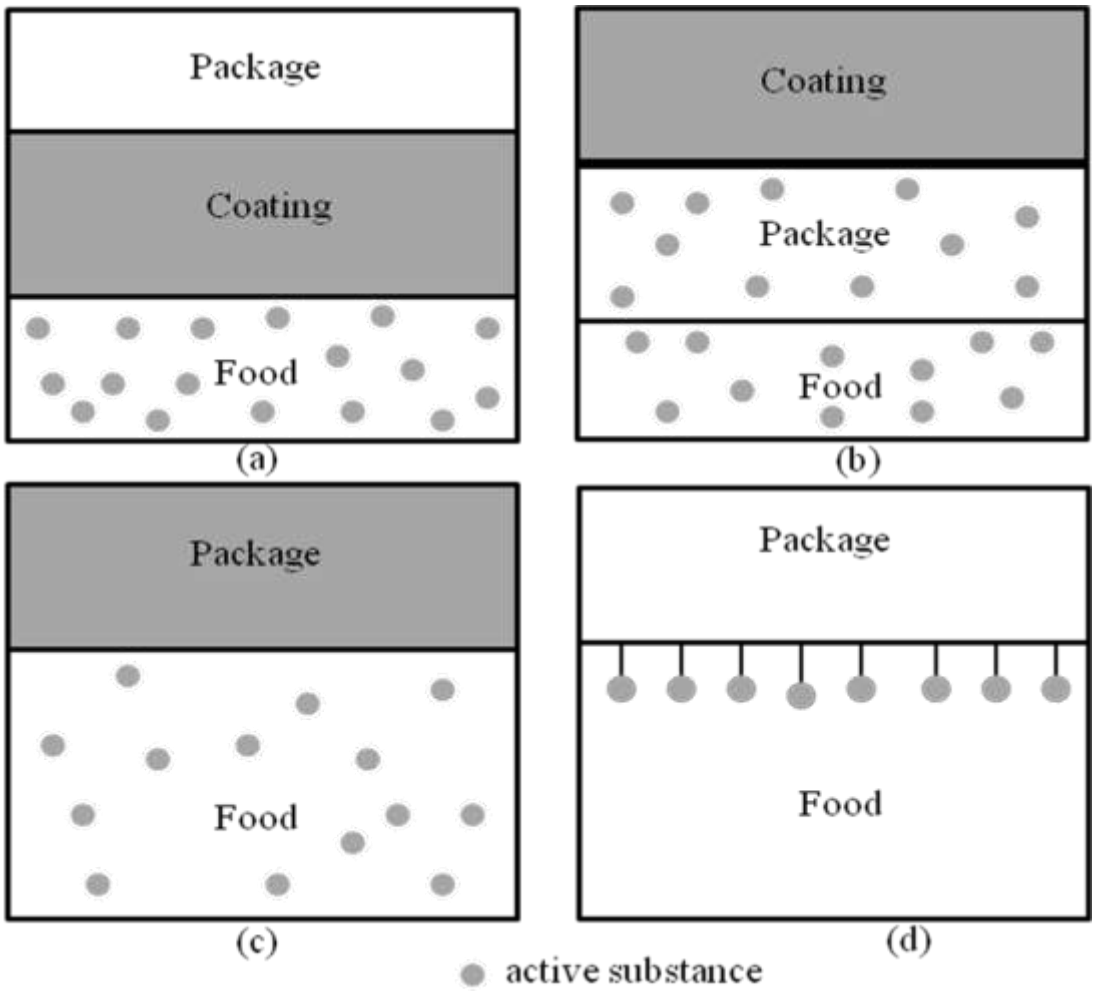

Figure 1.2. Migration of active substances from antimicrobial packaging systems: a) coating before packaging, b) coating after packaging, c) incorporation in the package and d) chemical immobilization on the package (adapted from Quintavalla and Vicini (2002) [19]).

PE and PE/ polyamide (PA) composite films, coated with sorbic acid, have exhibited significant inhibitory effect on *Escherichia coli*, when tested with Gouda cheese and pork

loin inoculated with the test bacteria [20]. Extruded low density PE (LDPE) films containing linalool or methychaviol have been proposed as antimicrobial active packaging materials [21]. Melt processed PP films containing thymol and carvacrol have demonstrated antimicrobial activity against bacterial strains potentially present in food [22]. LDPE, polylactic acid (PLA) and polycaprolactone (PCL) films containing lemon extract, thymol or lysozyme also showed antimicrobial efficacy [23]. The antimicrobial activity was found to be temperature dependent and the PCL films had a superior antimicrobial efficiency as they were processed at a lower temperature. PP films coated with whey protein isolate combined with nisin have exhibited significant bacterial growth inhibition against *Lactobacillus plantarum* [5]. PP/ PE films coated with soy protein isolate containing allyl isothiocyanate, *trans*-cinnamaldehyde, garlic oil or rosemary oil have been instrumental in extending the shelf life of fresh sprouts by reducing the total microbial counts of alfalfa, broccoli and radish sprouts [24]. Furthermore, PE films loaded with zinc oxide nanoparticles have shown potency for antimicrobial active food packaging applications as they illustrated biocidal action against *Escherichia coli* [25].

1.2.4 Antioxidants

Antioxidants are incorporated in packaging materials or added to food stuffs to improve oxidation stability of lipids [16]. When incorporated within the packaging material, the antioxidants diffuse through the polymer bulk, towards the surface, to accomplish the antioxidant activity [26, 27]. Butylated hydrxoytoluene (BHT) and butylated hydroxyanisole (BHA) are commonly used synthetic antioxidants in food applications [27, 28]. The chemical

structures of BHT and BHA are shown in Figure 1.3. However, due to consumer preference for natural food ingredients, the focus has shifted to natural antioxidants [3]. Natural antioxidants such as α-tocopherol, L-ascorbic acid, L-tyrosine, carvacrol and aromatic plant extracts have been utilized in antioxidant food applications [28-38].

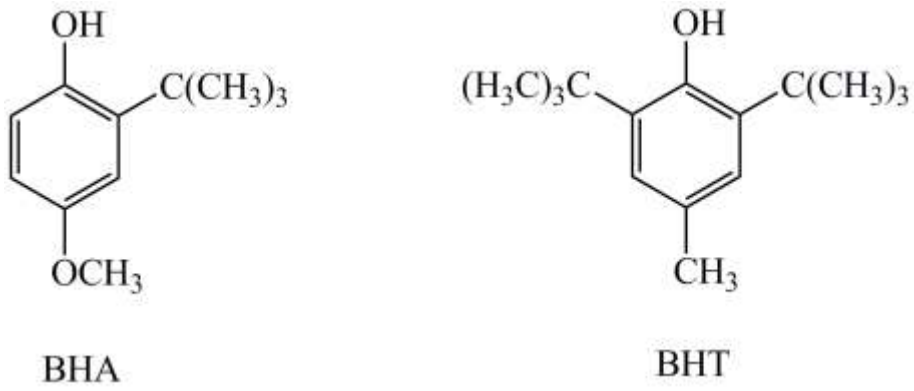

Figure 1.3. Chemical structures of BHA and BHT.

PET trays sprayed with citrus fruit extracts or α-tocopherol have been developed and tested for active packaging applications [39]. While the trays sprayed with citrus extracts showed considerable reduction in the oxidation of cooked turkey meat samples, the α-tocopherol sprayed trays did not show any antioxidant property as the active part of the antioxidant was not in contact with the meat surface. Extruded polylactic acid films (PLA), containing α-tocopherol and BHT have exhibited antioxidant activity [40]. PE films containing different antioxidants have also shown potency for antioxidant packaging applications. While LDPE films containing natural antioxidants from barley husks retarded the oxidation of polyunsaturated fatty acids (PUFA) in blue shark muscle [41], LDPE coated

with rosemary extracts delayed the lipid oxidation of minced chicken breast and thigh patties [42]. Moreover, ethylene vinyl alcohol copolymer (EVOH) films containing green tea extracts have been designed for antioxidant active packaging of aqueous as well as fatty foods [43, 44].

1.3 Principle of Lipid Oxidation

Food degradation is a complex phenomenon encompassing a wide range of chemical processes dependent on food constituents and their concentrations. While many reactions involved in food degradation are unknown, lipid oxidation is considered to be the most important and therefore, has been studied extensively [45-49]. Major food quality issues such as nutritional quality, toxicity, flavor, texture and color are influenced by lipid oxidation [50]. Triglycerides and phospholipids, structures of which are shown in Figure 1.4, are the two main groups of lipids. Triglycerides are found in cells responsible for storage of fats in animals while phospholipids form part of the cell membranes. The oxidative degradation of foodstuffs of animal or vegetal origin begins with the oxidation of the phospholipids [45].

Oxidation of lipids proceeds by a way of free radical mechanism, commonly known as autoxidation [46]. A scheme showing the autoxidation of unsaturated lipids is given in Scheme 1.1. Abstraction of a hydrogen atom from the methylene between a cis double bond pair of an unsaturated fatty acid initiates the autoxidation process. The abstraction of hydrogen adjacent to a double bond is favored because of the formation of a stable allylic radical in which the electrons are delocalized over three carbon atoms [46, 51-54]. The lipid radical then reacts with molecular oxygen to form a peroxy radical. In most oxygen

containing food systems, the lipid radicals react very quickly with oxygen resulting in a higher concentration of the peroxyl radicals than the lipid radicals [46, 51, 52, 55].

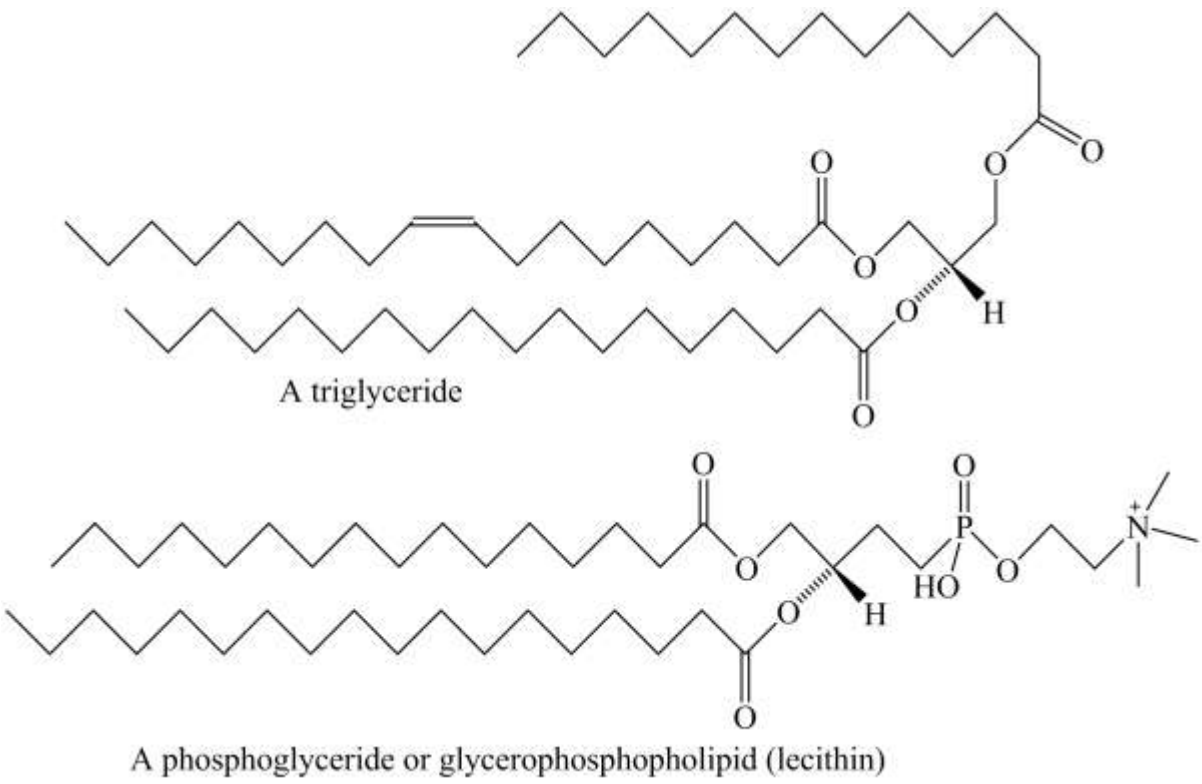

Figure 1.4. Structures of triglyceride and phospholipid.

The peroxy radical formed, reacts with another polyunsaturated fatty acid side chain of the lipid molecule to yield a lipid hydroperoxide (primary oxidation product) and a lipid radical thus, replenishing the number of lipid radicals in the reaction sequence. The newly formed lipid radical can abstract a hydrogen from another fatty acid, thereby propagating the reaction [46, 56]. The hydroperoxides are then converted into secondary non-radical oxidation products [48].

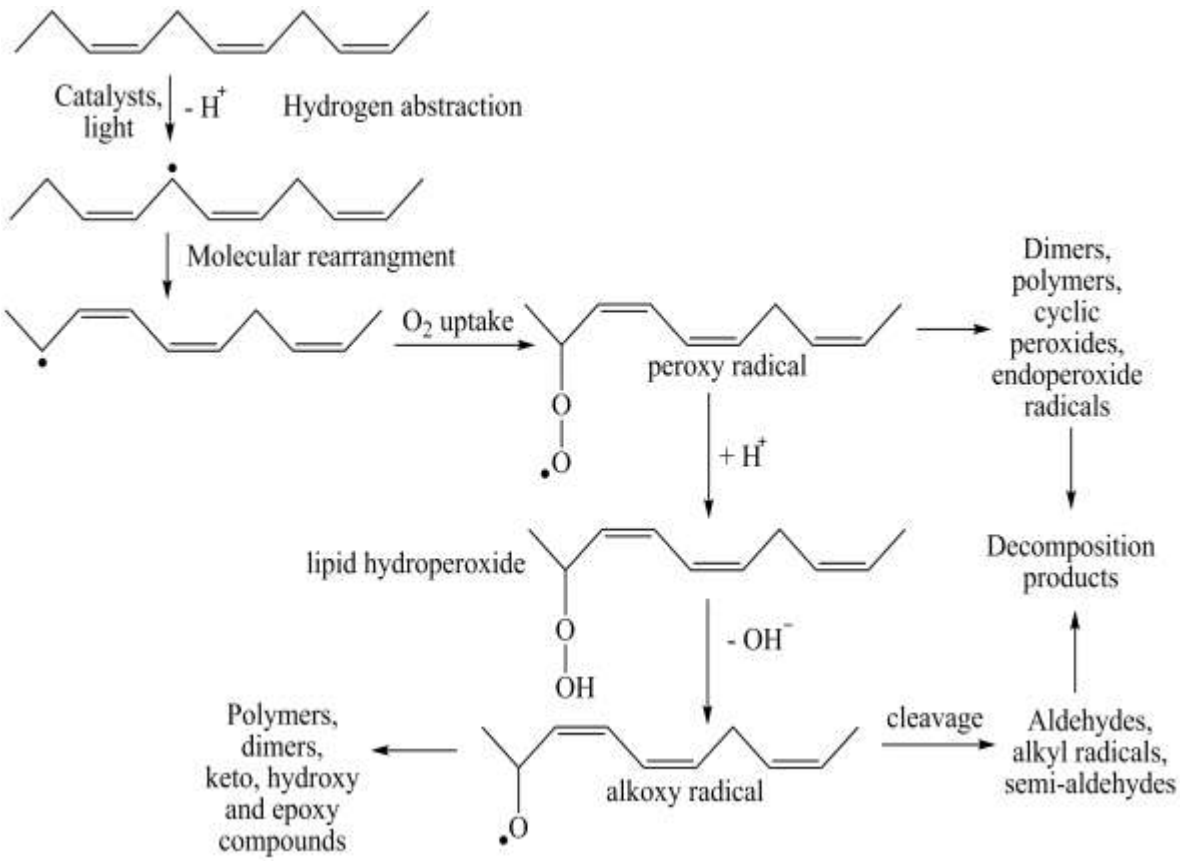

Scheme 1.1. Scheme of autoxidation of unsaturated fats (adapted from Kubow (1992) [46]).

At least three factors are necessary for the oxidation of organic substrates, namely the substrate (foodstuff), molecular oxygen and free radicals. The oxidation of foodstuffs can therefore, be lessened by eliminating either molecular oxygen or free radicals [45, 57]. Various oxygen scavengers and antioxidants, discussed previously, have been utilized for both these purposes. However, due to various reasons such as consumers not favoring foodstuffs containing sachets of oxygen scavengers and material processing issues, the addition of antioxidants to the packaging material is preferred over elimination of molecular

oxygen from foods using high barrier materials or oxygen scavengers [45]. Recently, intrinsically conducting polymers have been considered for use as solid antioxidant materials as they exhibit excellent free radical scavenging properties [58]. Traditional low molecular weight antioxidants like BHT, BHA or organic extracts of plants, are vulnerable at the high temperatures required for the processing of thermoplastic packaging materials. Their evaporation and volatility increases exponentially at higher temperatures and they may decompose leaving the substrates unprotected [59]. Higher molecular weight materials such as intrinsically conducting polymers have the potential to replace traditional antioxidants in active packaging applications due to their superior thermal stability [60-62].

1.4 Intrinsically Conducting Polymers

Intrinsically conducting polymers are a relatively recent class of novel organic materials that have typical properties of traditional polymers combined with those of electrically conducting materials [63]. They have electrical, magnetic and optical properties usually associated with metals, while retaining the advantageous mechanical properties and ease of processing usually associated with polymers [64, 65]. Intrinsically conducting polymers possess an extended π-conjugation along the polymer backbone which is the source of their conductivity. They also exhibit a high electron affinity and a low ionization potential [66]. PANI, polypyrrole, poly(3,4-ethylenedioxythiophene) and polyacetylene are examples of intrinsically conducting polymers. Their structures are presented in Figure 1.5.

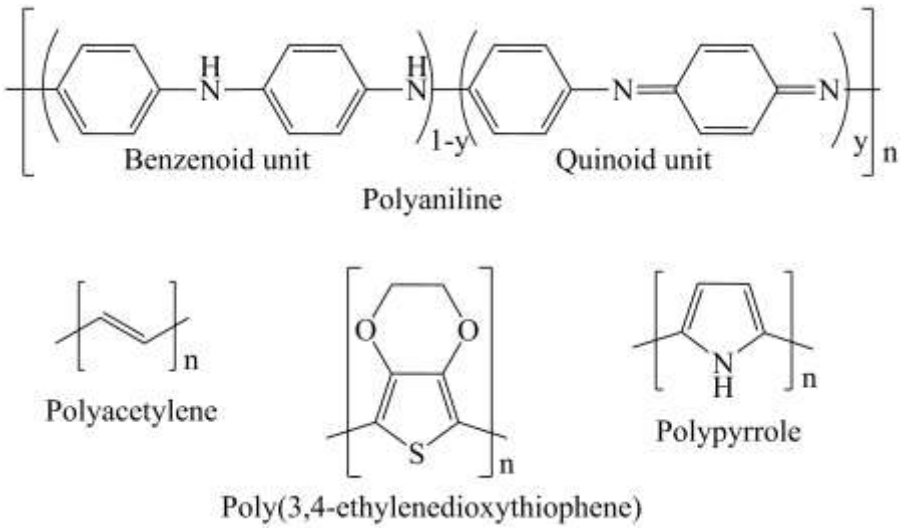

Figure 1.5. Structures of some intrinsically conducting polymers.

Intrinsically conducting polymers exhibit minimal electrical conductivity in the neutral or uncharged form. However, their conductivities can be elevated by several orders of magnitude upon doping. Fincher *et al*. (1978) found that the conductivity of polyacetylene, the first intrinsically conducting polymer to be reported, could be systematically varied over twelve orders of magnitude by carefully controlling the dopant concentration [67]. Thus, polyacetylene could be transformed from an insulator to a metal like conductor through doping. Doping generally involves addition (*n*-doping) or removal (*p*-doping) of electrons from the polymer backbone, which induces localized charge defects in the form of polarons [68]. The removal of one electron locally from a carbon atom forms a polaron, while the removal of a second electron from an oxidized section forms a bipolaron. The formation of polypyrrole polaron and bipolaron is demonstrated in Scheme 1.2. Consequently, the dopant counter ions stabilize the charges along the polymer chains [64]. The polarons and bipolarons

are believed to be the charge carriers in conjugated conducting polymers.

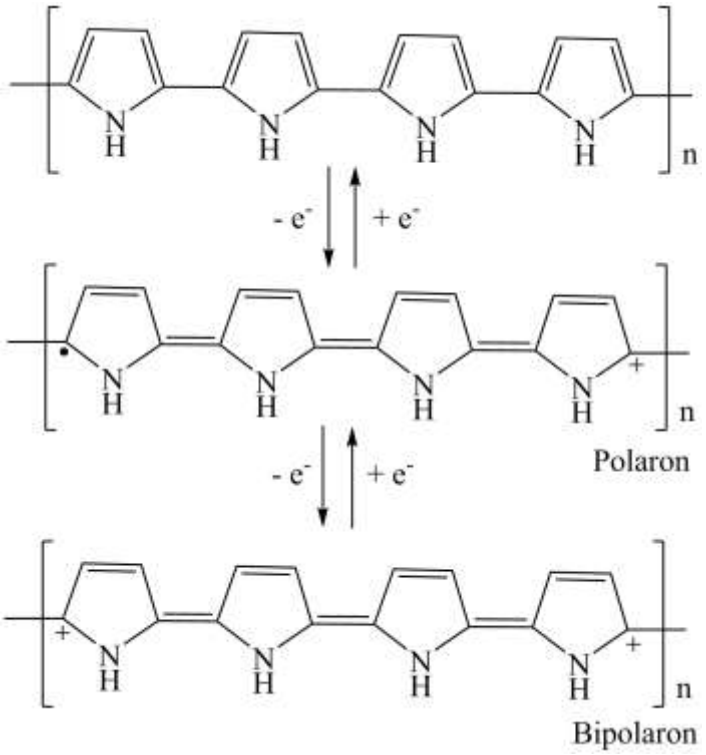

Scheme 1.2. Formation of polaron and bipolaron in polypyrrole.

Polypyrrole and PANI are usually doped with inorganic acids such as sulfuric acid or bulky organic acids such as dodecylbenzensulfonic and toluene-4-sulfonic acids [69-72]. The concept of doping is quite diverse and sometimes widely different processes are involved in doping different polymers. Polyacetylene, for example, is doped through partial oxidation (*p*-doping) or partial reduction (*n*-doping) of the π backbone whereas PANI is doped through protonation of the polymer backbone, a process which neither increases nor decreases the number of electrons associated with the polymer chain [64, 73]. This type of

doping, referred to as primary doping, has been found to be reversible. Furthermore, the concept of secondary doping has also been utilized to further increase the conductivity of organic polymers. Secondary doping involves treatment of a polymer, already doped by a primary dopant, with an apparently 'inert' substance such as *m*-cresol (secondary dopant) [73]. The effects of secondary dopants are permanent and persist even after the removal of the dopant. Although a range of intrinsically conducting polymers have been synthesized and studied, polypyrrole, polythiophene, PANI and their derivatives are the most intensely investigated polymers. This is attributed to their low cost, ease of synthesis and good environmental stability [74]. PANI is generally considered to display the optimum combination of stability, high conductivity and low cost [75-77].

The antioxidant capability of intrinsically conducting polymers was reported in 1998 by Ismail *et al*. when they evaluated the performance of PANI in protecting styrene butadiene rubber vulcanizates against oxidation and radiation deterioration [78]. Following this study, several researchers endeavoured to investigate the antioxidant properties of polyaniline and other intrinsically conducting polymers. Recently, the free radical scavenging properties of chemically synthesized polypyrrole, PANI and poly(3,4-ethylenedioxythiophene) have been reported with PANI exhibiting a superior free radical scavenging capacity [79-86]. Therefore, PANI and its derivatives remain the intrinsically conducting polymers that have been considered most widely in antioxidant studies. For example, the free radical scavenging activity of electrochemically synthesized PANI [87], and poly(anilinesulfonic acid), a derivative of PANI [88] have been reported. Gizdavic-Nikolaidis *et al*. (2010) have also reported the free radical scavenging activity of microwave

synthesized PANI copolymers, namely poly(aniline-*co*-2-sulfonic acid) and poly(aniline-*co*-2-aminobenzoic acid) [89].

1.5 PANI

PANI is a phenylene - based polymer having –NH- groups on either side of the phenylene ring. The –NH- groups can undergo oxidation, allowing PANI to exist in a continuum of oxidation states [90]. The principal structure of PANI consists of two types of segments: the reduced benzenoid amine and oxidized quinoid imine units as shown in Figure 1.5 [91]. Varying ratios of the benzenoid and quinoid units result in different oxidation states or forms of polyaniline. The three well defined oxidation states of PANI, shown in Figure 1.6, are leucoemeraldine, pernigraline and emeraldine [92, 93]. Leucoemeraldine is the fully reduced, pernigraniline is the fully oxidized and emeraldine is the partially oxidized form of PANI. The emeraldine form is environmentally stable and does not undergo any changes in the chemical structure upon prolonged storage [90]. The emeraldine base, an insulating form, can be easily converted to emeraldine salt, the conductive form, through protonation (doping) as shown in Scheme 1.3 [94]. On the other hand, the emeraldine salt form can also be converted back to the emeraldine base after treatment with a base (dedoping). Reduction of the emeraldine to leucoemeraldine or oxidation of emeraldine to pernigraniline results in diminution of the conductivity of PANI [92, 95, 96].

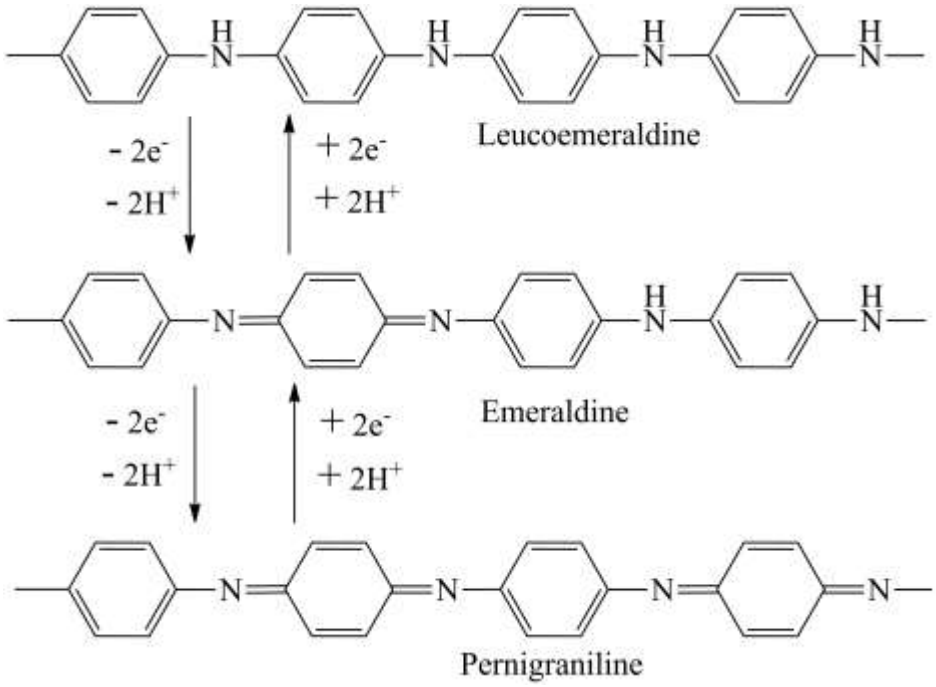

Figure 1.6. Different base forms of PANI.

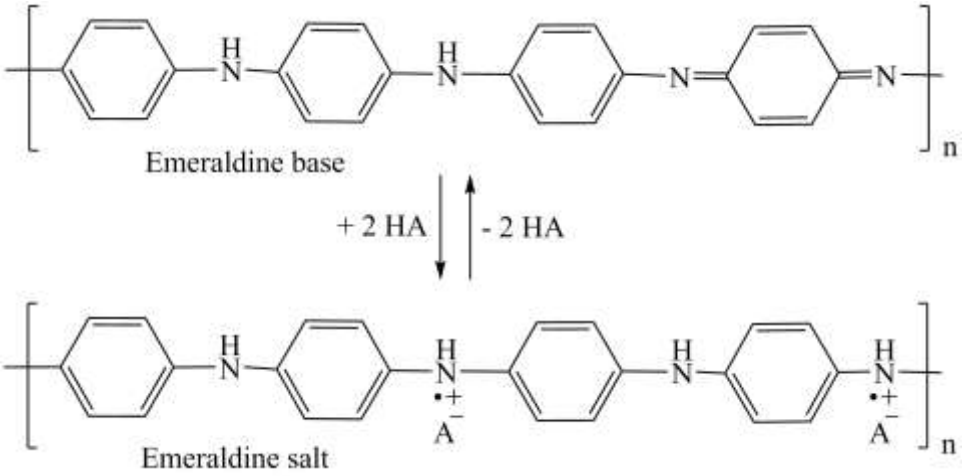

Scheme 1.3. Conversion of emeraldine base to emeraldine salt.

1.5.1 Synthesis of PANI

PANI is synthesized by the chemical or electrochemical oxidation of aniline in aqueous or non-aqueous solvents [90, 97-99]. The polymerization of aniline has also been carried out with the aid of enzymes, plasma, ultra sonic irradiation and photo-excitation of the aniline monomers [97]. However, chemical synthesis is the preferred technique where large quantities of PANI are required.

1.5.1.1 Chemical synthesis

The chemical synthesis of PANI occurs with the addition of an oxidant such as ammonium persulfate (APS) [100-110], hydrogen peroxide and ferric chloride [111, 112] or ferric sulfate and ferric nitrate [113] to the aniline monomer. The polymerization is usually carried out in acidic conditions and several organic as well as inorganic acids like hydrochloric acid (HCl) [114], phosphoric acid [115], sulfuric acid [116], dodecylbenzenesulfonic acid (DBSA) [117, 118], *p*-toluenesulfonic acid (*p*TSA) [119], camphor sulfonic acid (CSA) [83] or succinic acid [120] have been used for chemical synthesis of PANI. The product is the corresponding acid doped emeraldine salt form of polyaniline.

The mechanism of oxidative polymerization of aniline is shown in Scheme 1.4. Initially, an aniline dimer is formed through the reaction of an anilinium cation with aniline [121-123]. The dimer is then oxidized via a single two-electron step to quinoidal diimine form because of its lower oxidation potential in comparison with aniline, leading to the formation of the polymer [124, 125]. The polymerization of aniline is efficient only in acidic

medium, where aniline exists as an anilinium cation [126]. PANI has also been chemically synthesized with aniline salts; aniline hydrochloride [127-132] or aniline sulfate [133], as the starting materials. However, recently PANI was synthesized by oxidation of aniline in the absence of any added acids [79, 85]. In this approach, known as the "falling pH" method, the polymerization is initiated at a higher pH but the pH falls as the reaction progress due to the generation of protons. As shown in Scheme 1.5, the initial products formed at higher pH are phenazine structures and regular polyaniline forms at lower pH [92].

1.5.1.2 Electrochemical synthesis

Electrochemically activated polymerization by anodic current has been employed for the production of several intrinsically conducting polymers. Electrochemical synthesis, compared to chemical synthesis, yields purer polymers as no additional chemicals such as oxidants or surfactants are used [97, 134, 135], although scale-up to larger polymer quantities is more difficult. The mechanism of electrochemical oxidation of aniline is believed to be similar to that of chemical oxidation [125]. Electrochemical polymer synthesis is also very versatile and a range of approaches can be employed, including a constant current (galvanostatic), a constant potential (potentiostatic) and potential cycling [97, 135-139]. The galvanostatic method consists essentially of a two-electrode assembly dipped in an electrolyte solution containing the monomer. A specified level of current is passed so as to form the polymer film on the surface of an inert electrode such as platinum or stainless steel [97].

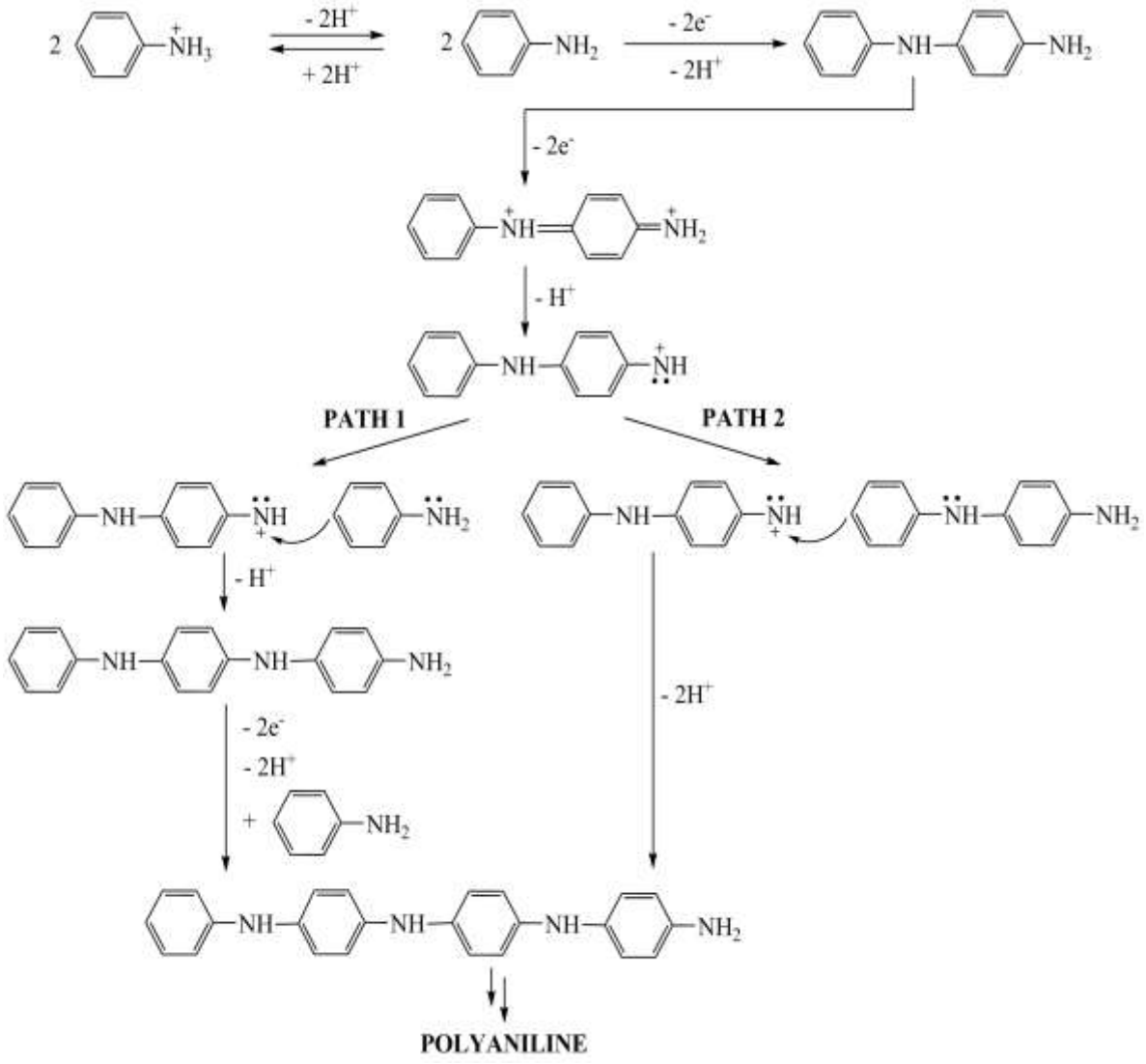

Scheme 1.4. Mechanism of polymerization of aniline in an acidic environment (adapted from Wei *et al*., (1989) [125]).

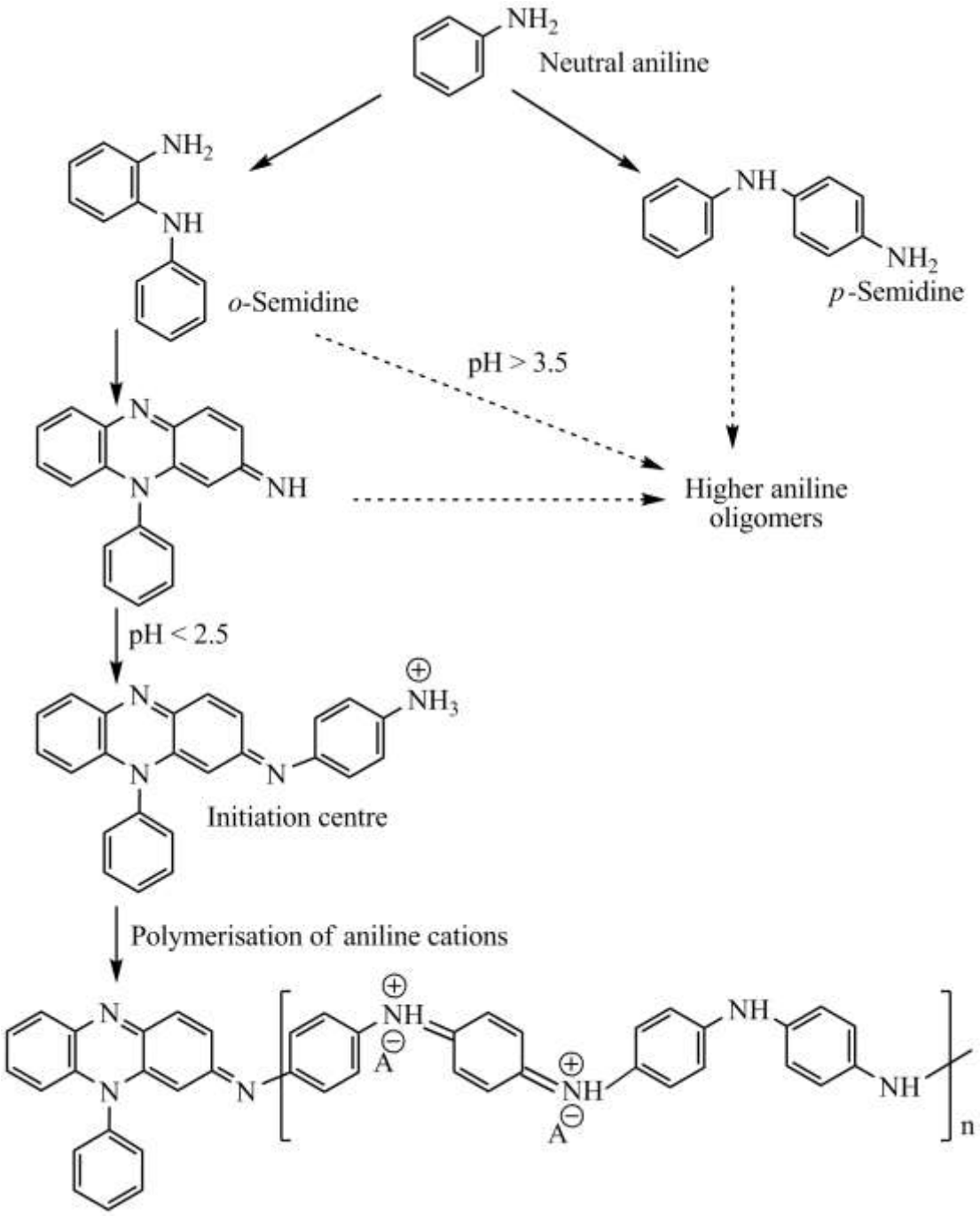

Scheme 1.5. Mechanism of polymerization of aniline in a "falling pH" environment (adapted from Stejskal *et al*., (2010) [92]).

While continuous cycling between the predetermined potentials produces a PANI film firmly adhered on the electrode surface [140], polymerization at a constant potential produces a polymer powder that adheres weakly on the electrode [141]. Electrochemical polymerization offers the option of finely controlling the thickness of the deposited polymer film that can be peeled of the electrode surface. Homogeneous PANI films of uniform thickness have been achieved using both the potentiostatic and galvanostatic regimes [142]. Bhadra *et al*. (2007) syntheiszed PANI powder by applying a constant potential of 1.3 V across the working graphite and the reference saturated calomel electrodes, in the presence of aniline solution and *p*TSA [143].

1.5.1.3 Other polymerization techniques

Conducting PANI has also been successfully synthesized via plasma polymerization [144, 145]. In this technique, monomer molecules are fragmented by the action of plasma to form smaller fragments and radicals, which are then recombined to materialize larger molecules. Repetitive radical formation and recombination leads to the formation of plasma polymers [144]. In a typical plasma polymerization setup, monomer vapours are introduced into a chamber where plasma is generated between electrodes and, following the fragmentation of the monomers, the polymer grows on the walls of the chamber or on substrates (glass, silicon, metal, etc) provided in the chamber. Plasma polymerization provides an all-dry, one-step, contaminant free and relatively rapid technique for polymer synthesis [144].

A less considered route to synthesize PANI is the photopolymerization technique. PANI was obtained by adding aniline in nitric acid to a silver nitrate solution and illuminating at 365 nm with a 20 W germicide mercury lamp. The interaction of the photon with the solution generated aniline radicals which could polymerize through head-to-tail coupling [146]. Similary, Jing *et al*. (2006; 2007) accomplished polymerization with the aid of ultrasonic irradiation [147, 148]. Another method to synthesize PANI is a biological route where enzyme initiated polymerization is employed. Polyaniline has been synthesized by horseradish peroxide, which catalyzed aniline oxidation via the hydrogen peroxide formed enzymatically [149, 150].

1.5.2 Morphology

The evolution of the structure of PANI consists of three steps: the generation of nucleates, their assembly and finally the growth of PANI chains from the nucleates [92]. Depending on the type of nucleate organization, due to the synthesis conditions and route, the subsequent PANI chain growth can produce a range of morphologies such as granules, spheres, fibers, tubes and other complex structures [92].

The granular structure is the most common morphology of PANI. This morphology is easily obtained by chemical polymerization when using strong oxidants and high aniline concentration under acidic conditions (pH < 2.5) [92, 151, 152]. Laslau *et al*. (2009) obtained nano-granules measuring 15 – 30 nm by oxidizing aniline with APS at pH 2.5 [153]. The as-prepared granular PANI, being doped by the corresponding acid in the synthesis media, is electrically conductive [92].

Nanofibers, sometimes also called nanowires, are prepared by oxidizing aniline at low concentrations in the presence of a strong acid. The diameters of the fibers are usually in the range 20 – 100 nm, but they can extend to several micrometers in length [92]. The diameters of the nanofibers are dependent on the acids employed in the synthesis. In the presence of HCl, CSA and perchloric acid, the average diameters of the PANI nanofibers were 30, 50 and 120 nm respectively [102]. The nanofibers can also extend into branched networks [121, 154, 155], arrays [156, 157] or bundles [158].

PANI nanotubes, one of the most interesting objects among conducting polymer nanostructures, differ from the nanofibers by the presence of an internal cavity [92]. However, like nanofibers, they can also extend to several micrometers in length. Nanotubes are synthesized as nanofibers but in the presence of a template. The synthesis of nanotubes is generally initiated at low acidity, pH > 3.5, and completed at pH < 2.5. Oligomers formed at the initial high pH act as the template for the formation of the nanotubes at lower pH [159-162]. While the cavities of the polyaniline nanotubes are usually in the range 10 – 150 nm, the wall thickness are generally in the range 50 – 200 nm. The walls can be compact and smooth or have a rough granular morphology [92, 163].

PANI microspheres have been prepared by initiating the oxidation of aniline in an alkaline medium [164, 165]. If the entire synthesis occurs in the alkaline medium then the microspheres consist largely of aniline oligomers [161]. The microspheres can be of several micrometers in size and depending on the synthesis conditions they can be hollow [166, 167]. Zhang *et al*. (2009) prepared hollow PANI microspheres with diameters from 310 nm to 1.2 μm. The shell thickness of the microspheres was 80 – 110 nm [113]. PANI nanospheres with

diameters less than 200 nm have also been occasionally observed alongside nanotubes [160]. However, they have never existed as dominant products [92].

A range of other morphologies of PANI such as tetragonal stars [168], 3D-boxes [169], hairy urchin [112], cauliflower [111], leaf-like [170], flower-like [171] and dendrites [172] have been obtained by tuning the pH profile during the polymerization of aniline. The "falling pH" synthesis regime yields a variety of nanostructured PANI morphologies within the same sample [91]. These morphologies include nanotubes, nanorods, nanoflakes and nanospheres [106, 173].

The origin of nanostructures consists of three steps: generation of nucleates, their self-assembly and growth of PANI chains from the nucleates [92]. Depending on the type of nucleates and subsequent PANI growth, different morphologies result. When aniline is oxidized in a weak acid, the intial phenazine groups formed stack due to π-π interactions and hydrogen bonding. The stacking mechanism produces nanocrystallites which act as templates for the adsorption of *N*-phenylphenazines arising in the reaction mixture. The starting template for tubular growth is thus produced by the short *N*-phenylphenazines stacked around the oligomeric nanocrystallites.The subsequent growth of PANI chains from the stacked *N*-phenylphenazine initiation centers gives rise to the walls of the nanotubes [161]. Under favourable conditions, PANI chains grow perpendicularly from single stack of nucleates and produce the body of a nanofiber [92]. A random aggregation of phenazine nucleates results in granular morphology [92]. At low pH and low aniline concentrations, dimers of aniline form. The non-availability of surface for dimer deposition, unlike the phenazine templates for tubular growth, leads to formation of trimers. Following trimer formation, nanoparticles form

through radial growth. Since spherical clusters will have a lower overall surface energy than an elongated chain, granular morphologies form [91]. Under alkaline conditions, aniline is not miscible with the aqueous media and constitutes a separate phase. Oxidation at the interface of the aniline droplets and the oxidant aqueous phase forms microspheres. These microspheres may be hollow or contain aniline which can be further oxidized [161].

1.5.3 Free radical scavenging capacity

The versatility of PANI, attributed to its tunable morphology, variable oxidation states and conductivity, has led to its application in a wide range of fields including metallic corrosion protection [174, 175], electromagnetic interference shielding [176], electrostatic discharge [177], sensors [93, 178] and actuators [179]. Recently, PANI has gained recognition for use as a solid antioxidant material [180-182].

The antioxidant activity of PANI, characterized by its free radical scavenging capacity, is attributed to its ability to switch easily between the reduced and oxidized states. The first oxidation process for the PANIs generally begins at around 100 to 200 mV (Ag/AgCl) in aqueous solutions, while potentials in excess of 800 mV are required to fully oxidize PANI under acidic conditions [88]. The similarity of PANI oxidation potentials to those of ascorbic acid and the most active antioxidant polyphenols in beverages (at 100 to 200 mV (Ag/AgCl) in neutral pH solutions), created interest in considering PANI as a solid antioxidant material [88]. At these potentials, the oxidation of PANI can be readily coupled with the reduction of active radicals such as $ROO^{\bullet}$ and $OH^{\bullet}$, with formal potentials of 800 and 2100 mV at pH 7, respectively [183]. These hydroxyl radicals, in particular are so active

that once formed, for example via the Fenton reaction in the presence of Fe(II) and peroxide, they will react with the first organic groups, of any functionality they encounter. By contrast, the reduction potential for the O_2/H_2O_2 couple, frequently the first process involving oxygen and its interaction with food and beverages, lies around 165 mV (Ag/AgCl) at pH 7, and at ca. 265 mV at pH 3.6, typical of many wines and fruit juices [184]. Only ascorbic acid and the more active polyphenols have reduction potentials low enough to react directly with molecular oxygen in beverages, as do several intrinsically conducting polymers. Therefore, PANI with a lower formal potential, acts as a strong reducing agent when in contact with free radicals. This interaction leads to the oxidation of PANI and reduction of the free radicals to neutral species [80, 88].

The free radical scavenging capacity of PANI has been assessed using the $DPPH^{\bullet}$ (1,1-diphenyl-2-picrylhydrazyl) [83, 88, 180] and $ABTS^{\bullet+}$ (2,2-azino-bis(3-ethylbenzothiazoline-6-sulfonic acid) assays [79]. The $DPPH^{\bullet}$ and $ABTS^{\bullet+}$ radicals are coloured but are decolourized upon reduction, for example, when intrinsically conducting polymers are introduced into solutions containing the free radicals. The extent of free radical reduction, more specifically the degree of decolourization, can be monitored by UV spectrophotometry, or alternatively electron spin resonance spectroscopy, and thus the free radical scavenging capacity of the intrinsically conducting polymers can be determined. Further test procedures can include the oxygen radical absorbance capacity (ORAC) assay, the extent of formation of peroxides in oil samples, or the formation of brown coloured pigments in juices, undertaken under conditions of accelerated aging [181].

1.5.4 Biocompatibility

PANI has always been treated with caution as the aniline monomer and subsequent polymerization intermediates such as aniline dimmers and oligomers can be potentially physiologically active. The most recognized threat is the carcinogenic effect of benzidine, the aniline dimer. However, pure PANI, after removal of low molecular weight polymerization products, has been found to be biocompatible and non-cytotoxic [185]. The biocompatibility and non-cytotoxicity of PANI has also been confirmed by several other studies.

PANI films exhibited good cell attachment and proliferation when tested with H9c2 cardiac myoblasts [186] and PC-12 pheochromocytoma cells [187, 188] indicating biocompatibity of the films. Kumar *et al*. (2010) have demonstrated the biocompatibility of heavy ion irradiated PANI nanofibers by studying their haemolysis prevention activity [189]. The nanofibers showed reduced potency to damage blood cells and therefore, an enhanced hemolysis prevention activity. Kamalesh *et al*. (2000) assessed the biocompatibility of PANI films through subcutaneous implantation into male Sprague-Dawley rats beneath the dorsal skin for a period ranging from 19 to 90 weeks and concluded that the films were biocompatible [190]. Furthermore, polymer composites [191-193] and hydrogels [194] containing PANI have also been found to be biocompatible. The biocompatibility and non-cytotoxicity of PANI is advantageous for applications such as food packaging where it will be in contact with food stuffs.

1.5.5 PANI based polymer substrates

The successful utilization of PANI as a solid antioxidant requires blending with commercially available polymers having suitable mechanical properties and processability. Various techniques like solution blending, melt processing, surface deposition and surface grafting have been used to prepare PANI containing polymer substrates. However, melt processing is the industrially preferred method for large scale production, PANI incorporated polymer matrices. PANI is thermally stable, circumscribed by ≤ 10 % weight loss other than moisture loss, up to 400 ºC [195]. However, the infusibility of PANI is the major drawback for melt processing [97]. Nevertheless, PANI has been successfully dispersed in the melt of commercially available polymers such as PE [196-199], PVC [200, 201], PS [202], PET [203] and poly(methyl methacrylate) (PMMA) [204, 205]. Ternary blends of PANI/ ethylene vinyl acetate (EVA)/ PE [206] and PANI/ PMMA/ poly(vinylidene fluoride) (PVDF) [207] have also been prepared via melt processing. The melt blending process generally involves mixing or extruding PANI with another melt processable polymer and compression moulding the mix or extrudate into films, as shown in Figure 1.7.

Furthermore, other techniques have been employed to prepare PANI/ host polymer composites. For example, PANI was polymerized in an aqueous dispersion of corn starch to yield PANI/ starch composites with antioxidant properties for consideration in biomedical applications [182]. The free radical scavenging capacity of the composite samples improved with increased PANI loading. Electrospun nanofibers of CSA doped PANI and polyethylene oxide (PEO) have been prepared [208]. Solution blending of PANI with other polymers has also been extensively exploited to yield blend films. Cast films of PANI blends with PS in *N*-

methyl-2-pyrrolidone (NMP) [209], poly(vinyl formal) (PVF) in chloroform [210], PS in *m*-cresol [211], poly(vinyl acetate) (PVAc) in dimethyl sulfonate oxide (DSMO) [212] and PVC in tetrahydrofuran (THF) [213] have been prepared.

PANI has been physically deposited on PET fibers [214-217], PET films [218-223], poly(tetrafluoroethylenelene) (PTFE) [224], and PE films [225, 226] by immersing the polymer substrates in the aniline polymerization media. Caramori and Fernandes (2008) have prepared PANI/ PET composites by polymerizing PANI on hydrazine activated PET [227]. To achieve improved adhesion, PANI has been chemically grafted on poly(acrylic acid) grafted polymer surfaces [228-231]. Similarly, Ji *et al*. (2002) carried out oxidative graft polymerization of aniline on PTFE films modified by surface hydroxylation and silanization [232].

The availability of a range of techniques to blend with other polymers fosters the applicability of PANI as a solid antioxidant. PE and PET are common plastics used in the packaging industry. Blending these plastics with PANI has the potential to yield novel packaging materials with antioxidant properties, which can then be used to enhance shelf life of cosmetics, beverages and other food products [181].

PANI has been exploited for its electrical conductivity; however, its application as a solid antioxidant is an emerging field of study. While few studies on the antioxidant property of PANI have emerged recently [83, 88, 180], PANI is yet to be applied as an antioxidant in active food packaging systems. PANI based active packaging systems have a huge potential in food packaging applications as the food packaging industry is in continuous need of improved packaging systems.

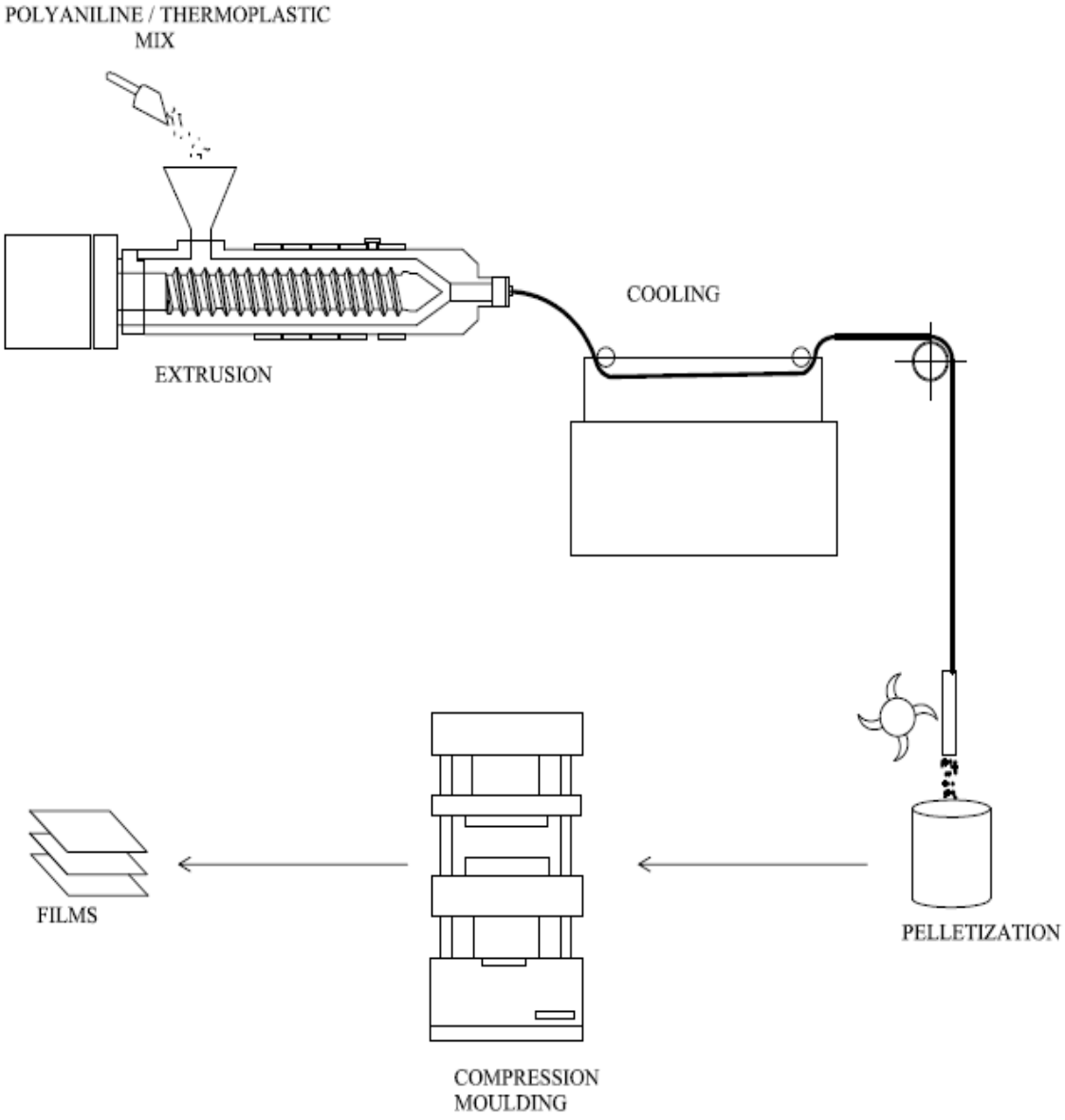

Figure 1.7. Melt processing of PANI/ thermoplastic blends.

1.6 Research Objectives

This research aims to explore the utilization of PANI in active packaging applications. Accomplishment of this aim will result in the availability of PANI based active materials, with antioxidant capabilities, for use in the food and packaging industries. The aim of this research was realized through a series of more detailed objectives:

(1) Examination of the factors affecting free radical scavenging capacity of PANI.

(2) Evaluation of the effect of thermal treatment on the free radical scavenging capacity of PANI.

(3) Incorporation of PANI in PET and PE matrices via melt processing.

(4) Characterization of the physical and chemical properties of the melt processed compositess.

(5) Assessing the suitability of the melt processed composites for active packaging applications.

CHAPTER TWO

Factors Affecting the Free Radical Scavenging Capacity of PANI

This chapter has been published as:

Nand A.V., Ray S., Easteal A.J., Waterhouse G.I.N., Gizdavic-Nikolaidis M., Cooney R.P., Travas-Sejdic J., Kilmartin P.A. (2011) Factors affecting the radical scavenging activity of polyaniline. *Synthetic Metals* 161: 1232-1237.

2.1 Introduction

For several years, PANI has been a prominent research subject within the group of electrically conducting polymers. It has attracted the attention of scientists due to its electrical and optical characteristics [233], environmental stability, low cost and ease of synthesis [234]. PANI also has the potential to exist in a continuum of oxidation states. These properties have enabled PANI to be used in a wide range of applications such as actuators, chemical/ biological sensors, for electrostatic discharge, electromagnetic interference shielding and corrosion protection [173-175, 179, 235, 236].

Recently PANI has been investigated for its antioxidant activity [180]. The scavenging of DPPH radicals has been used as a measure of the antioxidant activity of PANI [82, 83, 85]. The DPPH free radical method measures antioxidant activity at room temperature, so the risk of thermal degradation of the test molecules is minimized. Oxidation of conducting polymer segments is seen as the major mechanism involved in the reaction of DPPH radicals with PANI [84, 88].

PANI has been successfully used as an antioxidant to protect styrene butadiene rubber vulcanizates from oxidative deterioration [78]. Saikia *et al.* (2010) have prepared antioxidant starch/ PANI composites for biomedical applications [182]. Since PANI is being recognized for its antioxidant behaviour, it is imperative that the factors affecting its antioxidant activity be investigated, but only a handful of such studies have been reported in the literature. Banerjee *et al*. (2010) have found that polyaniline nanofibers had enhanced antioxidant activity [83], which was attributed to the increased surface area of the nanofibers. This

phenomenon has also been observed by Wang *et al*. (2007) who also reported that the antioxidant activity increased as the average diameter of the nanofibers decreased [82].

The oxidation level is one of the most important factors affecting the properties of PANI [234]. Being redox active, PANI can be switched between various oxidized and reduced forms. The oxidation of PANI generally involves transformations of amine (–NH-) groups to imine (–N=) [234]. It has been peviously observed that reduced PANI is a superior scavenger of $ABTS^{\bullet+}$ compared to as - prepared, partially oxidized, polymer samples [79]. The possible influence of surface area was also raised in this report, on the basis that nanotubular forms of PANI were superior in radical scavenging to the conventional granular PANI prepared in the presence of a strong acid. Nanorod or nanotubular forms develop from solutions that are originally acid-free and of a neutral pH, but whose pH falls during the chemical synthesis, due to the liberation of sulfuric acid as the ammonium persulfate oxidant is reduced, leading to nanotube and nanorod formation at intermediate pH values (around pH 2.5) [237, 238].

In the present study PANI samples with both granular and micro/nanorod morphologies were prepared, and the surface area directly determined using the Brunauer-Emmett-Teller (BET) methodology. The relationships between conductivity, surface area, oxidation state and the resulting radical scavenging activity were then examined.

2.2 Experimental

2.2.1 Materials

Aniline, obtained from Sigma Aldrich, was distilled under reduced pressure. The colourless distillate was stored under nitrogen at 5 °C before use. Methanol, APS, hydrochloric acid (HCl), ammonium hydroxide and DPPH were also purchased from Sigma Aldrich and used as received.

2.2.2 Synthesis of PANIs

Four samples (NR-PANI, NR-PANIdd, G-PANI and G-PANIdd) of PANI were synthesized. NR-PANI was synthesized by adding 250 mL of 0.3 M APS to 250 mL of 0.2 M aniline solution with mechanical stirring at 5°C for 24 h. The pH of the reaction mixture dropped from an initial value of 6.5 to 3.0 after 3 h and to 1.3 over the 24 h reaction period. The reaction mixture was then filtered, washed several times with water and methanol. The residue obtained was vacuum dried at 40 °C overnight. 4.5 g of NR-PANI was deprotonated by stirring in 250 mL of 2.5 % ammonium hydroxide solution for 19 h. The product was filtered, washed with water several times and dried at 40 °C to obtain NR-PANIdd.

G-PANI was synthesized by adding 4.6565 g of distilled aniline to 100 mL of 1 M HCl. The pH of the solution was adjusted to 1.0 and 250 mL of 0.3 M APS was then added to the reaction mixture. The reaction mixture was mechanically stirred at 5 °C for 24 h. The product was filtered, washed and dried as described previously. G-PANIdd was obtained in same way as NR-PANIdd.

2.2.3 Characterization

The surface morphology of the PANI samples was visualized using a Philips XL30S FEG scanning electron microscope. The samples were coated with platinum using a Polaron SC7640 Sputter Coater for 300 s at 5-10 mA and 1.1 kV.

Infrared spectra of the polyaniline powder samples were recorded with a Thermo Electron Nicolet 8700 Fourier transform infrared spectrometer using a single bounce ATR and a germanium crystal. The average of 64 scans with resolution 4 cm^{-1} was taken. All the spectra were atmosphere and baseline corrected.

The electrical conductivities of dry pressed pellets of NR-PANI and G-PANI were measured by the four–probe technique using a Jandel Model RM2 instrument.

N_2 adsorption isotherms were determined at liquid nitrogen temperature (-195 ^oC) using a Micromeritics Tristar 3000 instrument. Specific surface areas were calculated from the N_2 adsorption data according to the Brunauer-Emmett-Teller (BET) method. Cumulative pore volumes and pore diameters were calculated from the adsorption isotherms by the Barrett-Joyner-Halenda (BJH) method. Samples were degassed at 150 ^oC for 2 h under a dry N_2 gas purge prior to the N_2 adsorption measurements.

X-ray photoelectron spectroscopy (XPS) data of the samples were collected on a Kratos Axis UltraDLD instrument equipped with a hemispherical electron energy analyser. Samples were mounted on standard VG sample studs by means of indium wafers. Spectra were excited using monochromatic Al Kα X-rays (1486.69 eV) with the X-ray source operating at 150 W. The analysis area was a 300 by 700 µm spot. The core level scans were collected with pass energy 20 eV. The analysis chamber was at pressures in the 10^{-9} torr

range throughout the data collection. Data analysis was performed using CasaXPS. Core level data were fitted using Gaussian-Lorentzian peaks with a Shirley background. The peak full width at half maxima (FWHM) was maintained constant for all the components in a particular spectrum. The binding energy scale was corrected for the neutraliser shift using the C 1s signal from saturated hydrocarbon at 284.6 eV.

2.2.4 Radical scavenging activity assay

20 mL of a 255 μM methanolic DPPH solution was added to 1 mg of test sample, weighed using a 5 digit balance to ensure a weight in the range from 1.00 to 1.05 mg (weighing error <5 %). The samples were left to react at room temperature for 24 h after which the absorbance of the supernatant at 516 nm, λ_{max} of the DPPH solution, was measured using a Shimadzu UV-1700 UV-visible spectrophotometer. Three trials of each sample were undertaken. A control experiment, without any test sample, was also set up. The amount of $DPPH^{\bullet}$ which reacted over a 24 h period was then calculated after subtracting away the background loss of a $DPPH^{\bullet}$ solution without added test sample, using an adaptation of the DPPH assay for use with polymeric samples [79, 80].

2.3 Results and Discussions

2.3.1 Morphology

The scanning electron microscope (SEM) micrographs of the PANI samples, depicted in Figure 2.1, clearly present different morphologies for NR-PANI and G-PANI. While NR-

PANI consisted largely of micro/nanorods, the presence of some flakes was also evident. By contrast, G-PANI exhibited a granular morphology typical of high acid–doped PANI. All the samples were dark colored materials.

The morphologies of NR-PANIdd and G-PANIdd were not significantly different from NR-PANI and G-PANI respectively. NR-PANIdd consisted of micro/nanorods and flakes while G-PANIdd had a granular morphology. Dedoping with ammonium hydroxide did not have a substantial effect on the morphologies of PANI samples.

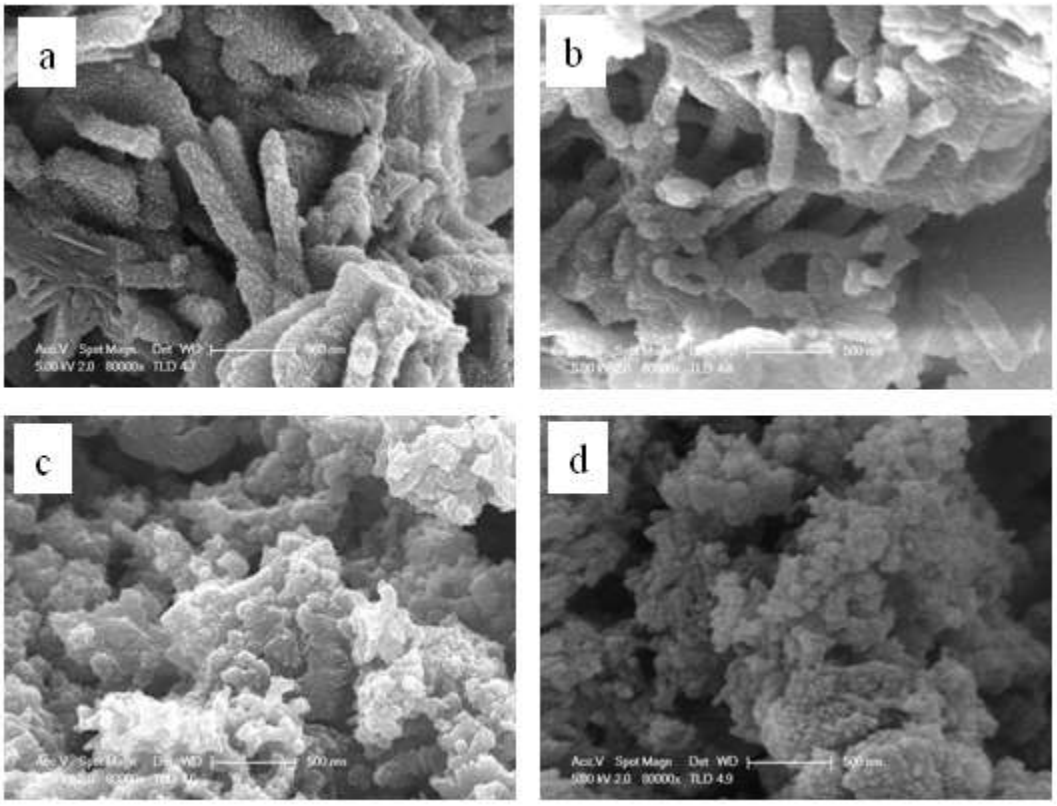

Figure 2.1. SEM micrographs of a) NR-PANI, b) NR-PANIdd, c) G-PANI and d) G-PANIdd.

2.3.2 Fourier–transform infrared spectroscopy (FTIR)

Figure 2.2 shows the FTIR spectra of NR-PANI, NR-PANIdd, G-PANI and G-PANIdd. All the samples show characteristic peaks at about 1585 cm^{-1} (C=C stretching mode of the quinoid rings), 1500 cm^{-1} (C=C stretching mode of benzenoid rings), 1310 cm^{-1} and 1250 cm^{-1} (C–N stretching mode), confirming that the samples were in a partially-oxidized state, referred to as the emeraldine PANI state. The vibrational bands at about 1155 and 830 cm^{-1} are assigned to the aromatic ring in–plane and out–of–plane C–H bending [87, 138]. The intensity of the C-N band of NR-PANI and G-PANI at about 1310 cm^{-1} decreased after dedoping. This suggests a higher proportion of quinoid units in the polymer chains of NR-PANIdd and G-PANIdd compared to NR-PANI and G-PANI. NR-PANI and NR-PANIdd exhibited a peak at 1040 cm^{-1} which could be assigned to sulfonate groups attached to the benzene rings [239], along with some bisulfate included as counterions [159, 173] but the peak persisted after dedoping. This peak was absent from G-PANI and G-PANIdd samples.

Further peaks at about 1413 and 1447 cm^{-1} are also characteristic of PANI nanostructures formed under falling pH conditions [239]. Previous studies indicate that flake-like morphology in PANI, synthesized in a falling pH environment, could contain phenazine-like, highly branched structures, which exhibit these bands [237, 238]. This authenticates the SEM results where flakes alongside micro/nanorods were visible for NR-PANI and NR-PANIdd. G-PANI and G-PANIdd, having a granular morphology, did not exhibit these bands. Previous studies of nanorod formation under falling-pH conditions have demonstrated that the interior core structures, formed at a higher pH and containing phenazine groups, are coated by a layer of more regular PANI under the lower pH conditions that apply later in the

synthesis [153, 238]. It is this outer polyaniline surface that will be exposed to test solutions in the first instance, although the contribution of interior material, and of phenazine groups, also needs to be considered for the likes of radical scavenging.

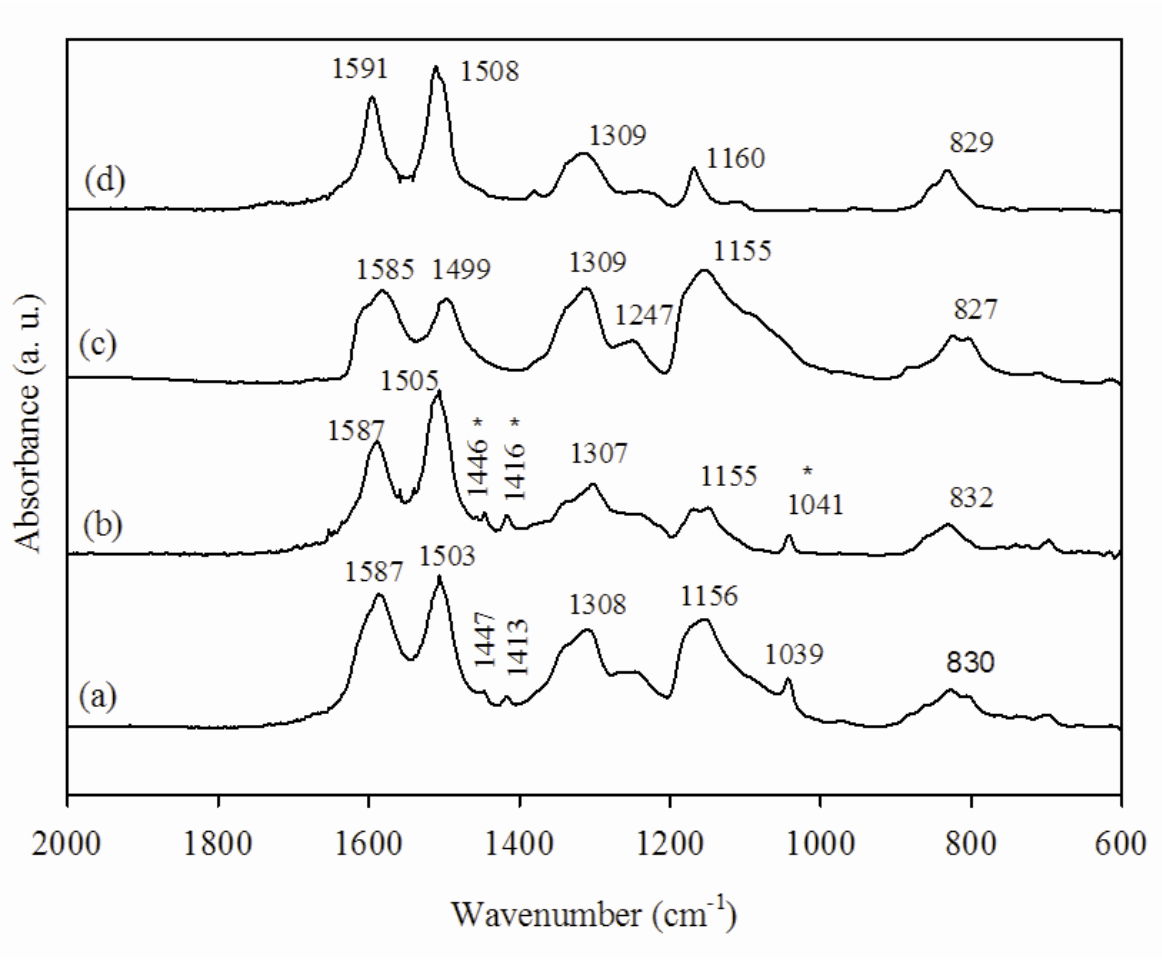

Figure 2.2. FTIR spectra of a) NR-PANI, b) NR-PANIdd, c) G-PANI and d) G-PANIdd. Typical micro/ nanorod peaks have been highlighted with asterisks.

2.3.3 Electrical conductivity

The electrical conductivities of NR-PANI and G-PANI were 2.3×10^{-3} and 5.2×10^{-1} S cm^{-1} respectively. As is well known, polyaniline exhibits its highest conductivity when partially oxidised and in an acid-doped state [21]. G-PANI, being doped by HCl, had a higher conductivity than NR-PANI which was synthesized in the absence of any initial acid. The conductivities of dedoped samples were too low to be determined by the technique employed in this study, and were likely less than 10^{-5} S cm^{-1} in each case.

2.3.4 Surface area

The specific surface areas, cumulative pore volumes and the average pore diameters of the PANI samples are presented in Table 2.1. The various samples had a similar specific surface area, cumulative pore volume and average pore diameter. The specific surface area was in fact about 25 % larger in the case of the granular samples formed under higher acid conditions: G-PANI and G-PANIdd. This finding was counter to the initial expectation that the micro/nanorod NR-PANI would have a higher surface area. The presence of flakes alongside micro/nanorods may have influenced the surface area values for NR-PANI.

The specific surface areas and average pore diameter of the samples investigated in this study compared well with those reported previously. The specific surface area and average pore size of PANI, synthesized by oxidizing aniline with APS in the presence of HCl without any stirring, were given as 18.8 m^2g^{-1} and 16.1 nm respectively [240]. Chowdhury *et al*. (2008) prepared PANI samples in a similar way and reported specific surface areas ranging from 11 to 29 m^2g^{-1} [241]. Moreover, PANI nanofibers, formed by interfacial

Table 2.1. Specific surface area, cumulative pore volume and average pore diameter of the PANI samples.

Sample	Specific surface area (± 0.2 m^2g^{-1})[a]	Cumulative pore volume ($\pm 0.01 cm^3g^{-1}$)[b]	Average pore diameter (± 2 nm)[b]
NR-PANI	22.3	0.13	25
NR-PANIdd	22.6	0.11	22
G-PANI	27.8	0.14	22
G-PANIdd	28.2	0.11	17

[a] determined from the N_2 physisorption isotherm by BET method
[b] determined from the N_2 physisorption isotherm by BJH method

polymerization, with specific surface areas ranging from 34.2 to 54.7 m^2g^{-1}, and microspheres with specific surface areas 46 m^2g^{-1} have also been reported [102, 242, 243].

Huang and Kaner (2004; 2006) have observed an 8.7–19.7 % increase in the specific surface area of polyaniline nanofibers after dedoping with base, indicating that the free volume of the nanofiber samples increased after the removal of dopants [102, 242]. However, in the present study dedoping did not affect the specific surface areas of NR-PANI and G-PANI to a significant extent; an increase of only about 1 % was observed. NR-PANI and G-PANI were degassed at 150 ºC and it is possible that the dopants exuded upon the thermal treatment. This would render the surface area of NR-PANI and G-PANI similar to that of NR-PANIdd and G-PANIdd respectively.

2.3.5 Level of oxidation

The N1s core level XPS spectra of NR-PANI, G-PANI, NR-PANIdd and G-PANIdd are given in Figure 2.3. The major peaks of all samples were decomposed into four sub-bands. The peaks corresponding to quinoid imine nitrogen (-N=) and benzenoid amine nitrogen (-NH-) are centered at 398.3 eV and 399.7 eV respectively. The two peaks centered at binding energies above 400 eV are attributed to positively charged nitrogen centres (N^+) [234]. The phenazine nitrogen peak also appears around 398 eV [244] and these could also contribute to the quinoid imine peaks of NR-PANI and NR-PANIdd. However, as XPS is a surface sensitive technique and mainly profiles the outer 10 nm of the sample, the inner phenazine-containing material formed initially at a higher pH is unlikely to contribute greatly to the measured XPS peaks. The relative contributions of various nitrogen groups in the samples resulting from fitting of Gausian-Lorentzian components are summarized in Table 2.2.

Table 2.2. Intensities of N 1s deconvoluted peaks and the oxidation level of PANI samples.

Samples	N1s deconvoluted peak intensities (%)			Oxidation level $\left[\frac{(-\mathrm{N}=)+(\mathrm{N}^+)}{\mathrm{Total\,N}}\right]$
	-N= [a]	-NH- [b]	N^+ [c]	
NR-PANI	3.0	82.8	14.2	0.17
NR-PANIdd	29.7	63.8	6.5	0.36
G-PANI	3.7	72.6	23.7	0.27
G-PANIdd	22.8	58.5	18.7	0.42

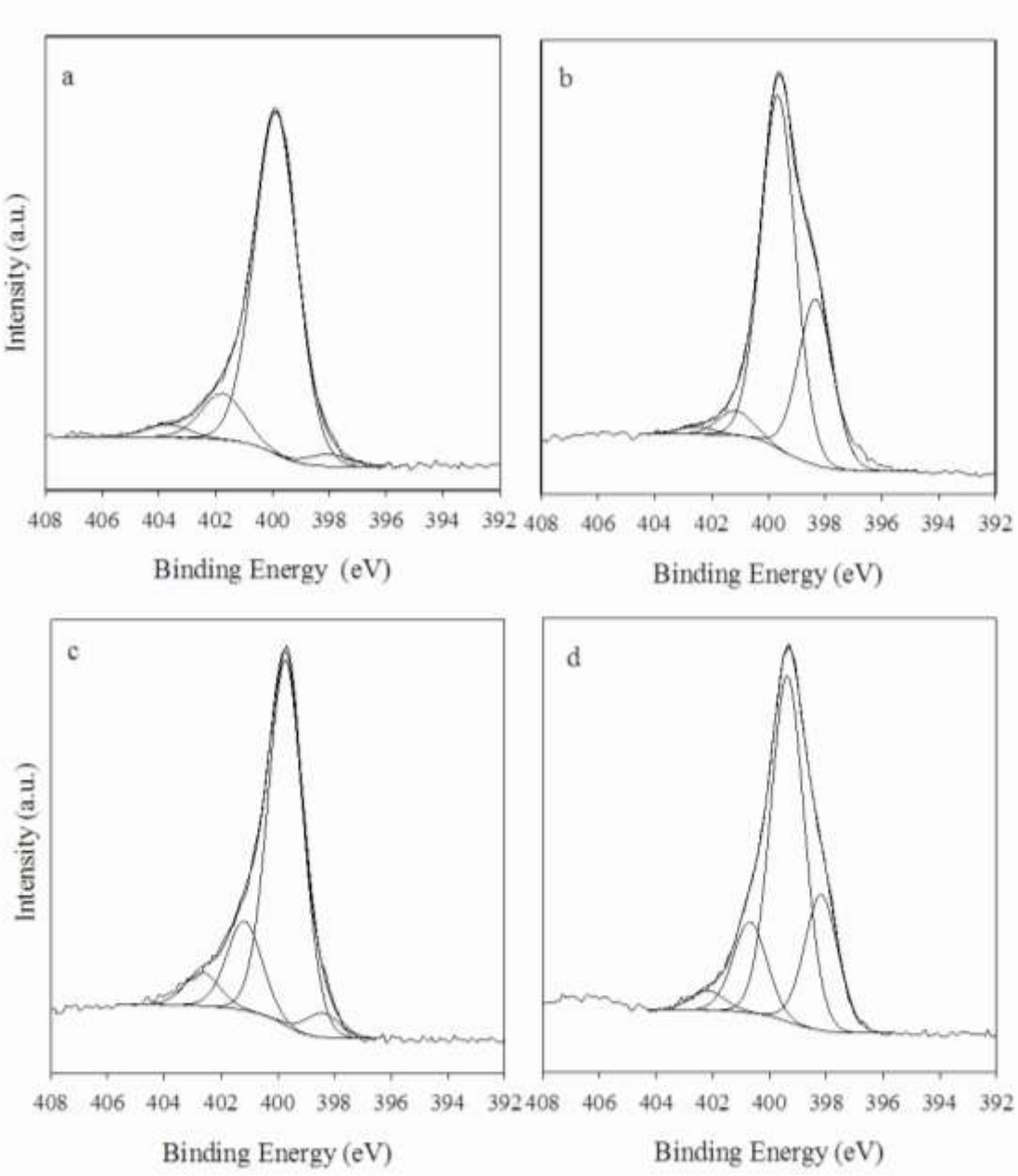

Figure 2.3. N 1s core level spectra of a) NR-PANI, b) NR-PANIdd,

c) G-PANI and d) G-PANIdd.

The oxidation of PANI entails the conversion of benzenoid to quinoid moieties. During this process, the amine nitrogens are transformed to positively charged species and then to imine nitrogens [245]. The degree of oxidation of polyaniline can therefore be determined by estimating the total imines and positively charged nitrogens in the sample. The oxidation levels of the PANI samples were calculated using the method employed by Kumar *et al*. (1990) [246].

The oxidation level of NR-PANI was lower than that of G-PANI, showing that the synthesis conditions had led to a more reduced polymer in the 'falling pH' synthesis method. The chemical nature of such micro/nanorod forms of PANI is still a matter of some discussion, with various branched and phenazine – type structures having been suggested [91, 237, 238]. NR-PANIdd and G-PANIdd had higher oxidation levels than NR-PANI and G-PANI, respectively. Treatment of NR-PANI and G-PANI with a base increased the –N= concentration and hence elevated their oxidation levels likely due to the influence of atmospheric oxygen during the procedure. This is consistent with other studies where an increase in –N= concentration was observed after treating the PANI samples with base [246, 247]. Overall, the oxidation levels of the PANI samples were in the following order: G-PANIdd > NR-PANIdd > G-PANI > NR-PANI.

2.3.6 Radical scavenging activity

The results for DPPH radical scavenging capacity, a widely used method to provide an estimate of antioxidant activity, are presented in Figure 2.4. The DPPH radical scavenging capacity of the PANI samples was in the following order: NR-PANI > G-PANI ≈ NR-

PANIdd > G-PANIdd. The important finding was that the micro/nanorod NR-PANI sample, while exhibiting a 25 % smaller BET surface area, showed a 16 % higher radical scavenging capacity compared to G-PANI. It can be noted here that NR-PANI was in the lowest oxidation state, and thus had a higher capacity to act as a reducing agent in scavenging DPPH radicals. Likewise treatment with a base increased the oxidation level of both NR-PANI and G-PANI, and this resulted in NR-PANIdd and G-PANIdd having a lower radical scavenging activity compared to the as-prepared samples. The phenazine type units of NR-PANI may have contributed to its higher radical scavenging capacity, and this is a matter of further investigation.

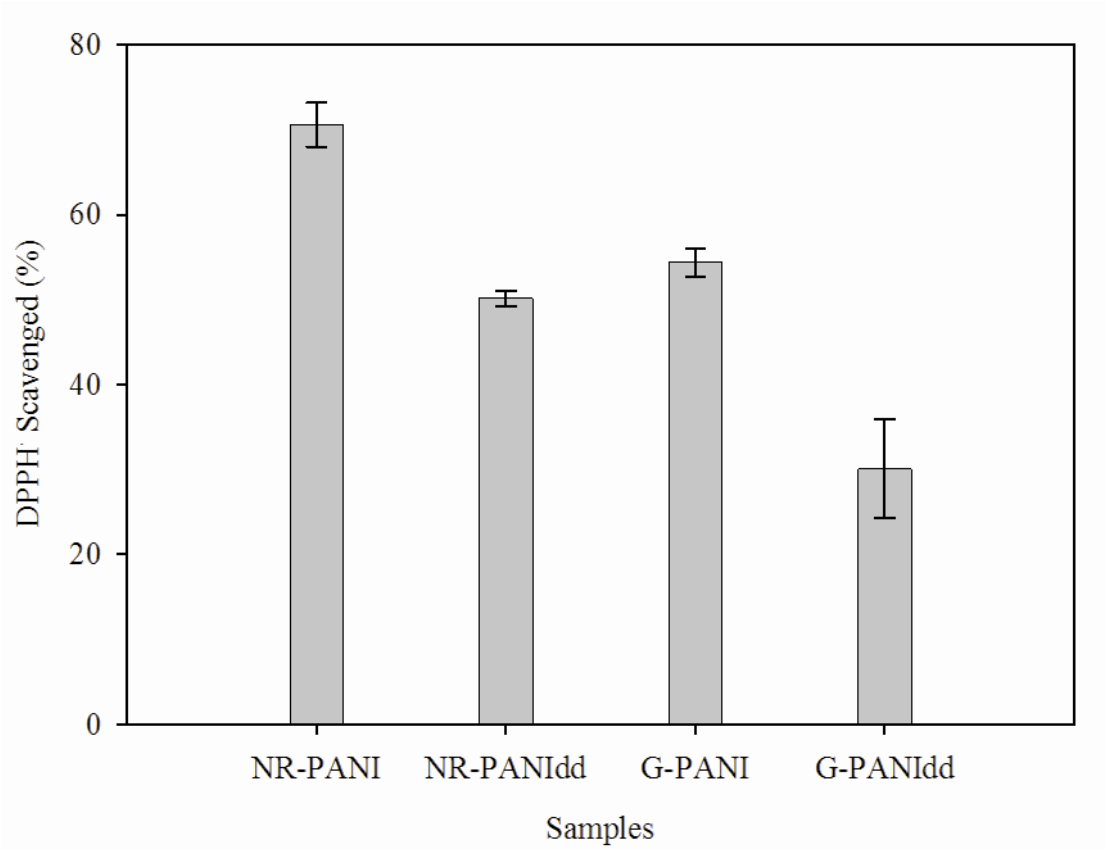

Figure 2.4. DPPH radical scavenging capacity of PANI samples.

The free radical scavenging capacity of PANIs has been shown in other studies to be dependent on the surface area, such that higher surface area samples were said to show better scavenging activity [82, 83, 89]. The radical scavenging activities in these studies were evaluated 15 [83] and 30 minutes [82, 89] after introducing the sample to the DPPH solution. In the present study the radical scavenging activity was evaluated after 24 h of exposure, found to be necessary to fully assess the radical scavenging capacity of conducting polymers [79, 85]. The prolonged time interval employed here allowed the DPPH solution to access the entire polymer sample. It is possible that the initial rate of radical scavenging is surface area related, as observed earlier [82, 83], although in these cases any difference in initial polymer oxidation state also needs to be considered. However, the overall radical scavenging activity will be related primarily to the total redox capacity, given by the amount of conducting polymer, its initial oxidation state, and its chemical nature; such as the unknown influence of phenazine-containing structures in the micro/nanorod interiors.

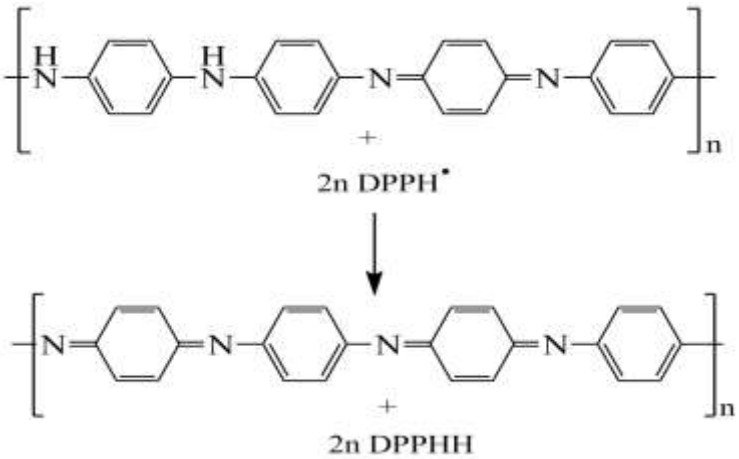

Scheme 2.1. Reaction of DPPH radical with PANI.

As reported earlier, DPPH radicals oxidize the reduced (benzenoid) units of PANI as shown in Scheme 2.1 [84]. This process involves the conversion of the benzenoid units of polyaniline to quinoid and quenching of the DPPH radical. Therefore, PANI samples having a low level of oxidation, characterized by a high proportion of benzenoid units, are able to scavenge more $DPPH^{\bullet}$ and exhibit superior antioxidant activity [85]. This effect held even when the conductivity of the samples was lowered by several orders of magnitude through alkaline dedoping. This further indicates that electroactivity, including the state of oxidation, is the more critical aspect of conducting polymer performance in free radical scavenging tests, rather than high polymer conductivity. NR-PANI had lower conductivity but higher radical scavenging activity than G-PANI. NR-PANIdd and G-PANIdd, being the dedoped non-conducting forms of PANI, also exhibited appreciable antioxidant activity. The chemical nature of NR-PANI, with phenazine type structures, could have also contributed to its higher free radical scavenging capability.

2.4 Conclusions

PANI samples with similar surface areas but varying oxidation levels were synthesized and the radical scavenging activity of the as-prepared and the dedoped samples were evaluated using DPPH assay. Micro/nanorod forms of PANI did not exhibit higher BET surface area values compared to regular PANI, and there was no correlation between the conductivity and the radical scavenging activity. The oxidation level of the samples, arising from the reaction conditions, in decreasing order was G-PANIdd, NR-PANIdd, G-PANI and NR-PANI. The antioxidant activity of the samples was in the reverse order: NR-PANI > G-

PANI ≈ NR-PANIdd > G-PANI. Higher antioxidant activities were observed with lower oxidation level. Hence, obtaining a more reduced conducting polymer, either during the original synthesis or through later treatments, is important to take into account when preparing conducting polymers for antioxidant applications.

CHAPTER THREE

The Effects of Thermal Treatment on the Antioxidant Activity of PANI

This chapter has been published as:

Nand A.V., Ray S., Gizdavic-Nikolaidis M., Travas-Sejdic J., Kilmartin P.A. (2011) The effects of thermal treatment on the antioxidant activity of polyaniline. *Polymer Degradation and Stability* 96: 2159-2166.

Nand A.V., Ray S., Easteal A.J., Gizdavic-Nikolaidis M., Cooney R.P., Travas-Sejdic J., Kilmartin P.A. (2012) Evaluation of polyaniline for packaging applications. *Materials Science and Forum* 700: 236-239.

3.1 Introduction

PANI has received considerable attention as an antioxidant [80, 83, 84, 89 182]. The ability to scavenge free radicals is the motivation for considering the application of PANI as a solid antioxidant material. PANI has been shown to be a proficient scavenger of ABTS and DPPH free radicals [79]. Free radicals are considered to be a prime cause of the deterioration and rancidity of foodstuffs [83]. Therefore, the free radical scavenging properties of PANI, when included within packaging materials, can potentially be utilized for the protection of foodstuffs.

Blending PANI with conventional thermoplastics has the potential to yield novel packaging materials with antioxidant properties. From an industrial point of view, melt processing would be the preferred method of incorporating PANI into thermoplastics [248]. PANI has been melt processed with poly(vinyl chloride) [200, 248] and poly(ethylene terephthalate) [203]. Melt processing involves subjecting PANI to the high processing temperatures of conventional thermoplastics. Therefore, it is important to assess the influence of thermal treatments on the stability and final properties of PANI samples.

The thermal stability of PANI has been investigated previously. Thermogravimetric analysis (TGA) showed that the chemically synthesized polyemeraldine base form of PANI was thermally stable up to 400 °C [249, 250]. Doping with DBSA elevated the degradation temperature of PANI to 450 °C [251]. PANI electropolymerized in HCl degraded above 440 °C [245], while the degradation of chemically synthesized HCl doped PANI started at 250 °C [252]. Phosphoric acid doped PANI also degraded above 250 °C [253]. It has been suggested that PANI undergoes a range of changes upon thermal treatment, including doping,

dedoping, oxidation, chain scission, cross-linking and changes in crystal structure [245, 250, 252, 254-257].

The electroactivity and electrical conductivity of PANI have been reported to be affected by thermal treatments. The electroactivity of HCl doped PANI started to decrease after 70 °C, when heated in air, and showed additional modest deterioration until 150 °C after which it became unstable and conductivity decreased until the polymer became an insulator after treatment above 200 ºC [99]. While the effects of thermal treatment upon the conductivity and electroactivity of PANI have been examined, the influence of thermal treatments on the radical scavenging capacity remains unexplored.

In this study we evaluated, for the first time, the influence of thermal treatment upon the radical scavenging activity of chemically prepared PANI. PANI samples having granular (G-PANI and G-PANIdd) and "nanorod" like (NR-PANI and NR-PANIdd) morphologies were prepared by oxidizing aniline with ammonium persulfate in the presence and absence of HCl, respectively. The free radical scavenging capacity of these samples have been assessed previously and found to be critically dependent upon the oxidation state ahead of BET surface area or conductivity [258]. The samples were thermally treated in air at various temperatures in the range 100 to 300 ºC and were characterized using SEM, electron spin resonance (ESR) and FTIR spectroscopies. The free radical scavenging capacity was evaluated using the DPPH assay.

3.2 Experimental

3.2.1 Materials

Sodium hydroxide, copper (II) sulfate and DPPH were also purchased from Sigma-Aldrich and used as received. The sources of all other chemicals have been listed in section 2.2.1.

3.2.2 Synthesis of the PANIs

Four samples of PANI (NR-PANI, NR-PANIdd, G-PANI and G-PANIdd) were prepared as described in section 2.2.2. An additional sample was prepared using the same conditions and reactants as for NR-PANI but keeping the pH of the reaction mixture constant at 6.5 using a Metrohm titration system consisting of 836 Titrando base, 800 Dosino dosing unit, 804 Ti stand and electrode [106]. The reaction mixture was continuously titrated with a 0.25 M sodium hydroxide solution during the 24 h synthesis period to maintain the reaction pH at 6.5. The product was filtered, washed with water and methanol and dried as was done for NR-PANI.

3.2.3 Thermal treatment

600 mg samples were heated isothermally in air for 30 min at 100, 125, 150, 175, 200 and 250 ºC in a Heraeus convectional oven, and at 300 ºC in a Thermolyne 1400 furnace. A treatment time of 30 min was chosen as major structural changes in PANI have been reported

to occur within 30 min of heat treatment [245]. The thermally treated samples were allowed to cool to room temperature and were then kept in a dessicator until further characterization.

3.2.4 Characterization

The surface morphology of the PANI samples was visualized using a Philips XL30S FEG Scanning Electron Microscope. The samples were coated with platinum using a Polaron SC7640 Sputter Coater for 300 s at 5-10 mA and 1.1 kV.

Infrared spectra of the samples were recorded on a Thermo Electron Nicolet 8700 FTIR spectrometer using a single bounce ATR and a germanium crystal. An average of 64 scans with a resolution of 4 cm^{-1} was taken.

ESR spectra of known masses of sample powders, contained in ESR quartz tubes, were recorded using a JEOL (JES-FA-200) ESR spectrometer operating in the X-band. The spectrum of a known mass of copper (II) sulfate was also recorded under the same conditions as the samples, for the calculation of spin concentrations.

X-ray diffraction (XRD) patterns of the samples were recorded on a Rigaku Geiger – Flex series diffractometer, in the range 5 - 45° (2θ) using a Cu Kα radiation.

The weight loss of the as-prepared samples in air was measured using a Rheometrics STA 1500 Thermogravimetric Analyzer over a temperature range of 25 to 500 °C at a scan rate of 10 °C min^{-1}.

The electrical conductivities of dry pressed pellets of as-prepared and thermally treated NR-PANI and G-PANI samples were measured by the four – probe technique using a Jandel Model RM2 instrument.

3.2.5 Radical scavenging assay

The DPPH radical scavenging capacity of 1.00 ± 0.05 mg samples were evaluated as described in section 2.2.4.

3.3 Results and Discussions

3.3.1 Morphology

The SEM images of the PANI samples, after thermal treatment at 100 °C and 300 ºC are shown in Figure 3.1. The G-PANI and G-PANIdd samples had a granular morphology, typical of PANI synthesized in the presence of a strong acid [116, 161]. By contrast, the NR-PANI and NR-PANIdd samples consisted of a mixture of nanorods and flakes. This morphology, characteristic of PANI synthesized under falling pH conditions, has also been observed [91]. Thermal treatment did not have a pronounced effect on the morphology of the PANI samples. G-PANI and G-PANIdd retained their granular morphology after being thermally treated up to 300 ºC. NR-PANI and NR-PANIdd continued to exhibit the morphology of nanorods alongside flakes after thermal treatment up to 300 ºC. Similar observations have been made in previous studies where the thermal treatment did not affect the nanofibrous [252], nanotubular [120] or globular [132] morphology of chemically synthesized PANI.

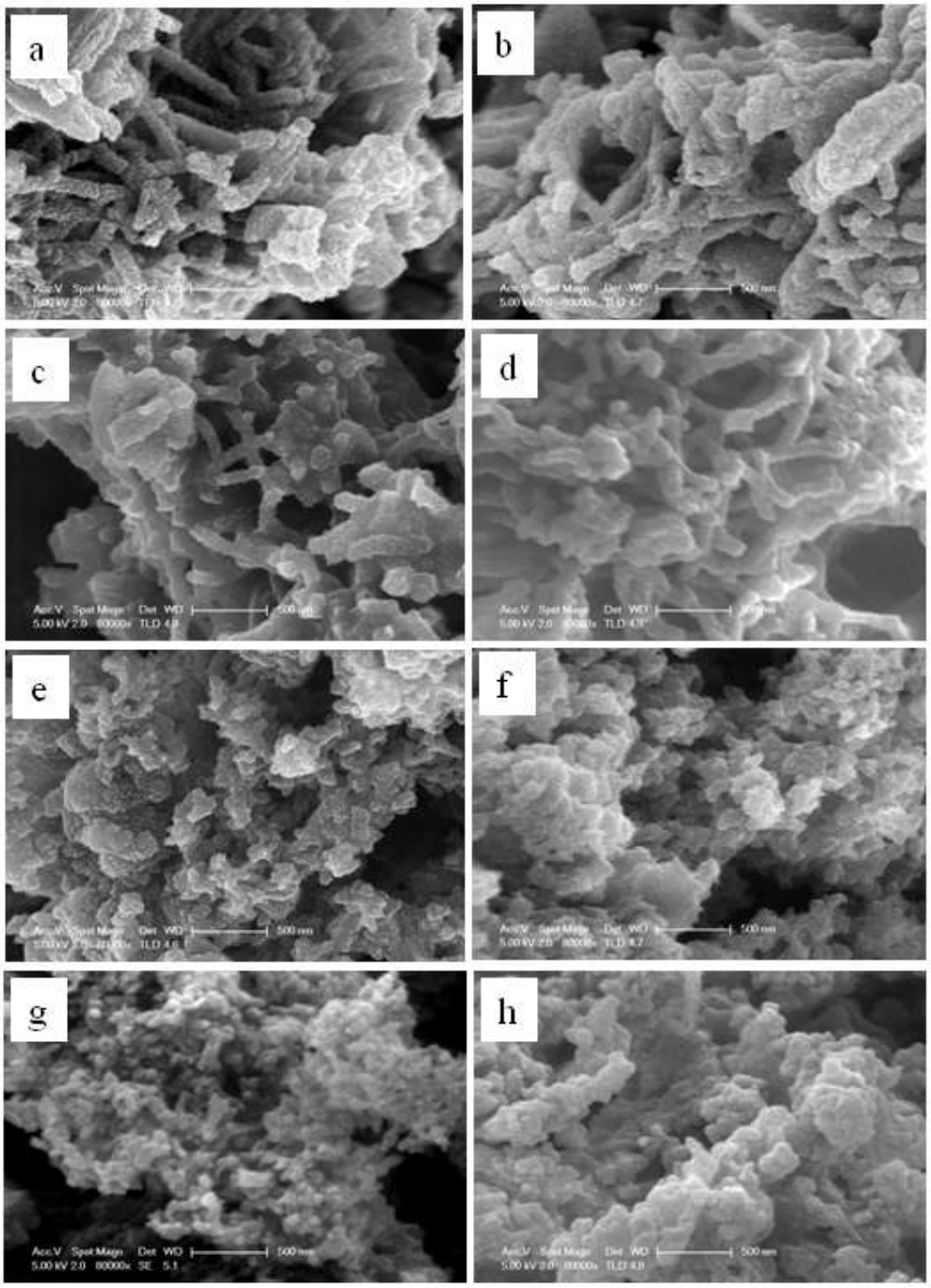

Figure 3.1. SEM micrographs of NR-PANI treated at a) 100 °C and b) 300 °C; NR-PANIdd treated at c) 100 °C and d) 300 °C; G-PANI treated at e) 100 °C and f) 300 °C; G-PANIdd treated at g) 100 °C and h) 300 °C.

3.3.2 Thermal stability

The thermo gravimetric analysis (TGA) plots of the as-prepared PANI samples are presented in Figure 3.2. All the samples exhibited a three – step weight loss behaviour. A three – step weight loss of PANI has been previously described by Palaniappan and Narayana (1994), in which the first and second steps were in the 20 – 110 ºC and 110 – 250 ºC ranges, respectively, while the third step started at 250 ºC [253]. The weight losses of all as-prepared PANI samples in various temperature ranges are summarized in Table 3.1.

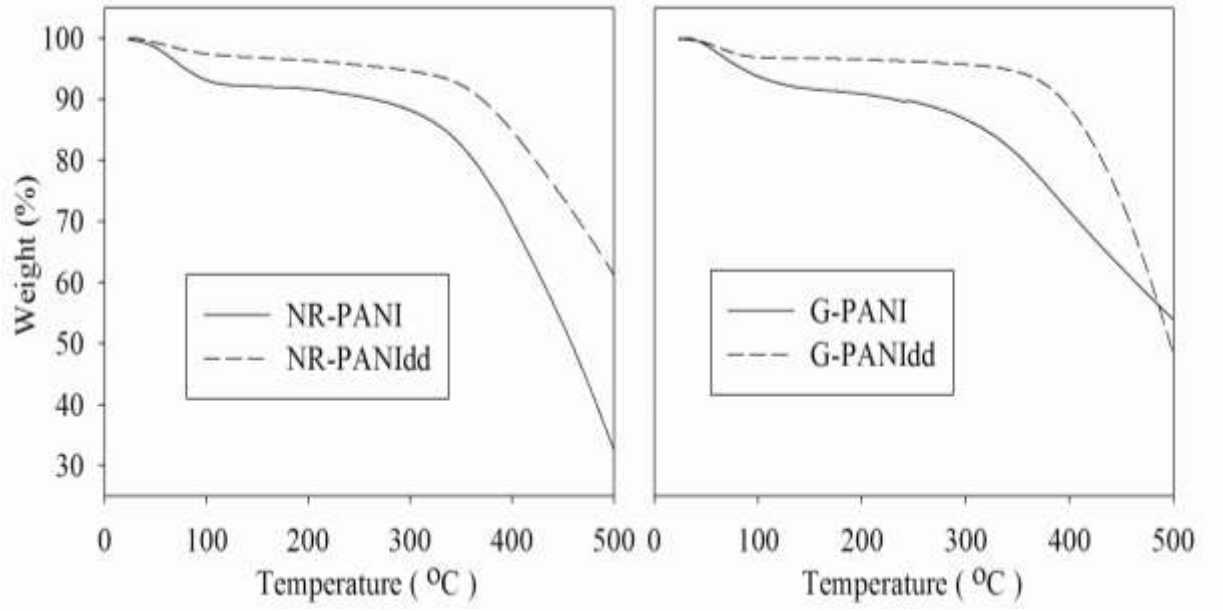

Figure 3.2. TGA curves of NR-PANI, NR-PANIdd, G-PANI and G-PANIdd.

Table 3.1. Results of thermogravimetric analysis of the as-prepared PANI samples.

Sample	Initial temperature (T_I), °C	Intermediate temperature (T_F), °C	Weight loss between T_I and T_F (%)	Total weight loss (%)
NR-PANI	25	120	7.8	
	120	300	3.7	
	300	500	54.8	66.3
NR-PANIdd	25	120	2.7	
	120	340	3.9	
	340	500	31.7	38.3
G-PANI	25	120	7.3	
	120	250	3.4	
	250	500	34.9	45.6
G-PANIdd	25	100	3.1	
	100	350	2.3	
	350	500	45.1	50.5

The first weight loss in all samples can be attributed to the loss of occluded moisture [245, 252, 253, 257], out gassing of small molecules [254] and removal of dopants. The first weight losses of NR-PANI and G-PANI, 7.8 and 7.3 % respectively, were relatively higher than the first weight losses of NR-PANIdd and G-PANIdd, 2.7 and 3.1 % respectively. The loss of dopants from NR-PANI and G-PANI could have contributed to their higher weight

losses as NR-PANIdd and G-PANIdd, being the dedoped forms, were deficient in dopants. The modest second weight loss in all samples could be due to chemical changes including cross-linking [195, 259] and oxidation [245] by means of deprotonation of the polymer chains. The third weight loss in all samples was of much higher magnitude compared to the first and second weight losses. This weight loss is attributed to significant degradation of polymer backbone [195, 245, 252, 254, 257]. Conklin *et al*. (1995) have defined degradation as ≥ 10 % weight loss excluding the contribution from moisture [260]. Therefore, it can be inferred from the TGA results that NR-PANI, NR-PANIdd, G-PANI and G-PANIdd are thermally stable, to the point of commencement of the third weight loss, up to 300, 340, 250 and 350 °C respectively. NR-PANI and G-PANI had a lower thermal stability compared to their dedoped forms. It has been previously reported that in HCl doped PANI, dedoping predominates other changes at 250 ºC, resulting in the loss of bound water and bound HCl [245]. While G-PANI was synthesized in presence of HCl, the protons released from the persulfate oxidant would have created an acidified environment for NR-PANI [259]. It is likely that NR-PANI and G-PANI begin to lose their bound acids from deep inside the bulk of the polymer clusters at 300 and 250 ºC respectively [245], followed by degradation of the polymer chains at higher temperatures. Therefore, the third weight loss for NR-PANI and G-PANI was observed at lower temperatures compared to NR-PANIdd and G-PANIdd.

The degradation kinetics of the PANIs were investigated over the temperature range 300 – 500 ºC for NR-PANI and 250 – 500 ºC for G-PANI. The plot of natural log of percentage weight loss versus temperature, given in Figure 3.3, were nearly a straight line for both the samples suggesting the degradation followed first order kinetics. The degradation

kinetics of thermal degradation of polyemeraldine base has been previously reported to be first order [195].

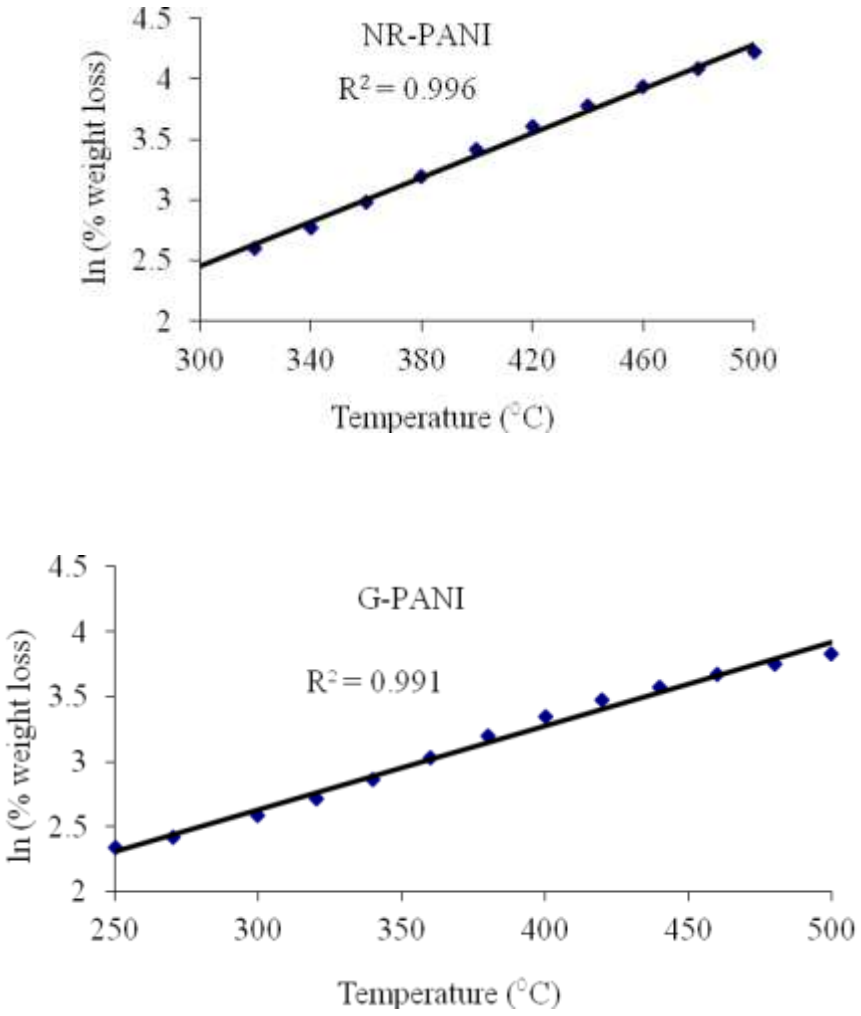

Figure 3.3. Plots of ln(% weight loss) as a function of temperature for NR-PANI and G-PANI.

3.3.3 Spectroscopy

The FTIR spectra of the as-prepared and thermally treated PANI samples are presented in Figure 3.4. All the as-prepared samples showed characteristic peaks at about 1585 cm^{-1} (C=C stretching mode of the quinoid rings), 1500 cm^{-1} (C=C stretching mode of benzenoid rings), 1310 cm^{-1} and 1250 cm^{-1} (C–N stretching mode), confirming the partially-oxidized, emeraldine state, of PANI. The vibrational bands at about 1155 and 830 cm^{-1} are assigned to the aromatic ring in–plane and out–of–plane C–H bending [87, 138]. NR-PANI and NR-PANIdd showed additional peaks at about 1040, 1413 and 1447 cm^{-1}. These are characteristic peaks of aniline oxidation products formed under falling pH conditions. While the peak at 1040 cm^{-1} can be assigned to sulfonate groups attached to the benzene rings [239] along with some bisulfate included as counterions [173], the peaks at about 1413 and 1447 cm^{-1} are considered to be due to phenazine and branched aniline oligomeric structures formed in a falling pH environment [238]. Various aniline oxidation products can be expected at neutral pH, including the formation of flakes and compounds with phenazine-type structures, with nanorods appearing as the pH lowers to 3 – 4. During the final synthesis stage at lower pH values, a coating of regular PANI is expected on the nanostructures that have already formed [106].

The absorbance intensities of all of the FTIR bands were remarkably suppressed upon thermal treatment above 200 ºC. Moreover, the vibrational bands between 1400 cm^{-1} and 1200 cm^{-1} coalesced together to give a broad band after treatment above 200 ºC. However, the bands at about 1585 and 1500 cm^{-1} were still prominent in the IR absorption of all

samples after thermal treatment. The absorbance peak intensity ratios of these two peaks (*Q/B*), quinoid

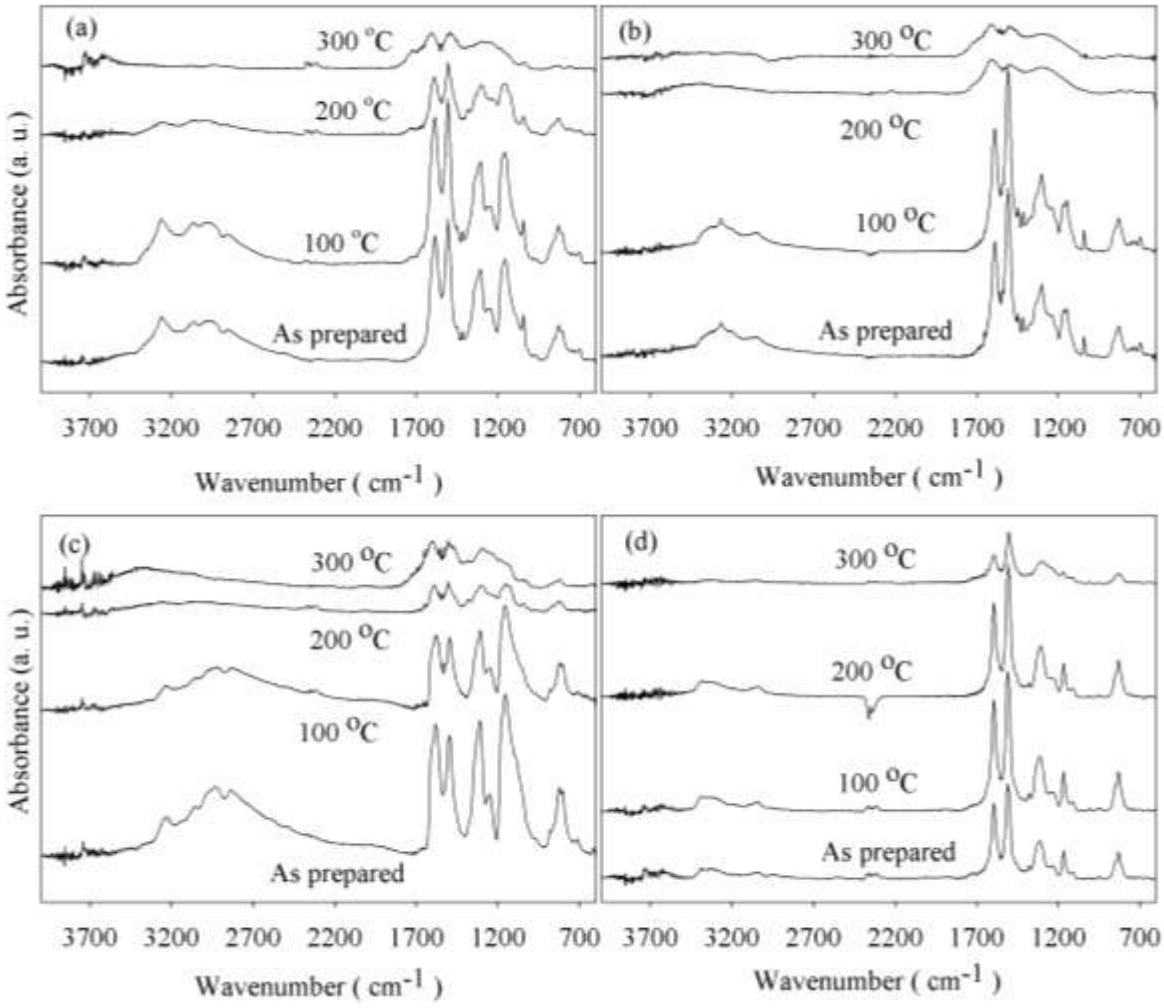

Figure 3.4. FTIR spectra of as-prepared and thermally – treated samples of a) NR-PANI, b) NR-PANIdd, c) G-PANI and d) G-PANIdd.

(*Q*) to benzenoid peak (*B*), has been successfully utilized to evaluate the chemical changes in a PANI sample upon thermal treatment [245]. The *Q/B* ratios of all samples after treatment at

various temperatures are given in Table 3.2. The magnitude of changes in the *Q/B* ratios obtained in the present study was comparable to a previous study [245]. Acid doped PANI samples are known to contain NH_2^+ groups resulting from the protonation of NH groups [261]. The quinoid absorption region is also characteristic of the NH_2^+ deformation of secondary amines and their salts [262]. The 1585 cm^{-1} peak of NR-PANI and G-PANI exhibit a shoulder on the higher wavenumber side which could be attributed to the NH_2^+ deformations. These shoulders were absent in the spectra of the dedoped samples. Therefore, adhering to a previous study [245], the *Q/B* ratios were used to probe chemical changes due to thermal treatment within the same sample rather than to compare different samples. The oxidation levels of the four as-prepared samples are reported in chapter 2 [259].

NR-PANI and NR-PANIdd showed a decrease in the *Q/B* ratio upon thermal treatment up to 175 ºC and an increase after that. G-PANI and G-PANIdd also showed a similar trend with the ratios increasing after thermal treatment above 200 ºC. A decrease in the *Q/B* ratio can indicate conversion of quinoid rings to benzenoid rings. However, the change in *Q/B* ratio can also be attributed to a cross-linking reaction occurring during thermal treatment. It is envisioned that cross-linking is established through a link of the imine nitrogen with its neighbouring quinoid ring, as suggested in earlier studies [128, 263] and shown in Scheme 3.1. The cross-linking reaction produces cyclized phenazine-like segments containing ternary nitrogen. However, no specific peaks in the FTIR spectra of the thermally-treated samples could be assigned to the tetra-substituted phenyl groups or the tertiary amines of the cross-linked polymer, as also reported by Mathew *et al.* (2002) [255]. Since the quinoid units were utilized in the cross-linking of the polymer chains, a decrease in the *Q/B*

ratio was observed. The later increase in *Q/B* ratios denotes conversion of some benzenoid to quinoid rings, an oxidation reaction, although some further processes may occur to create chemical structures that absorb in the 1550 to 1600 cm^{-1} range. The oxidation reaction, as proposed in an earlier study [245], occurs through the release of electrons and formation of nitrogen cation radicals followed by stepwise release of protons, electrons and further protons. The intrinsic chemical changes, cross-linking and oxidation, are followed by further polymer degradation at higher temperatures, as evidenced by the TGA results. The broad band above 2000 cm^{-1}, prominent in NR-PANI and G-PANI, is the characteristic of conducting form of PANI. The decrease in the intensity of this band after treatment above 200 ºC maybe attributed to the loss in conductivity [127, 245].

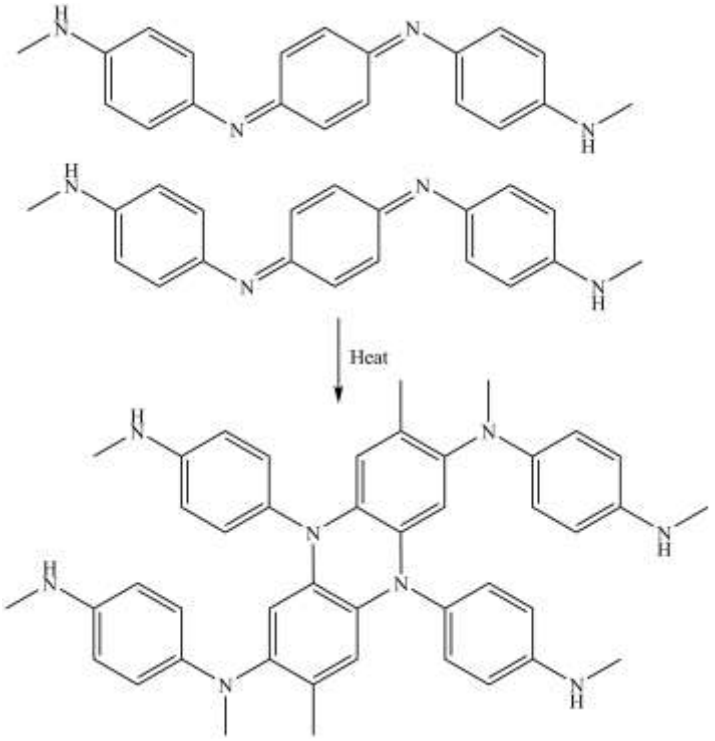

Scheme 3.1. Cross-linking scheme for PANI upon heating, adapted from [255, 263].

Table 3.2. *Q/B* ratios and spin concentrations of as - prepared and thermally – treated PANI samples.

Thermal treatment temperature (°C)	NR-PANI		NR-PANIdd		G-PANI		G-PANIdd	
	Q/B	[Spin] (x 10^{19} spins g^{-1})	*Q/B*	[Spin] (x 10^{19} spins g^{-1})	*Q/B*	[Spin] (x 10^{19} spins g^{-1})	*Q/B*	[Spin] (x 10^{19} spins g^{-1})
As-prepared	0.95	3.53	0.70	2.59	1.14	12.2	0.79	0.42
100	0.91	3.93	0.67	2.65	1.12	13.0	0.79	0.38
125	0.89	4.05	0.66	2.71	1.10	16.5	0.78	0.38
150	0.86	6.06	0.63	2.72	1.05	18.3	0.77	0.41
175	0.87	7.70	0.62	2.66	1.00	20.6	0.73	0.48
200	0.90	7.52	1.10	1.13	0.95	14.6	0.65	0.75
250	0.98	2.47	1.18	1.11	0.98	6.80	0.68	1.92
300	1.04	1.21	1.19	0.86	1.01	3.90	0.69	1.03

ESR spectroscopy was also employed to study the changes in PANI polaron content upon thermal treatment. A representative set of spectra of as-prepared and thermally-treated G-PANI is given in Figure 3.5. All of the as-prepared and thermally-treated samples showed a single signal with g values in the range 2.0033 to 2.0038 compared to the free electron g value of 2.0023. This indicates the presence of the radical on or near the nitrogen atom. A g value shift of at least 10^{-3} occurs when the radical is localized on or near a heteroatom [104, 253]. The g values were temperature–independent, as observed for PANI salts by Palaniappan and Narayana [253].

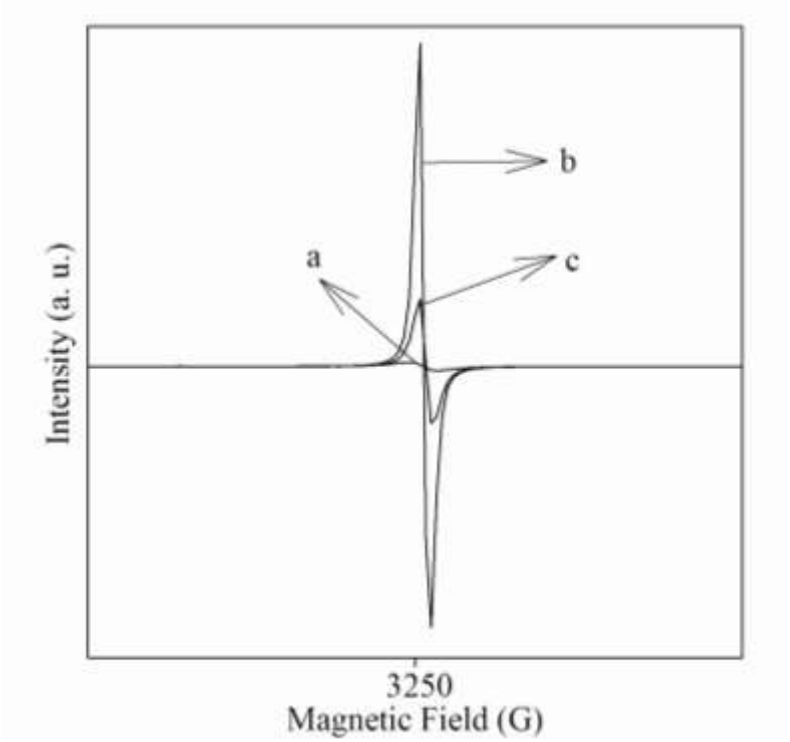

Figure 3.5. ESR spectra of G-PANI: a) as – prepared, b) treated at 175 °C, and c) treated at 300 °C.

The spin concentrations of the samples were obtained from the integrated ESR signals using Equation 3.1, and are recorded in Table 3.2.

$$N_{sample} = \frac{I_{sample}}{I_{CuSO_4}} \times \frac{\left(n_{CuSO_4} \times N_A\right)}{m_{sample}} \qquad \text{(Eq. 3.1)}$$

where N_{sample} is the spin concentration of the sample (spins g^{-1}), n_{CuSO_4} is the moles of copper sulfate, N_A is the Avogadro constant, I_{sample} and I_{CuSO_4} are the areas under the integrated ESR signals of the sample and copper sulfate respectively, and m_{sample} is the mass of the PANI sample (g). NR-PANI, NR-PANIdd, G-PANI as well as G-PANIdd initially showed thermally activated paramagentism, that is, an increase in spin concentration, upon thermal treatment. However, after treatment above a certain temperature; 175 ºC for NR-PANI and G-PANI, 150 ºC for NR-PANIdd and 250 ºC for G-PANIdd, a Curie – Weiss type paramagnetism, that is a decrease in spin concentration, was observed. This behaviour with PANI has also been observed in a previous study [253].

The initial increase in spin concentration upon thermal treatment of the PANIs may be due to bipolarons being thermally excited to two neighbouring paramagnetic polarons [264] resulting in an increase in spin concentration. Upon thermal treatment at the higher temperatures indicated above, a dedoping process occurs where the polarons are destroyed by a deprotonation reaction. This involves conversion of some benzenoid units to quinoid through pairing of polarons to form bipolarons [245], resulting in a decrease in spin concentration. This is also evidenced by *Q/B* ratios from FTIR spectra of the samples. The decrease in spin concentration upon thermal treatment in PANI has also been attributed to oxygen reacting with the paragmagnetic centres [257]. Overall the spectroscopy results reveal that PANIs undergo cross-linking and oxidation reactions, along with doping and dedoping upon thermal treatment.

3.3.4 XRD

The XRD patterns of as prepared and thermally treated NR-PANI and G-PANI are given in Figure 3.6. NR-PANI exhibited crystalline peaks at about 2θ = 6.5°, 19° and 26°. The peak about 2θ = 6.5° is characteristic of an interlayer repeat distance of spacers between parallel planes of stacked PANI backbone [204]. The intensity of all peaks decreased as the treatment temperature increased with the peak about 6.5º disappearing above 200 ℃ and the peaks about 19° and 26° merging to give a broad reflection. The diffraction pattern of as – prepared NR-PANIdd was similar to NR-PANI, with the broad reflection appearing after treatment above 175 ºC. G-PANI showed crystalline peaks at about 2θ = 15º, 20º and 25º, typical of HCl doped PANI [265]. The peaks disappeared above 200 ºC and resulted in a broad reflection about 2θ = 22º. The broad reflection, more commonly known as the 'halo' is characteristic of amorphous PANI [266]. The as – prepared G-PANIdd was amorphous, with the 'halo' appearing at around 20°; the loss of crystallinity was probably due to removal of counter ions leading to chain rearrangement during the dedoping process. G-PANIdd continued to display amorphous character after thermal treatment.

However, these results confirm that a PANI losses its crystallinity after treatment at high temperatures. This could be due to chemical processes such as chemical crosslinking during the thermal treatment process. A three-dimensional chemical structure, resulting from crosslinking, is known to decrease the crystallinity and apparently increase the amorphous state of PANI [267].

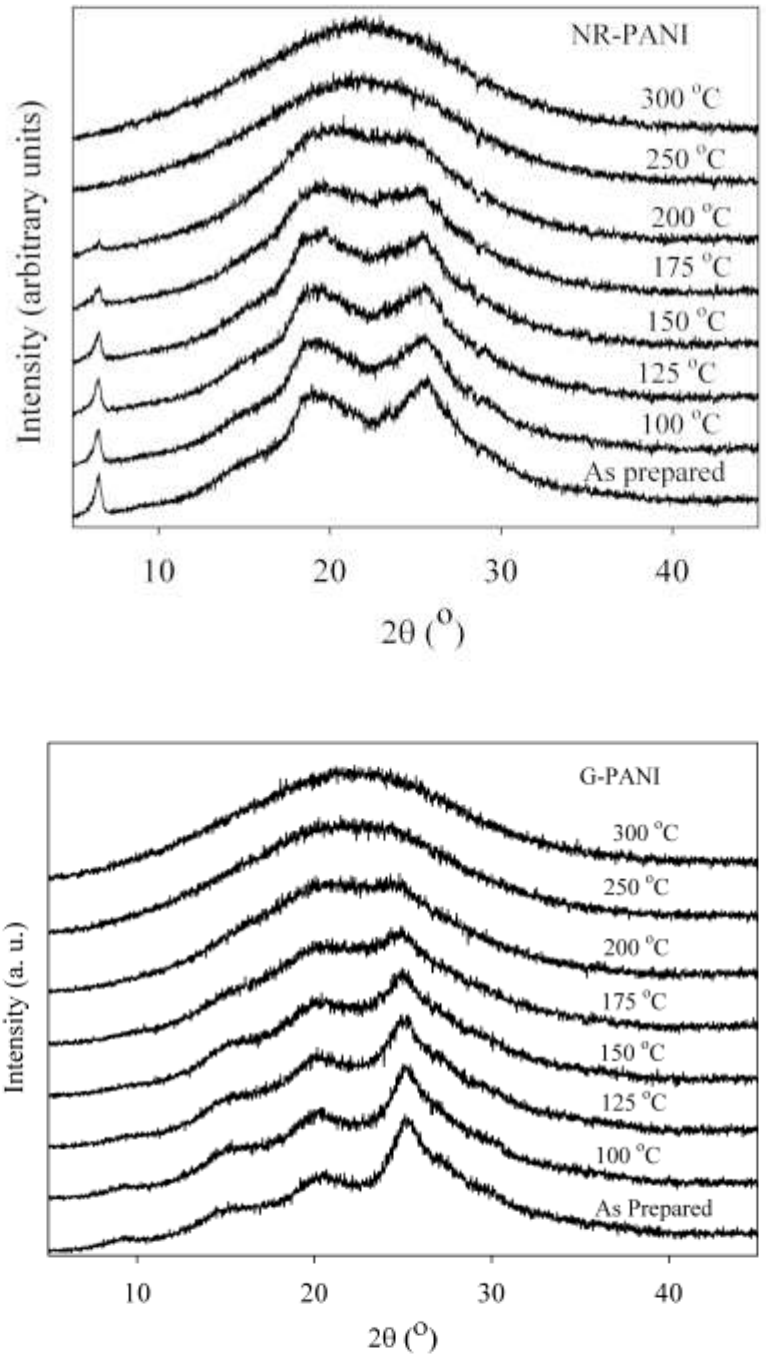

Figure 3.6. XRD patterns of as – prepared and thermally – treated NR-PANI and G-PANI.

3.3.5 Conductivity

The electrical conductivities of as prepared and thermally treated NR-PANI and G-PANI samples are given in Table 3.3. The as prepared G-PANI, synthesized a low pH, had a higher conductivity than NR-PANI. Upon thermal treatment, the conductivity of both samples initially increased slightly up to 100 ºC then decreased as the treatment temperature increased. The slight initial increase can be attributed to the loss of moisture [268]. More ordered crystalline PANI is known to exhibit higher conductivity [269]. As seen in the XRD patterns, thermal treatment decreased the crystallinity of both NR-PANI and G-PANI samples. In addition to the loss of dopant due to thermal treatment, the irregularity in polymer chain arrangement could have contributed to the observed decrease in conductivity. The conductivity of samples treated at 250 and 300 ºC could not be determined as the samples could not be pelletized, a setback also encountered by Palaniappan (1997) [270].

3.3.6 Free radical scavenging capacity

The free radical scavenging capacities of the as-prepared and thermally-treated polyanilines are presented in Figure 3.7. The as-prepared NR-PANI exhibited a higher free radical scavenging capacity (70.6 %) than the as-prepared G-PANI (54.4 %), which has been associated with the more reduced state of the as-prepared nanorod samples [258]. The radical scavenging capacity of both the PANIs decreased after proton dedoping with NR-PANIdd and G-PANIdd exhibiting a 51.9 % and 31.8 % radical scavenging capacity, respectively.

Table 3.3. Conductivity of NR-PANI and G-PANI.

Treatment Temp. (ºC)	Conductivity (S cm^{-1})	
	NR-PANI	G-PANI
As Prepared	2.33×10^{-3}	5.20×10^{-1}
100	7.46×10^{-3}	1.08×10^{0}
125	4.25×10^{-3}	3.60×10^{-1}
150	9.73×10^{-4}	1.20×10^{-1}
175	9.49×10^{-5}	6.38×10^{-3}
200	2.99×10^{-6}	5.22×10^{-7}
250	NM	NM
300	NM	NM

NM – not measured.

This decrease in radical scavenging capacity has been attributed to an incidental increase in the oxidation level of NR-PANI and G-PANI upon treatment with a base [258].

To further examine the contribution of the inner aniline oxidation products formed initially under the higher pH conditions that led to the formation of the NR-PANI sample, a further sample, rich in phenazine type units [106], was prepared at a static pH of 6.5. It is expected that the NR-PANI sample, prepared under falling pH, would have an interior like the sample prepared at pH 6.5, only coated with regular PANI. The DPPH radical scavenging capacity of the pH 6.5 sample was 66.3 %, which can be compared to the 70.6 % radical scavenging capacity of NR-PANI on a mass basis. This result indicates that the aniline

oxidation products formed at higher pH can contribute positively to the radical scavenging activity of the falling-pH nanorod samples.

NR-PANI and NR-PANIdd exhibited a trivial decrease in $DPPH^{\bullet}$ scavenging capacity upon thermal treatment up to 175 ºC. After thermal treatment above 175 ºC, a rapid decrease in radical scavenging capacity was seen. A similar trend was observed for G-PANI and G-PANIdd, however, the rapid decrease in free radical scavenging capacities in these samples were seen a little later after thermal treatment above 200 ºC. At low temperatures NR-PANI exhibited higher free radical scavenging capacity than G-PANI but the opposite was observed above 175 ºC. However, after treatment at 300 ºC both NR-PANI and G-PANI showed comparatively similar free radical scavenging activities.

The interaction of DPPH radicals with PANI results in neutralization of the DPPH radicals through the oxidation of benzenoid units of PANI as shown previously Scheme 2.1. This process involves the conversion of benzenoid units of PANI to quinoid through the loss of hydrogen from the amine nitrogens [84]. The thermal treatment of NR-PANI and NR-PANIdd up to 175 ºC results in partial cross-linking of the polymer chains as evidenced by the Q/B ratios in FTIR spectroscopy. The resulting cyclized phenazine–like units containing ternary nitrogen of the cross-linked PANI chains, may still participate in the DPPH radical scavenging through oxidation of the organic structures that are produced. Moreover, the small decrease in the radical scavenging activity after treatment up to 175 ºC shows that oxidation of some benzonoid units of the PANI may also have occurred alongside the cross-linking reaction. Upon thermal treatment above 175 to 200 ºC, the PANI polymer chains for each of the samples undergo oxidation reactions, as indicated by the Q/B ratios, and

degradation on further heating, as shown by TGA results. The oxidized and degraded units of PANI, comprising mainly quinoid units, will have a lower tendency to neutralize DPPH radicals [79]. Therefore, a decline in free radical scavenging capacity was observed after treatment at temperatures above 175 ºC.

The spin concentrations of the samples increased when the polymer samples showed an initial decrease in radical scavenging capacity up to 175 ºC. It has been previously shown that radical scavenging activity is not related primarily to PANI conductivity [258], and an associated high number of polaron charge carriers. However, upon thermal treatment at higher temperatures the spin concentrations decreased as did the radical scavenging capacity of the polyanilines.

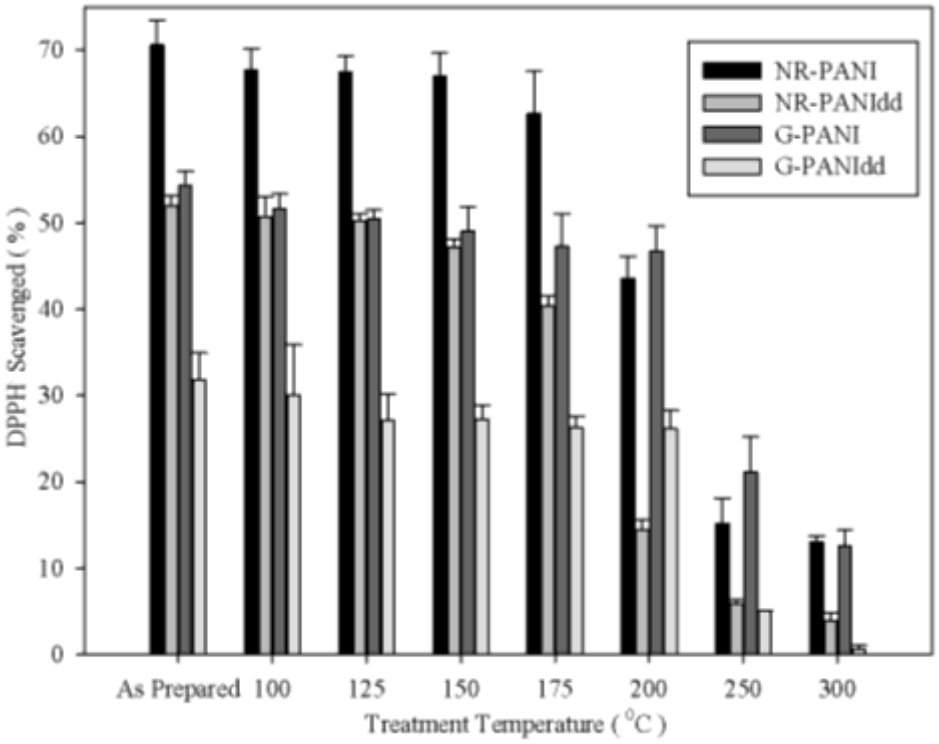

Figure 3.7. DPPH radical scavenging capacity of the PANIs.

3.4 Conclusions

The as-prepared NR-PANI, NR-PANIdd, G-PANI and G-PANIdd were thermally stable up to 300, 340, 250 and 350 °C respectively. No major morphological changes for the granular (G) and the nanorod (NR) PANI samples were evident upon thermal treatment up to 300 ºC. The free radical scavenging capacity of the as-prepared and thermally treated PANI samples synthesized in different chemical environments was evaluated using the DPPH assay. NR-PANI and NR-PANIdd showed a slight decrease in free radical scavenging capacity upon thermal treatment up to 175 ºC and a rapid decrease after treatment at higher temperatures. G-PANI and G-PANIdd also exhibited a slight decrease in free radical scavenging capacity upon thermal treatment up to 200 ºC and a rapid decrease thereafter. The rapid decrease in the free radical scavenging capacity is attributed to the oxidation of the polymer samples as evidenced by FTIR spectroscopy, but was not related to the spin concentration obtained by ESR. Hence, the nanorod PANI can be thermally processed up to 175 ºC, and the granular PANI to 200 ºC for antioxidant applications with little loss of radical scavenging activity. Reduced antioxidant activity can be expected if the PANIs are processed at temperatures higher than these.

CHAPTER FOUR

Characterization of PET/ PANI Composites as Potential Antioxidant Materials

This chapter has been published as:

Nand A.V., Ray S., Travas-Sejdic J., Kilmartin P.A. (2012) Characterization of polyethylene terephthalate/ polyaniline blends as potential antioxidant materials. *Materials Chemistry and Physics* 134: 443-450.

4.1 Introduction

PET, a semi-crystalline thermoplastic polyester, is widely used because of its low cost and good mechanical properties [271]. Apart from its application as a substrate for flexible electronics, optical components and micro-sensors [272, 273], PET has created a niche in the food packaging industry in bottles that contain soft drinks [274]. Efforts are being made to improve the properties of PET in order to augment its packaging applications. Blending with other materials is one route to compensate for the deficiencies, or to enhance the existing properties of PET. PET has been blended with ethylene-vinyl alcohol copolymer [275], a liquid crystalline polyester [276] and aromatic polyamides [271], in order to improve gas barrier properties.

Blending PANI with PET has the potential to yield novel antioxidant packaging materials. PET/ PANI composites have been prepared by the *in situ* polymerization of absorbed aniline within PET fibres [221]. On the other hand, thermomechanical processing is the preferred method for blending polymers in the polymer industry [277] but the infusibility of PANI limits its thermomechanical processing [118]. Alternatively, polyaniline has been successfully dispersed in a melt of processable polymers [207]. Mitzakoff and Paoli (1999) endeavoured to produce conducting PET/ polyaniline blends for large scale utilization but the product was a hard and brittle material due to the hydrolysis of PET ester bonds induced by the acid dopants of polyaniline [203].

PANI synthesized via the falling pH method (NR-PANI) creates nanorods, and has demonstrated a high free radical scavenging capacity [258]. It has also shown adequate thermal stability, characterized by less than 10 % weight loss other than losses due to

moisture, up to 300 ºC [278]. In the present work, NR-PANI was blended with PET through thermomechanical processing at 265 ºC. The composites have been characterized using optical microscopy, FTIR, XPS, differential scanning calorimetry (DSC) and dynamic thermomechanical analysis (DMTA). The static mechanical properties, conductivity and the free radical scavenging capacity of the composites, using the DPPH assay, have also been examined.

4.2 Experimental

4.2.1 Materials

PET resin (intrinsic viscosity = 0.82 ± 0.02 dL g^{-1}) was kindly provided by Frucor Beverages (NZ) Limited. Details of other chemicals are given in section 2.2.1.

4.2.2 Synthesis of NR-PANI

NR-PANI, consisting of micro/ nanorods and flake-like structures, was synthesized by the falling pH method as described in section 2.2.2. The dried NR-PANI was ground to a fine powder; sieved using a 106 µm sieve and particle size analysis was carried out by means of laser diffractometry using a Malvern Mastersizer 2000 instrument. The NR-PANI powder was kept in an air – tight container for further use.

4.2.3 Preparation of NR-PANI/ PET composites

Melt blending of PET and NR-PANI, with 1% (PETPA1), 2% (PETPA2) and 3% (PETPA3) loading of NR-PANI, was undertaken using a Prism TSE16 twin screw extruder with a L/D ratio of 12.5. PET pellets were dried in a Moreto dehumidification dryer at 135 ºC overnight and NR-PANI was dried overnight at 60 ºC in a vacuum oven prior to blending. PET and NR-PANI were manually mixed and quickly fed into the extruder operating at 265 ºC with a screw speed of 10 rpm. The molten composites were extruded through a 2 mm die as a rod, quenched in water and pelletized. A PET sample without any NR-PANI was also extruded as described above. The extruded pellets were dried at 60 ºC in a vacuum oven for 24 h and compression moulded between teflon sheets at 265 ºC to obtain 0.20 ± 0.02 mm thick films. The pellets were heated in the press for 4 min with repeated application and release of pressure to remove air bubbles, and kept at 2.5 kPa for an additional 4 min. The films were cooled in a flow of air immediately after removal from the hot press and stored in air tight containers until further characterization. The film thickness was measured using a Mitutoyo Absolute 500 series digital calliper. Composites with more than 3% NR-PANI content had poor mechanical strength and could not be processed.

4.2.4 Characterization

XPS data of the film samples were collected on a Kratos Axis UltraDLD instrument equipped with a hemispherical electron energy analyser. Samples were mounted on standard VG sample studs by means of double sided carbon tapes. The spectra were taken using monochromatic Al Kα X-rays (1486.69 eV) with the X-ray source operating at 150 W. The

analysis area was a 300 by 700 µm spot. The core level scans were collected with 20 eV pass energy. The analysis chamber was at a pressure in the 10^{-9} torr range throughout the data collection. Data analysis was performed using CasaXPS. Core level data were fitted using Gaussian-Lorentzian peaks with a Shirley background. The binding energy scale was corrected for the neutraliser shift using the C 1s signal from saturated hydrocarbon at 284.6 eV.

The infrared spectra of the films were recorded using a Thermo Electron Nicolet 8700 Fourier transform infrared spectrometer using a single bounce ATR and a germanium crystal. An average of 64 scans with a 4 cm^{-1} resolution was taken. The film samples were also examined using the Nicolet Continuµm FTIR microscope equipped with a digital camera for image acquisition.

DSC studies were performed on the film samples, contained in aluminium pans, using a TA Instruments Q1000 DSC from 25 to 300 ºC at a 10 ºC min^{-1} heating rate in a nitrogen atmosphere.

Dynamic mechanical properties were measured using a Rheometric Scientific DMTA IV working in the tensile mode. Storage modulus (*E*'), loss modulus (*E*'') and loss tangent (tan δ) of each sample were determined at 1.5 Hz from 25 to 100 ºC at a heating rate of 3 ºC min^{-1} under a liquid nitrogen flow. The test specimens were presented as rectangular strips measuring 12 x 20 x 0.2 mm^3 (width x length x thickness).

The melt flow index (MFI) of PET and the composite samples was determined using a Dynisco Polymer Test melt indexer according to ASTM D 1238. The sample pellets were

forced through a capillary, after melting at 253 ºC for 3 min, by application of a 2.16 kg weight.

The static mechanical properties of the samples were determined at ambient temperature, using an Instron 5567 universal testing machine equipped with a video extensometer. The measurements were undertaken in accordance with ASTM D822-02. The stress-strain curves of rectangular test specimens measuring 7 x 80 x 0.2 mm^3 (width x length x thickness) were measured at a constant crosshead speed of 5 mm min^{-1} and a 1000 N load cell. The distance between the sample grips was 50 mm. The modulus of elasticity, tensile strength and elongation at break were determined from at least six measurements of each sample.

The technique of measuring the conductivity between two electrodes (DIN-53596) was employed to determine the electrical conductivity of PET and the composite films. All measurements were undertaken at ambient temperature using a Keithley 6517A electrometer.

4.2.5 Radical scavenging assay

An adaptation of the DPPH assay for use with polymeric samples [79, 80] was applied for the assessment of PET and the composite samples. 20 (1 x 1 cm^2) film pieces were added to 20 mL of a 55 µM methanolic DPPH solution. The samples were left to react at room temperature for 24 h, after which the absorbance of the supernatant at 516 nm was measured using a Shimadzu UV-1700 UV-visible spectrophotometer. Three trials of each sample were undertaken. A control experiment, without any test sample, was also set up. The

amount of $DPPH^{\bullet}$ which reacted over a 24 h period was then calculated after subtracting away the background loss of a $DPPH^{\bullet}$ solution without added test sample.

4.3 Results and Discussions

4.3.1 Microscopy

The optical micrographs of PET, PET/ NR-PANI composite films and pure NR-PANI are presented in Figure 4.1. The PET film was transparent with no traces of additional components. An even distribution of NR-PANI particles in the PET matrix was observed, indicated by the 'dark spots' in the micrographs. NR-PANI was previously confirmed in section 2.3.1, to consist of micro and nanorods along with flake-like morphologies, within PANI aggregates. The NR-PANI aggregates were measured to be an average of 17 μm with particles as large as 85 μm. Similar sized NR-PANI particles were present in the composite films, indicating that the NR-PANI particles did not form larger aggregates upon dispersing in PET, but rather produced an appreciable dispersion. The particle size distribution of NR-PANI in the composites, processed using the ImageJ software, is shown in Figure 4.2. The density of NR-PANI 'dark spots' in the composite films increased in the order PETPA3 > PETPA2 > PETPA1, in accordance with the composite formulations.

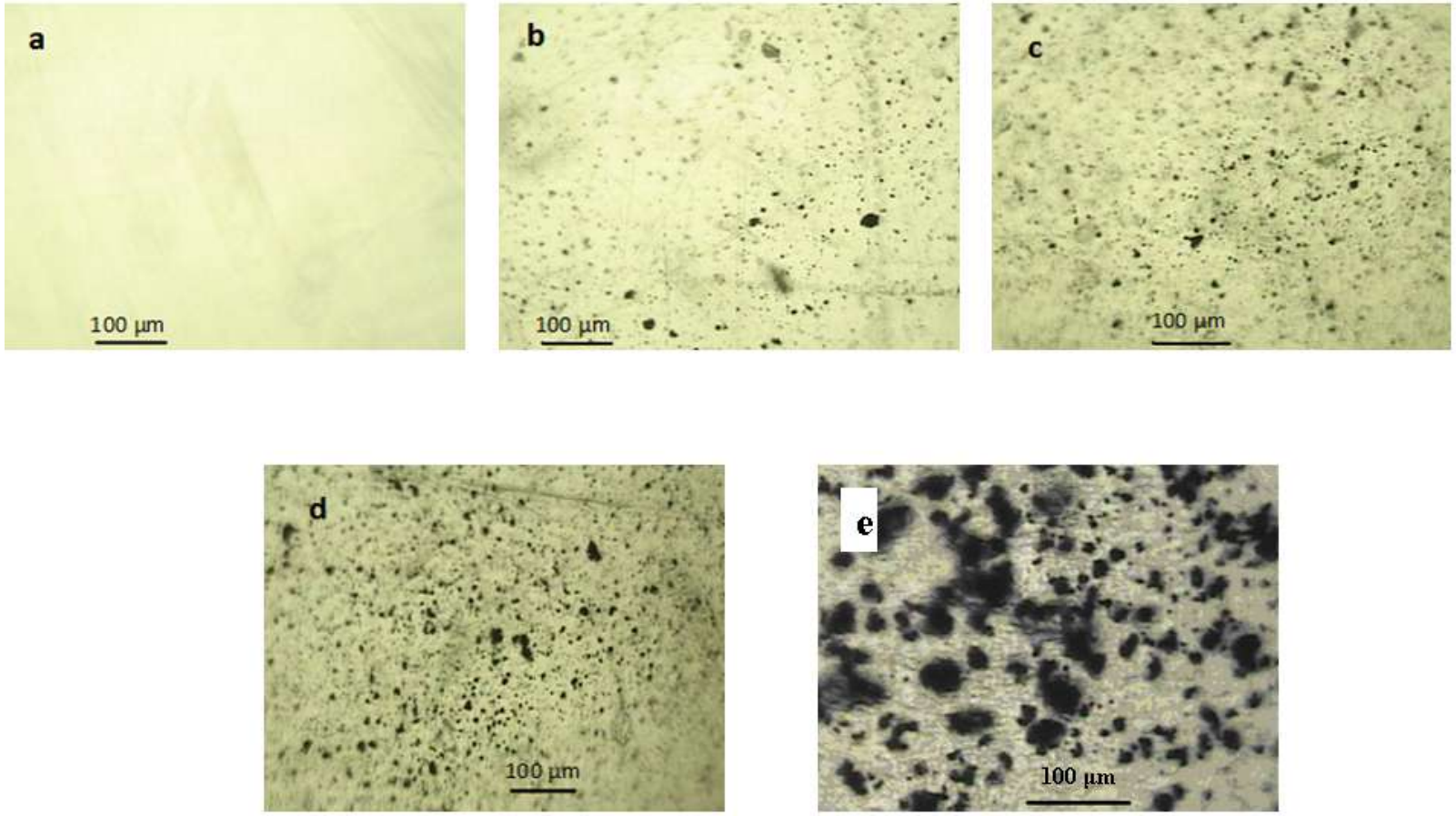

Figure 4.1. Optical micrographs of a) pure PET; along with composites containing 1, 2, and 3 % added NR-PANI: b) PETPA1, c) PETPA2, d) PETPA3 and e) pure NR-PANI.

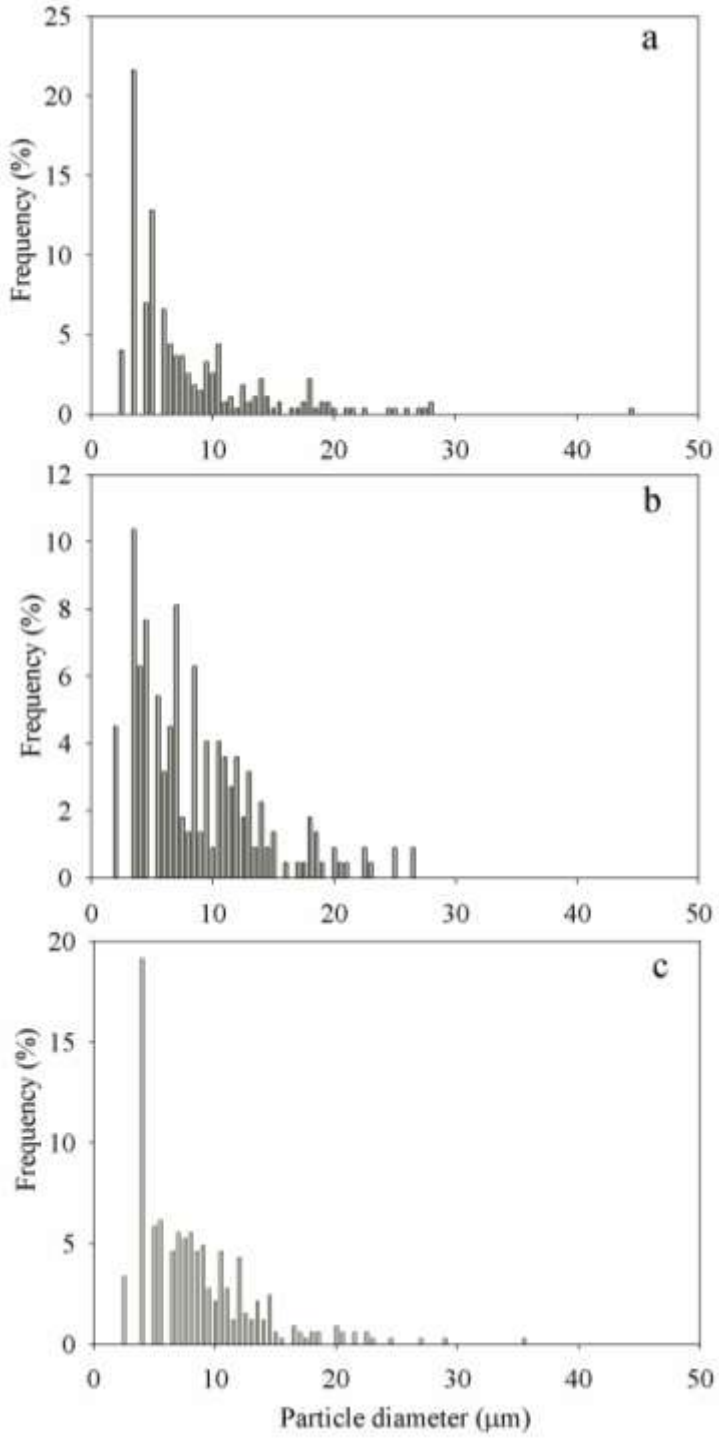

Figure 4.2. NR-PANI particle size distribution in:

a) PETPA1, b) PETPA2 and c) PETPA3.

4.3.2 Conductivity

The electrical conductivities of PET, PETPA1, PETPA2 and PETPA3 were 7 x 10^{-16}, 5 x 10^{-15}, 7 x 10^{-13} and 1 x 10^{-12} Scm^{-1} respectively. The conductivity of as-prepared NR-PANI was 2.3 x 10^{-3} Scm^{-1} [258]. With the inclusion of 3% NR-PANI in the composite, the conductivity of the PET increased by 4 orders of magnitude. The gradual increase in conductivity of the NR-PANI/ PET composites, with an increased loading of NR-PANI, suggests good dispersion and an improved conducting network of NR-PANI in the PET matrix, as observed in optical microscopy studies [207]. The conductivities of the composite films were much lower compared to an earlier study where addition of 5% of *p*TSA doped PANI increased the conductivity of PET by 11 orders of magnitude to 10^{-5} S cm^{-1} [203]. In the present study, NR-PANI was not doped by additional acids, beyond the sulfuric acid produced from the ammonium persulfate oxidant during synthesis, so a lower conductivity for NR-PANI/ PET composites was expected.

4.3.3 Melt flow index (MFI)

The MFI values of PET, PETPA1, PETPA2 and PETPA3 were 23 ± 3, 29 ± 1, 38 ± 1 and 48 ± 1 g $(10\ min)^{-1}$. Pesetskii *et al*. (2011) have also reported the MFI of pure PET as 23 g $(10\ min)^{-1}$ at 265 ºC and 21.6 N [279]. The MFI values thus increased with a greater amount of NR-PANI in the composites indicating easier flow of the melt. This suggests a lowering of the molecular weight of PET units upon incorporation of NR-PANI. Once molten, PET is known to undergo hydrolysis as well as thermo-oxidative degradation [280]. While PET undergoes significant hydrolysis under humid conditions at temperatures above

its glass transition temperature (T_g) [281], the thermal degradation is more pronounced at temperatures above 400 ºC [282]. These processes can be accelerated in the presence of an acid [281, 283]. Under acidic conditions the accelerated hydrolysis involves protonation of the in–chain oxygen atom of the ester group followed by reaction with water to produce hydroxyl and carboxyl end groups, resulting in scission of the PET chains as shown in Scheme 4.1. Moreover, thermal degradation of PET occurs through a chain scission mechanism resulting in carboxyl end groups and a lowering of the molecular weight [283].

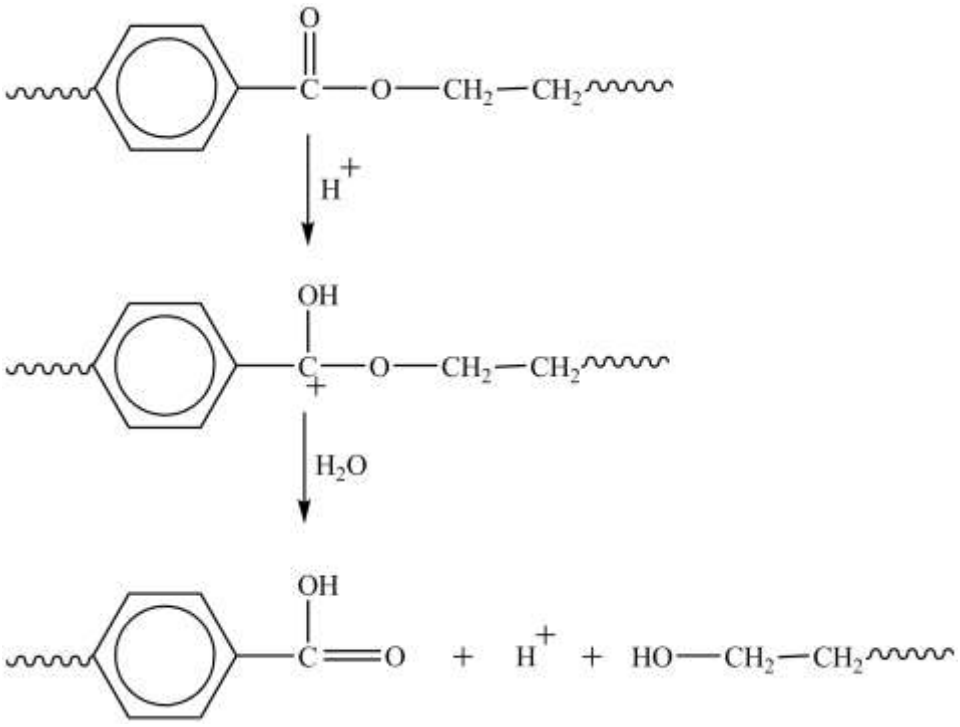

Scheme 4.1. Hydrolysis of PET.

NR-PANI contains occluded moisture and bisulfate dopant ions, which could create an acidic environment, ideal for the hydrolysis of PET. Paoli and Mitzakoff (1999) have previously observed hydrolysis of PET chains when blended with acid doped PANI at 270 ºC [203]. Similarly, hydrolysis of the PET ester groups was seen when PET was blended with nylon at 265 to 275 ºC [284]. While thermal degradation is not excluded in the present study, PET chains in the PET/ NR-PANI samples are expected to undergo hydrolysis catalysed by the dopants associated with NR-PANI.

4.3.4 FTIR spectroscopy studies

The FTIR spectra of PET, PETPA1, PETPA2, PETPA3 and NR-PANI are presented in Figure 4.3. The spectrum of PET is similar to that reported in the literature [285]. Major bands in the PET spectrum can be assigned to $_{\nu}$(C=O) at 1721 cm^{-1}, ring $_{\delta}$(CH) at 1505 and 1410 cm^{-1}, $_{\nu}$(O-CH_2) and ring $_{\nu}$(C-C-C) at 1018 cm^{-1}, $_{\delta}$(C=O) at 873 cm^{-1}, and a combination of $_{\delta}$(C=O) and ring $_{\delta}$(CH) at 727 cm^{-1}. A blend of ring $_{\delta}$(CH), $_{\delta}$(OCH) and $_{\delta}$(CCH) in *trans*-OCH_2CH_2O shows up at 1342 cm^{-1} while a blend of ring-ester $_{\nu}$(C-C), ring $_{\nu}$(C-C-C), $_{\tau}$(CH_2), $_{\delta}$(C=O) and $_{\nu}$(C-O) in C(=O)-O shows up at 1263 cm^{-1} [286]. Furthermore, the bands at 1121 and 1101 cm^{-1} are attributed to $_{\nu}$(C-O) in the crystalline and amorphous phases respectively [287]. NR-PANI exhibited peaks typical of polyaniline prepared by the 'falling pH' method. The major peaks are assigned to quinoid ring $_{\nu}$(C=C) at 1585 cm^{-1}, the benzenoid ring $_{\nu}$(C=C) at 1500 cm^{-1} and $_{\nu}$(C-N) at 1310 and 1250 cm^{-1} [14]. Peaks at about 1413 and 1447 cm^{-1} are attributed to phenazine-like highly branched structures formed at high pH. However, as the

pH of the synthesis mixture falls, the core structures containing phenazine-like groups are coated with more regular polyaniline [258].

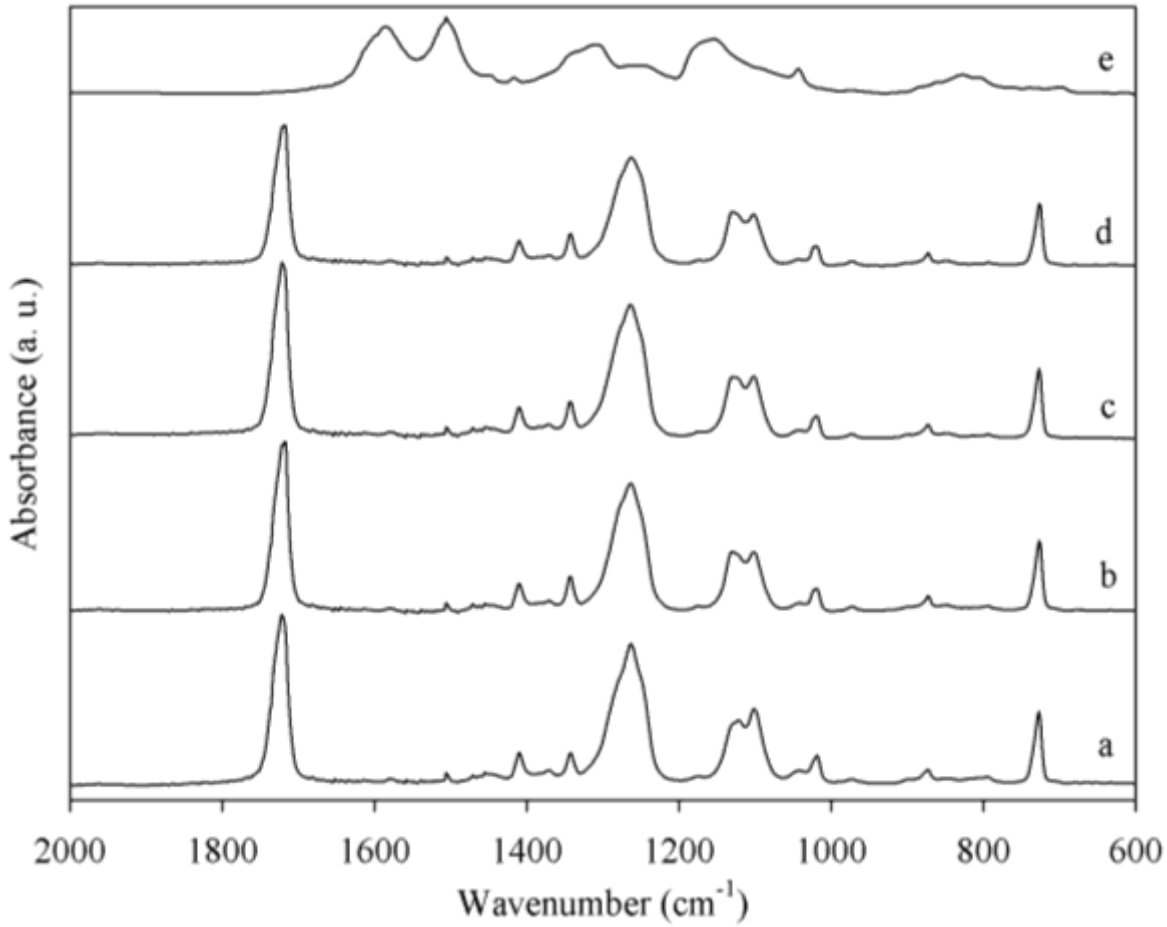

Figure 4.3. FTIR spectra of a) PET, b) PETPA1, c) PETPA2, d) PETPA3 and e) NR-PANI.

The spectra of PET/ NR-PANI composites were very similar to the spectra of pure PET. Although the presence NR-PANI in the composites was evident from optical microscopic studies, peaks corresponding to NR-PANI were not seen in the spectra of the

composites, as the NR-PANI was present at low concentrations and its contribution would have been largely diluted by the PET present. The PET peaks did not shift or broaden significantly upon addition of NR-PANI. The lack of large peak shifts suggests that specific interactions between the molecules of the two polymers were limited [288]. However, one notable change was blue shift of the band at 1121 cm^{-1} to 1130 cm^{-1} and the increase in intensity of the band at 1130 cm^{-1} compared to 1101 cm^{-1} band upon addition of NR-PANI. These observations suggest an increase in the degree of crystallinity of PET when blended with NR-PANI. The intensity of the 1342 cm^{-1} band also increased upon incorporation of NR-PANI implying an increase in the crystallinity of PET as observed by Liang and Krimm (1959) [287]. The increase in the intensity of the 1342 cm^{-1} band could also have been due to contributions from the $_{\nu}$(C-N) of NR-PANI.

4.3.5 XPS studies

The effect of NR-PANI on PET upon blending was also investigated by surface analysis using XPS. The elemental compositions of the samples determined from the wide scans are given in Table 4.1. PETPA2 and PETPA3 had 0.3 and 0.4% nitrogen content respectively, indicating the presence of NR-PANI, at least at the surface of the films. These PANI segments would be available for the scavenging of free radicals. However, no nitrogen was detected on the surface of PETPA1, possibly due to its presence at a very low level. The XPS wide scan analysis of NR-PANI revealed the following composition: 74.8% carbon, 9.7% nitrogen, 13.3% oxygen and 2.2% sulfur. Therefore, the theoretical nitrogen content of PETPA2 and PETPA3, based upon a 2% and 3% NR-PANI addition, would be 0.2 and 0.3%

respectively. The experimental nitrogen content of PETPA2 and PETPA3 were thus in accordance with the theoretical approximations.

Table 4.1. XPS data for PET, PETPA1, PETPA2 and PETPA3.

Sample	Elemental composition (at. %)			O/C	C1s deconvoluted peak quantification (at. %)		
	C	O	N		C-C/ C-H (284.6 eV)	C-O (286.4 eV)	O-C=O (288 eV)
PET	80.5	19.5	n/d	0.24	82.4	10.4	7.2
PETPA1	79.0	21.0	n/d	0.27	77.0	13.0	10.0
PETPA2	75.5	24.2	0.3	0.32	71.8	15.0	13.2
PETPA3	73.0	26.6	0.4	0.36	68.7	17.5	13.8

n/d: not detected

The O/C ratios, given in Table 4.1, increased with a greater amount of NR-PANI in the composites. The O/C ratio of NR-PANI, PET and PETPA3 were 0.18, 0.24 and 0.36, respectively. Theoretically, the addition of 3% NR-PANI to PET would have changed the O/C of PET by about 0.002. However, a much higher increase in the O/C ratio was observed. The –OH end groups produced by hydrolysis of PET chains contributed to the increase in the O/C ratio. The moisture and acid dopants present in NR-PANI can be expected to escalate the hydrolysis of PET chains, resulting in higher O/C ratios in the composites.

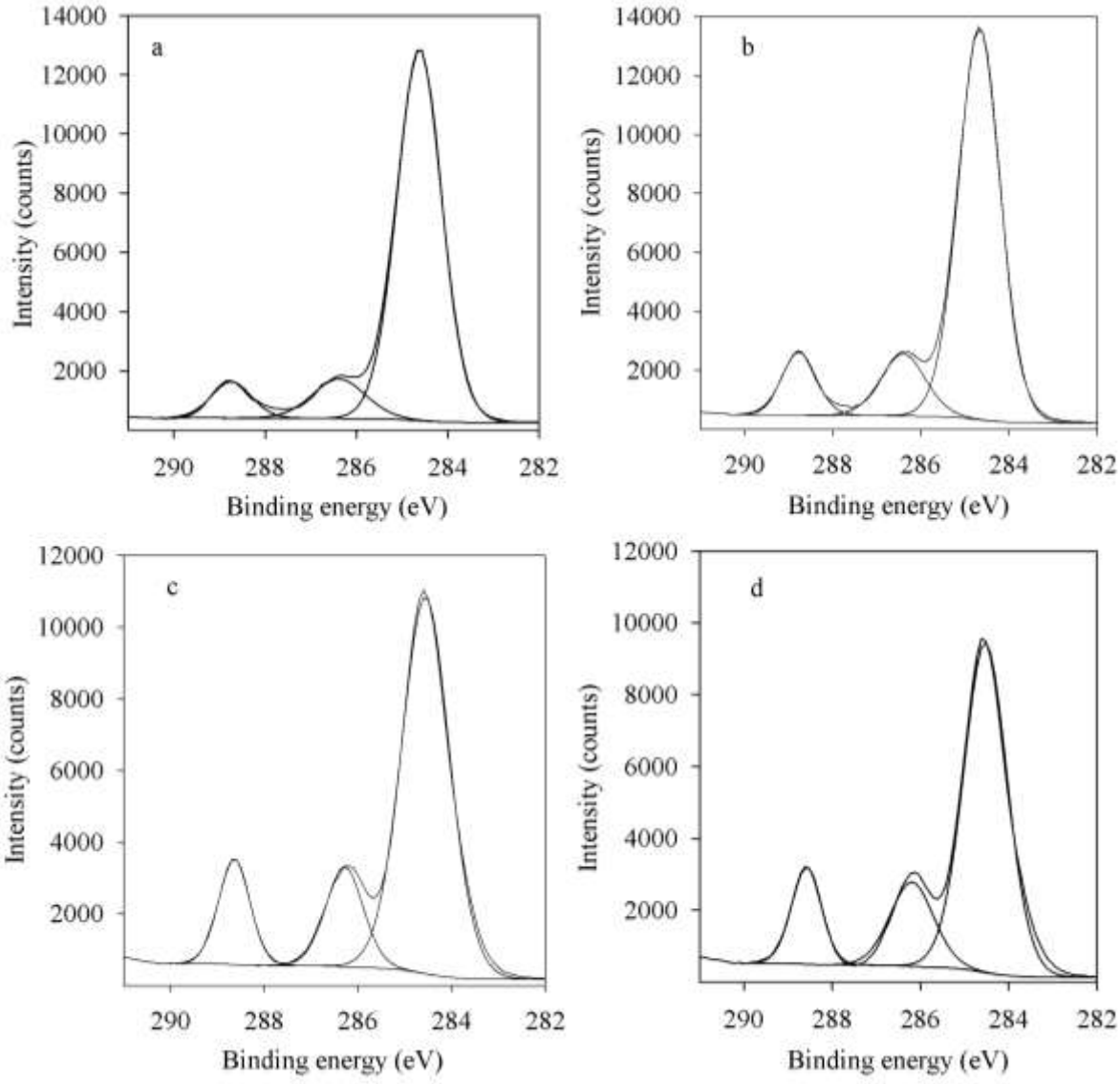

Figure 4.4. Deconvoluted C 1s spectra of a) PET, b) PETPA1, c) PETPA2 and d) PETPA3.

The carbon 1s spectra, deconvoluted into three components, are given in Figure 4.4 and their contributions are summarized in Table 4.1. The first component at 284.6 eV corresponds to carbon associated with C-C or C-H groups, the second component at 286.4 eV corresponds to C-O, and the third component at 288 eV is assigned to carbon in O-C=O species [289]. A peak corresponding to C-N groups of PANI in the composites typically occurs at 285.5 eV [190], but this could not be fitted in the carbon 1s spectra during the deconvolution process, likely due to its low concentration. The C-O group concentration increased as more NR-PANI was included in the composites. This was due to the production of hydroxyl end groups via hydrolysis of the PET chains. Interestingly, an increase in the concentration of C=O species with an increase in the amount of NR-PANI in the composites was also seen. This could be attributed to the formation of additional functional groups, such as anhydrides, upon PET chain bond scission due to thermal degradation [290, 291].

4.3.6 DSC studies

The DSC thermograms of NR-PANI, PET and the composites are given in Figure 4.5. The endothermic peak about 100 ºC in the thermogram of NR-PANI can be attributed to moisture loss. PET and the composites exhibited a glass transition (jump in heat flow), a cold crystallization (exothermic peak) and subsequent melting of the crystallites (endothermic peak) when heated from 25 to 300 ºC. The thermal transition temperatures, the glass transition (T_g), crystallization (T_c) and melting (T_m) as well as the corresponding enthalpies for cold crystallization (ΔH_c) and melting (ΔH_m), along with the degree of crystallinity (X_c) of PET in the composites are compiled in Table 4.2.

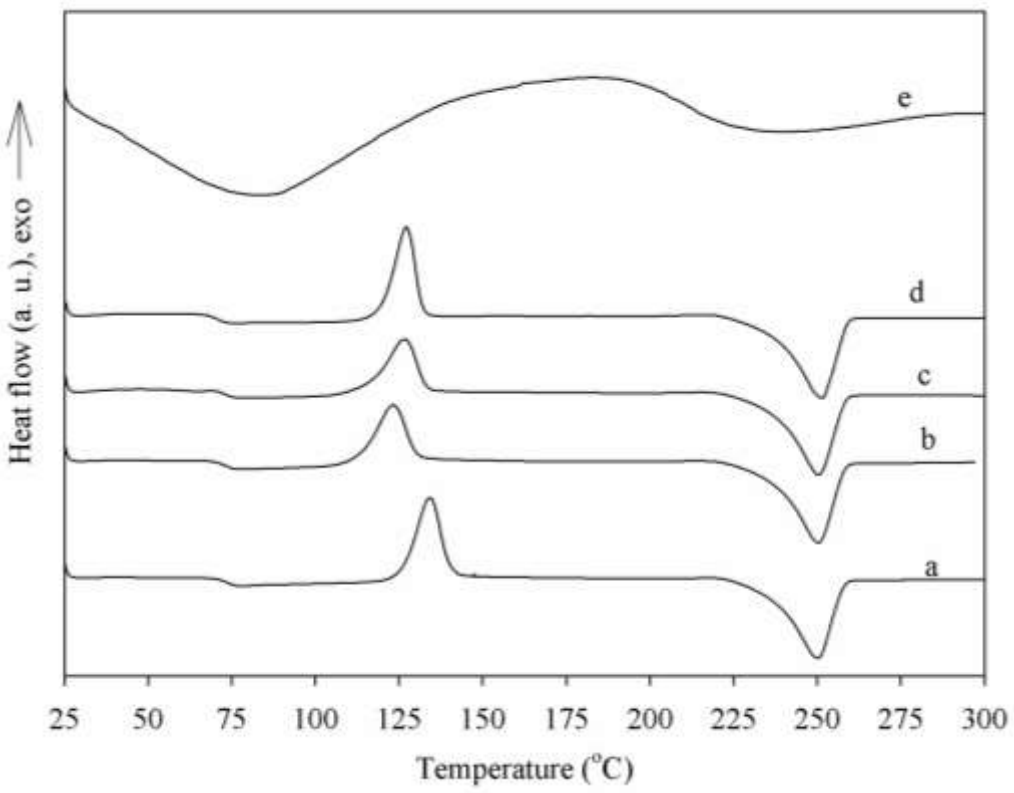

Figure 4.5. DSC thermograms of a) PET, b) PETPA1, b) PETPA2, c) PETPA3 and d) NR-PANI.

Table 4.2. DSC results of PET and NR-PANI/ PET composites.

Sample	T_g (ºC)	T_c (ºC)	T_m (ºC)	ΔH_c (J g^{-1})	ΔH_m (J g^{-1})	X_c (%)
PET	74	134	250	31.3	47.9	11.9
PETPA1	73	123	250	27.7	50.0	16.1
PETPA2	72	126	250	26.2	49.6	17.1
PETPA3	72	127	251	20.1	51.3	23.0

The degree of crystallinity was calculated using Equation 4.1, where ΔH^o_m is the enthalpy of melting of 100% crystalline PET, taken to be 140 J g^{-1} [284] and *w* is the weight fraction of PET in the composites.

$$X_c = \left(\frac{\Delta H_m - \Delta H_c}{w \Delta H^o_m} \right) \times 100 \quad \text{(Eq. 4.1)}$$

The degree of crystallinity of the PET film was 11.9%. The degree of crystallinity of PET increased with a greater amount of NR-PANI in the composites, with PETPA1, PETPA2 and PETPA3 showing a 35%, 44% and 93% increase, respectively. The increase in crystallinity of PET is also reflected in the decreasing ΔH_c values as the amount of NR-PANI increased in the composites. The increase in crystallinity can be attributed to hydrolysis of PET whereby small chain segments were created, which are capable of realigning and crystallizing easily. While a lowering in the molecular weight of PET upon hydrolysis has been reported previously [292], Ramao *et al*. (2009) have also observed an increase in crystallinity upon scission of PET chains [290].

The T_c of PET decreased upon addition of NR-PANI as shown in Table 4.2. Domains of an added phase are known to nucleate the cold crystallization of PET, thus lowering the T_c [284]. The T_g of PET in the pristine form and in the composites, also given in Table 4.2, did not differ significantly, indicating the absence of interactions between the two polymers, although an increase in the crystallinity of PET was observed. This was counter to a previous study where an increase in T_g was observed as the degree of crystallinity of cold-drawn PET

increased [293]. However, in another study, the T_g values did not change when the crystallinity of the PET films was increased by stretching the samples [284].

4.3.7 DMTA studies

The DMTA curves showing the *E′*, *E″* and tan δ of PET and PET/ NR-PANI composites are given in Figure 4.6. Upon increasing the temperature, *E′* decreased sharply above 65 ºC as the materials approached the glass - rubber region. *E″*, on the other hand, started to increase above 70 ºC as small parts of the macromolecular chains were able to move within the free volume [294]. *E′* of the composites, at 25 ºC, was slightly higher than that of PET, indicating that the composites were stiffer than PET. The *E′* increased with the composition of NR-PANI in the composites. This could be attributed to an increase in the degree of crystallinity of the composites.

The T_g values, given as the temperature corresponding to the maximum of the tan δ peak of PET, PETPA1, PETPA2 and PETPA3, were 82 ± 2, 81 ± 2 , 80 ± 2 and 79 ± 2 ºC, respectively. The T_g values for the samples did not vary significantly, as was the case with the T_g values obtained by DSC analysis. However, the T_g values from DMTA were about 8 ºC higher than the corresponding T_g values obtained by DSC. Such differences between the T_g values obtained by the two methods is common, as the exact position of T_g depends on the studied frequency in DMTA, whereas in DSC it depends on the heating rate used [294].

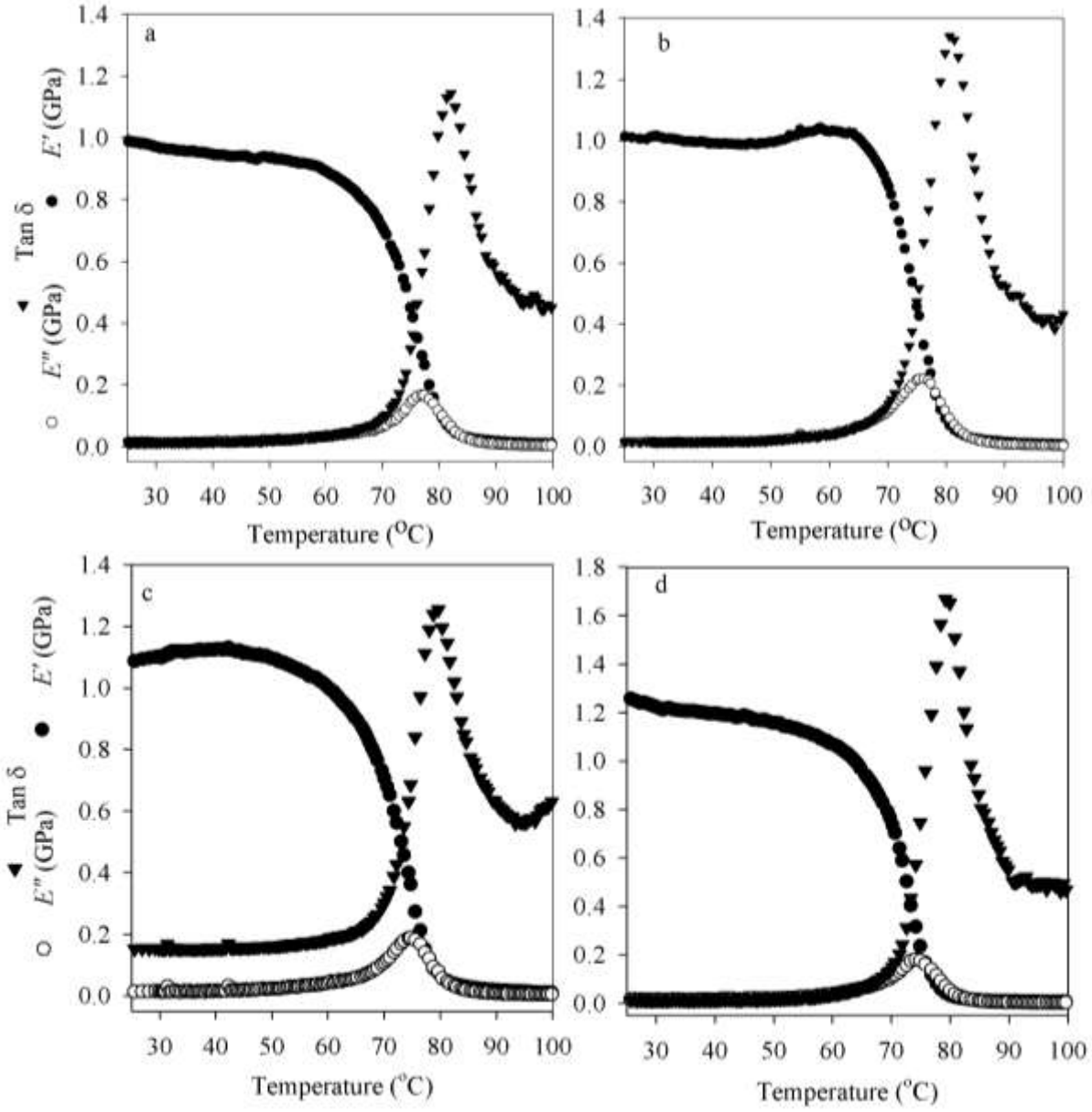

Figure 4.6. DMTA curves of a) PET, b) PETPA1, c) PETPA2 and PETPA3.

4.3.8 Static mechanical properties

The Young's moduli, tensile strength and elongation at break of PET and the PET/ NR-PANI composites are shown in Figure 4.7. The Young's moduli of the composites was higher than that of PET indicating that the composites were stiffer than PET. A 9% increase in the Young's modulus was observed upon loading 3% NR-PANI into the PET matrix. The increase in Young's modulus was proportional to the NR-PANI loading. This trend in Young's modulus is consistent with the trend in *E'* values from DMTA. The increase in Young's modulus can be attributed to an increase in the crystallinity of the composites. The Young's moduli of PET/ starch blends have been found to increase with starch loading. This was ascribed to the stiffness of the filler chains [282].

The tensile strength and the elongation at break of PET decreased after incorporation of NR-PANI. While the tensile strength decreased from 43 to 21 MPa with 3% NR-PANI loading, the elongation at break showed a marked decrease from 46 to 0.8%. The decline in the mechanical properties of the composites is due to insufficient interfacial adhesion between the NR-PANI particles and PET [198]. The hydrolysis of PET chains could have also contributed to the inferior mechanical properties of the composites. Annala and Lofgren (2006) have reported a decrease in the mechanical properties of polyethylene upon addition of PANI complexes. However, the mechanical properties of the blends were improved with the aid of functionalized metallocene polyethylene as a compatibilizer [198].

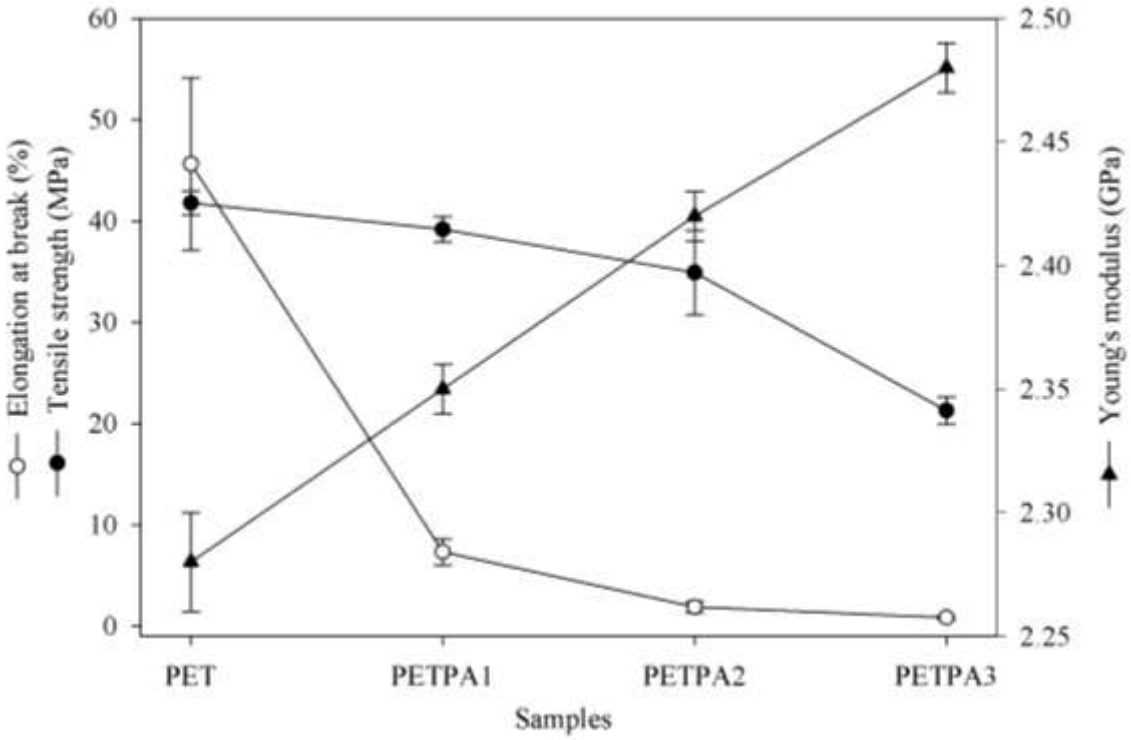

Figure 4.7. Mechanical properties of PET, PETPA1, PETPA2 and PETPA3.

4.3.9 Antioxidant activity

The free radical scavenging capacity, used as a measure of antioxidant activity, of the PET and PET/ NR-PANI composites are presented in Figure 4.8. The free radical scavenging capacity of the composites increased with an increase in the NR-PANI loading. On the other hand, pure PET did not exhibit any DPPH radical scavenging activity. Saikia *et al.* (2010) have made similar observations with starch/ PANI composites where higher free radical scavenging, also measured using the DPPH assay, was achieved with increased PANI loading [182]. It has been previously established that the free radical scavenging capacity is

independent of the associated electrical conductivity [258]. However, when composites are considered, the free radical scavenging capacity [182] as well as their conductivity [203] were both dependent on the amount of PANI present in the sample.

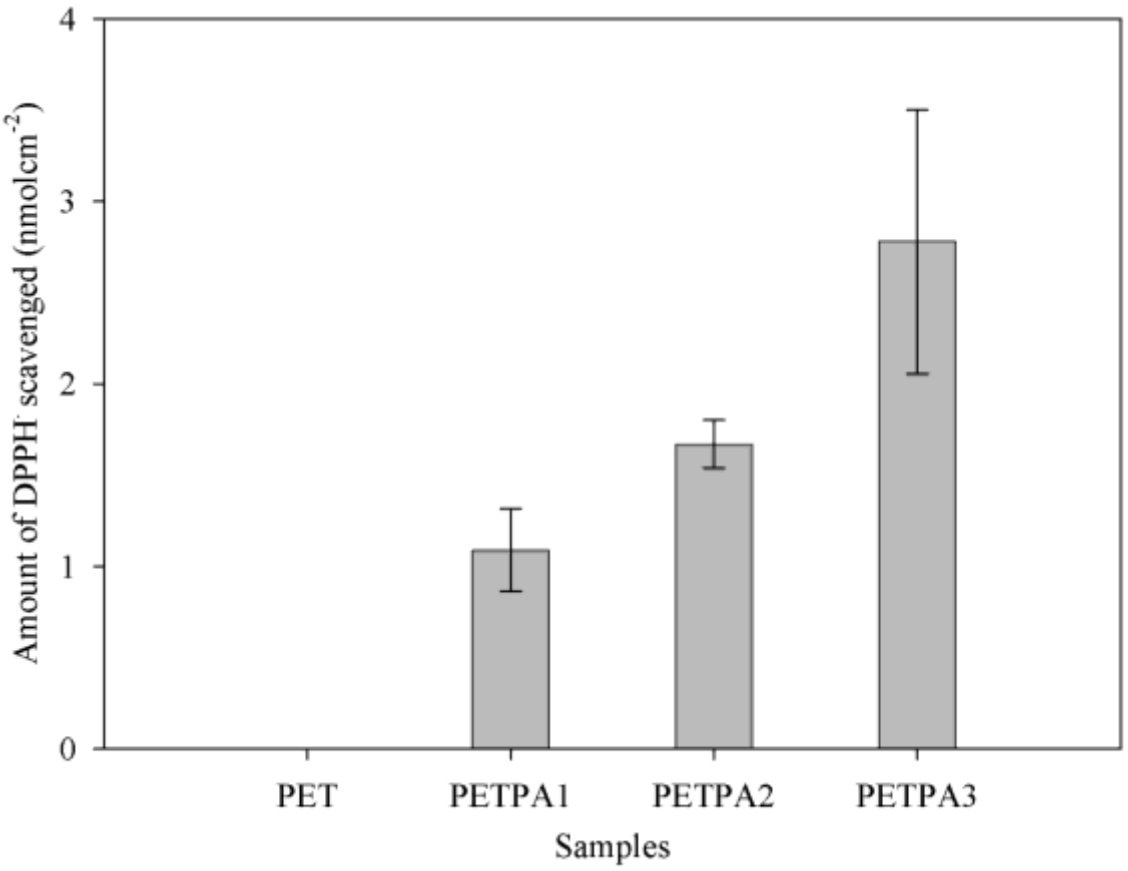

Figure 4.8. Free radical scavenging activity of PET, PETPA1, PETPA2 and PETPA3.

NR-PANI reduces DPPH$^{\bullet}$ radicals by donating hydrogen atoms, while the PANI segments are in turn oxidized to the pernigraniline form when in contact with DPPH radicals [258]. Therefore, having a higher concentration of NR-PANI molecules exposed to the

DPPH test solution would result in a higher free radical scavenging activity. The free radical scavenging capacity of the composite films was limited by the low loading level and more importantly the low concentration of NR-PANI at the surface of the composite films, as revealed by XPS. However, blending NR-PANI does bequeath free radical scavenging capabilities to PET as the PET/ NR-PANI composites clearly showed higher activity than the pure PET sample. The low loading of NR-PANI may be sufficient for the radical scavenging performance of the composites as PANI has a reversible redox property and can be readily oxidized and reduced by species in contact with the composites.

4.4 Conclusions

PET/ NR-PANI composites, with 1, 2 and 3 wt% NR-PANI loading, were prepared by melt processing. Optical microscopy revealed an even distribution of NR-PANI particles in the PET matrix, and a lack of aggregation. The electrical conductivities of the composites increased with NR-PANI loading, suggesting good dispersion and the formation of a conducting network of NR-PANI in the PET matrix. Spectroscopic and MFI results indicated that the PET chains underwent hydrolytic degradation upon addition of NR-PANI. The increase in the O/C ratios with the increase in NR-PANI content also suggested hydrolysis of the PET chains. An increase in the degree of crystallinity of PET was observed upon incorporation of NR-PANI, as the lower molecular weight chains were capable of realigning and crystallizing easily. The composites, owing to the increased crystallinity, were stiffer than pure PET at 25 ºC. Blending with NR-PANI, however, decreased the tensile strength and elongation at break of PET. This was due to insufficient interfacial adhesion between

PET and NR-PANI. The composites exhibited an increase in free radical scavenging capacity, a measure of antioxidant activity, with increasing NR-PANI loading. The PET/ NR-PANI composites, with low NR-PANI loading, could be potentially used for antioxidant packaging applications. However, their mechanical properties need to be improved if higher NR-PANI loading is to be considered.

CHAPTER FIVE

Characterization of Antioxidant LLDPE/ PANI Composites Prepared via Extrusion

This chapter is being published as:

Nand A.V., Ray S., Travas-Sejdic J., Kilmartin P.A. (2012) Characterization of antioxidant low polyethylene/ polyaniline blends prepared via extrusion *Materials Chemistry and Physics* 135: 903-911.

5.1 Introduction

PE is a commonly used polymer in the plastics industry due to its good thermal and electrical insulation properties, high resistance to chemicals [295], good mechanical and optical properties, a competitive market price [296] and ease of fabrication [297]. It makes up approximately 64% of all produced polymers [298]. PE has found use in applications such as pipes [299], grocery bags [300], agricultural films [296], biomedical implants [301] and liners for landfills [302]. Moreover, it is widely used as a food packaging material, both as free films and as coatings in containers [303].

Many researchers have attempted to fabricate superior packaging materials by blending PE with other materials. The oxygen barrier and mechanical properties of PE were improved upon blending with starch [304], or by incorporating PET microfibrils in the PE matrix [305]. The inclusion of zeolites in the PE matrix improved its water vapour transfer rate [306]. Furthermore, PE has been coated with garlic oil, rosemary oil [24] and zinc oxide nanoparticles [25] to yield packaging films with antimicrobial properties.

Recently, active food packagings with the ability to extend shelf life of foodstuffs have attracted much attention [16, 307]. Free radical mediated oxidation is known to be the primary cause of food deterioration and rancidity [45]. While most researchers have focused on the use of oxygen absorbers in packaging materials [45], little consideration has been given to the use of antioxidants, acting as free radical scavengers, to prevent the oxidation of foodstuffs. Free radical scavengers, when incorporated in packaging materials such as PE, have the potential to break the oxidation chain reaction and enhance the shelf life of foodstuffs [45]. However, to be successfully utilized, the free radical scavengers need to be

able to withstand the high temperatures and aggressive processing conditions required to process plastics.

PANI, an electrically conducting polymer, has been shown to exhibit excellent free radical scavenging capabilities [79, 80, 85, 258]. PANI synthesized via the "falling pH" route (NR-PANI), having a nanorod-like morphology, exhibited a higher free radical scavenging capacity compared to the conventional sample synthesized in a HCl media, attributed to a lower oxidation level in the NR-PANI [85]. NR-PANI has also demonstrated good thermal stability, characterized by a < 10% weight loss, other than that due to moisture, and high free radical scavenging activity up to 200 ºC [278]. Therefore, it is an ideal candidate for melt processing with PE, which is usually processed at temperatures below 200 ºC.

In the present work, composites of NR-PANI, synthesized via the "falling pH" route, and linear low density polyethylene (LLDPE) have been prepared by thermomechanical processing. The composites have been characterized using a range of spectroscopic and thermal analytical techniques. The static mechanical properties, conductivity and the DPPH free radical scavenging capacity of the composites have also been examined.

5.2 Experimental

5.2.1 Materials

LLDPE resin (FC21HN) having a melt flow index of 1.0 g $(10\ min)^{-1}$ and 0.918 g cm^{-3} density was obtained from TCL Hunt Ltd (New Zealand). Details of other chemicals used are given in sections 2.2.1 and 3.2.1.

5.2.2 Synthesis of NR-PANI

NR-PANI, consisting of micro- and nanorods and flake-like structures, was synthesized by the falling pH method as described in section 2.2.2. The dried NR-PANI was ground to a fine powder and sieved using a 106 µm sieve. The NR-PANI powder was kept in an air – tight container for further use. The degree of oxidation of NR-PANI has been previously determined by the XPS analysis of the N1s peak to be 17 % [258].

5.2.3 Preparation of NR-PANI/ LLDPE composites

Blending of LLDPE and NRPANI, with 5 %, 10 %, 15 % and 20 % loading of NR-PANI, designated as PEPA5, PEPA10, PEPA15 and PEPA20 respectively, was undertaken using a Brabender DSE25 twin screw extruder with a L/D ratio of 42. LLDPE pellets were dried in a Moreto dehumidification dryer at 80 ºC overnight and NR-PANI was dried overnight at 60 ºC in a vacuum oven prior to blending. LLDPE and NR-PANI were manually mixed and quickly fed into the extruder operating at 150 ºC with a screw speed of 20 rpm at a torque of 200 Nm. The molten composites were extruded through a 3 mm die as a rod,

cooled in air and pelletized. For comparison purpose, a control sample of LLDPE without any NR-PANI was also extruded as described above. The extruded pellets were compression moulded between Teflon sheets at 150 ºC to obtain 0.35 ± 0.05 mm thick films. The pellets were heated in the press for 1 min with repeated application and release of pressure to remove air bubbles, and kept at 10 kPa for an additional 4 min. The films were cooled in a flow of air immediately after removal from the hot press and stored in air tight containers until further characterization. The film thickness was measured using a Mitutoyo Absolute 500 series digital calliper.

5.2.4 Characterization

XPS data of the film samples were collected on a Kratos Axis UltraDLD instrument equipped with a hemispherical electron energy analyser. Samples were mounted on standard VG sample studs by means of double sided carbon tapes. The spectra were taken using monochromatic Al Kα X-rays (1486.69 eV) with the X-ray source operating at 150 W. The analysis area was a 300 by 700 µm spot. The core level scans were collected with 20 eV pass energy. The analysis chamber was at a pressure in the 10^{-9} torr range throughout the data collection. Data analysis was performed using CasaXPS. Core level data were fitted using Gaussian-Lorentzian peaks with a Shirley background. The binding energy scale was corrected for the neutraliser shift using the C 1s signal from saturated hydrocarbon at 284.6 eV.

FTIR transmission spectra of the LLDPE and NR-PANI/ LLDPE thin films were recorded using a Thermo Electron Nicolet 8700 fourier transform infrared spectrometer. The

spectrum of NR-PANI was recorded using the same instrument but equipped with a single bounce ATR and a germanium crystal. An average of 64 scans with a 4 cm^{-1} resolution was taken for all samples.

ESR spectra of known masses of film samples, contained in ESR quartz tubes, were recorded using a JEOL (JES-FA-200) ESR spectrometer operating in the X-band. The spectrum of a known mass of copper (II) sulfate was also recorded under the same conditions as the samples, for the calculation of spin concentrations.

XRD patterns of the NR-PANI powder, LLDPE and NR-PANI/ LLDPE films were recorded on a Siemens D5000 diffractometer, using Cu Kα radiation, in the range 5 to 45º (2θ). While the powder sample was compressed into the sample holder, the film samples were fixed to the sample holder with the aid of grease.

The cross-sectional surface morphology of cryo-fractured LLDPE and NR-PANI/ LLDPE film samples was visualized using a FEI Quanta 200FE environmental electron scanning microscope (ESEM). The samples were coated with platinum using a Polaron SC7640 Sputter Coater for 300 s at 5-10 mA and 1.1 kV. The NR-PANI particle size, dispersed in the composites, was obtained by the ImageJ software. The surface morphology of the NR-PANI sample was visualized using a Philips XL30S FEG SEM. Particle size analysis of NR-PANI was carried out by means of laser diffractometry using a Malvern Mastersizer 2000 instrument with water as the dispersant.

DSC analysis were performed on the samples, contained in aluminium pans, using a TA Instruments Q1000 DSC from 25 to 200 ºC at a 10 ºC min^{-1} heating rate in a nitrogen atmosphere.

The static mechanical properties of the samples were determined at ambient temperature, using an Instron 5567 universal testing machine equipped with a video extensometer. The measurements were undertaken in accordance with ASTM D822-02. The stress-strain curves of dog bone shaped test specimens were measured at a constant crosshead speed of 5 mm min^{-1} and a 1000 N load cell. The distance between the sample grips was 65 mm. The dimensions of the test region of the samples were 25 mm x 3 mm x 0.35 mm (length x width x thickness). The Young's modulus, tensile strength and elongation at break were determined from at least six measurements of each sample.

The technique of measuring the conductivity between two electrodes (DIN-53596) was employed to determine the electrical conductivity of LLDPE and the NR-PANI/ LLDPE films. All measurements were undertaken at ambient temperature using a Keithley 6517A electrometer. The electrical conductivity of dry pressed pellets of as prepared NR-PANI was measured by the four-probe technique using a Jandel Model RM2 instrument.

5.2.5 Radical scavenging assay

An adaptation of the DPPH assay for use with polymeric samples [79, 80] was applied for the assessment of LLDPE and the composite samples. 10 pieces of 1 x 1 cm^2 film samples were added to 20 mL of a 55 µM methanolic DPPH solution. The samples were left to react at room temperature for 24 h, after which the absorbance of the supernatant at 516 nm was measured using a Shimadzu UV-1700 UV-visible spectrophotometer. Three trials of each sample were undertaken. A control experiment, without any test sample, was also set

up. The amount of $DPPH^{\bullet}$ which reacted over a 24 h period was then calculated after subtracting away the background loss of a $DPPH^{\bullet}$ solution without added test sample.

5.3 Results and Discussions

5.3.1 Morphology

The ESEM images of the cryo-fractured surfaces of LLDPE, NR-PANI/ LLDPE composites, and the SEM image of pristine NR-PANI, are shown in Figure 5.1. Pure LLDPE exhibited a continuous homogeneous phase with network-like features resulting from the brittle fracture of the sample. Moreover, the ESEM images of the surface of the cryo-fractured composite samples clearly showed irregular shaped NR-PANI lumps, with rough surfaces, dispersed in the LLDPE continuous phase. The absence of nanorod and flake-like morphologies of NR-PANI, presented in Figure 5.1(e), in the composites could be attributed to coalescence of the nanorods and flakes into lump-like aggregates during processing. Annala and Lofgren (2006) have also observed two different morphologies in the fracture surfaces of PE/ PANI extrudates [198]. Distinct phase boundaries between the host LLDPE matrix and NR-PANI aggregates were also apparent from the ESEM images of the composites, especially at higher loadings of NR-PANI, namely in the PEPA15 and PEPA20 samples, indicating the absence of any significant interfacial adhesion between LLDPE and NR-PANI. This is attributed to the dissimilarity in the polarity of the two polymers. While LLDPE is a typical non-polar hydrocarbon polymer [308], NR-PANI possesses higher polarity due to the presence of amine groups in its macromolecular structure.

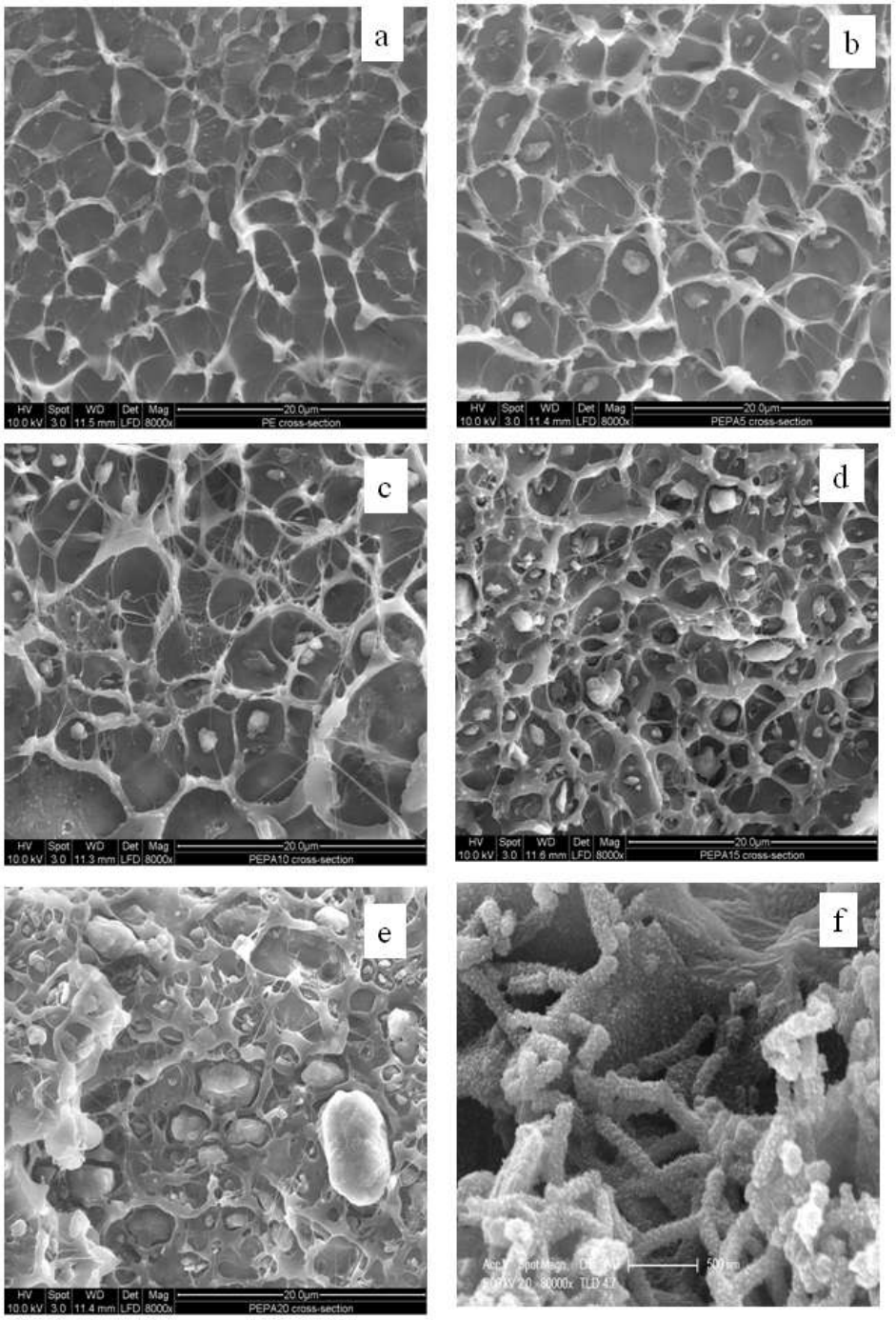

Figure 5.1. ESEM micrographs of the cryo – fractured cross – sectional surfaces of LLDPE, b) PEPA5, c) PEPA10, d) PEPA15, e) PEPA20 and f) SEM micrograph of NR-PANI.

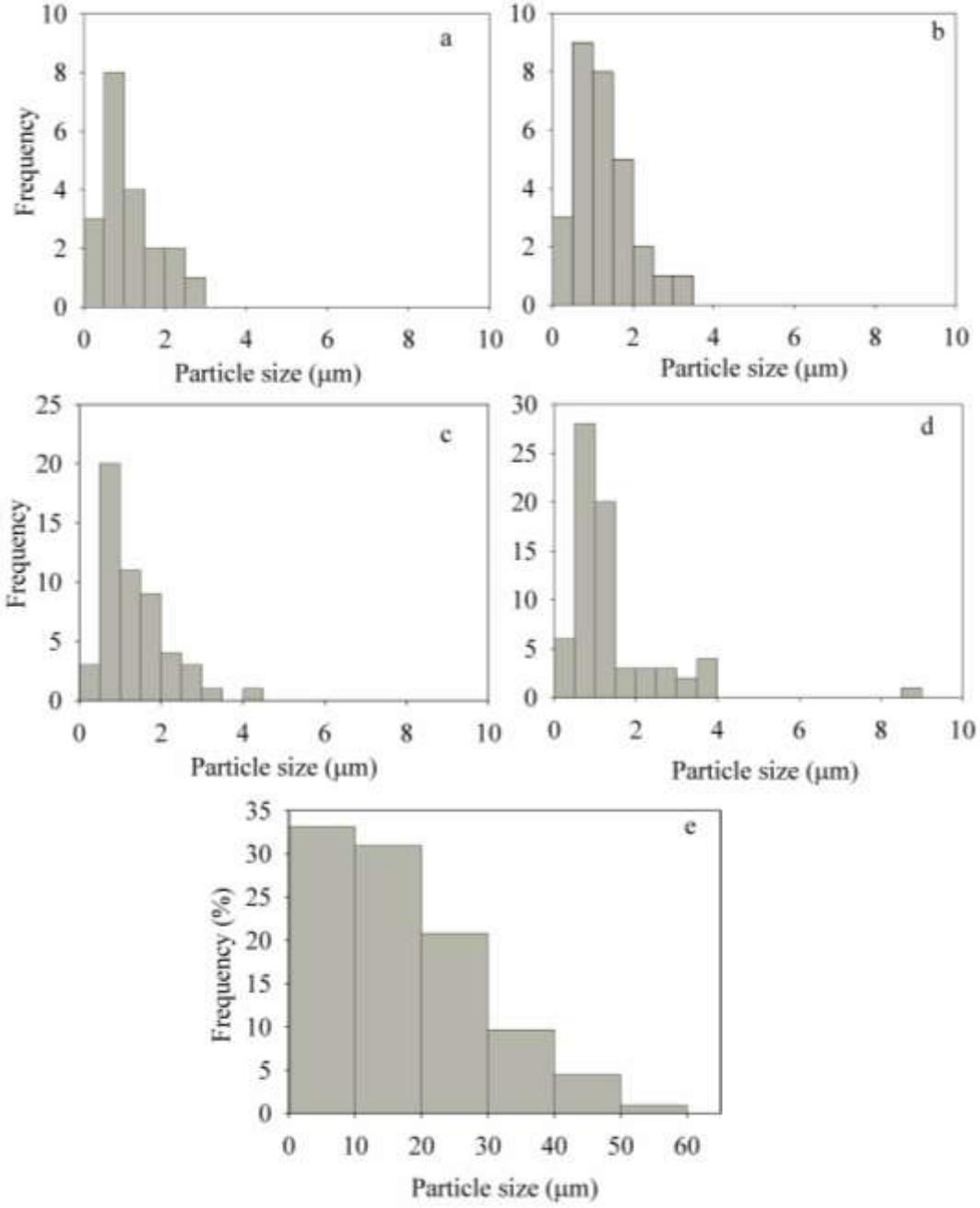

Figure 5.2. NR-PANI particle distribution in a) PEPA5, b) PEPA10, c) PEPA15, d) PEPA20 and e) particle size distribution of pristine NR-PANI obtained using laser diffractometry.

Although NR-PANI particles were well dispersed in the LLDPE matrix, their average particle sizes increased as the NR-PANI fraction in the composites increased. The particle size distribution of pristine NR-PANI and NR-PANI aggregates in the composites are shown in Figure 5.2. The average particle size of NR-PANI aggregates employed in this study, measured by laser diffractometry, prior to blending with LLDPE, was 17 μm. These aggregates broke down into smaller particles during blending as shown in the particle size distribution diagram of the composites in Figure 5.2. However, the NR-PANI particle size increased as the fraction of NR-PANI in the composites increased. The morphology and final size of the dispersed phase are known to be influenced by blending conditions, viscosity forces that tend to deform the dispersed phase, and the interfacial tension forces. At low fractions of the dispersed phase, an equilibrium particle size results primarily from continuous breakup of the dispersed phase. However, as the fraction of the dispersed phase increases, the particle size becomes progressively larger due to increased coalescence of the dispersed phase [304], as was observed with the PAPA15 and PEPA20 samples.

5.3.2 Spectroscopy studies

5.3.2.1 FTIR

The FTIR spectra of NR-PANI, LLDPE and the NR-PANI/ LLDPE samples are presented in Figure 5.3. The spectrum for LLDPE is similar to those reported in the literature [225, 297, 298, 309]. It consists of doublets, characteristic of partially crystalline PE, in the regions 1470 – 1463 cm^{-1} and 729 – 719 cm^{-1} [310]. These doublets are assigned to CH_2

bending and rocking vibrations respectively. An additional broad band at 1370 cm^{-1} is attributed to the CH_3 bending [297]. The major peaks in the spectrum of NR-PANI can be assigned to C=C stretching modes of the quinoid and benzenoid rings at 1585 cm^{-1} and 1500 cm^{-1} respectively, a C-N stretching mode at 1310 cm^{-1} and aromatic ring in-plane and out-plane C-H bending vibrations at 1155 cm^{-1} [258]. The peak at 1040 cm^{-1} is attributed to sulfonate and bisulfate groups, contributed by the ammonium persulfate oxidant during synthesis and included within NR-PANI chains as counterions [159, 239]. Further, weak vibrational bands at 1413 cm^{-1} and 1447 cm^{-1}, characteristic of polyaniline synthesized under falling pH conditions, are attributed to the phenazine-type highly branched structures [238, 258]. It is expected that as the pH of the synthesis falls, the phenazine type structures are coated with more regular polyaniline [153].

The spectra of the NR-PANI/ LLDPE samples included bands corresponding to both of the constituent polymers and the intensity of the bands due to NR-PANI increased as the fraction of NR-PANI was raised in the composite samples. However, there were no significant changes in the peak positions of the characteristic bands of both NR-PANI and LLDPE upon blending. Moreover, no additional peaks were observed in the spectra for the NR-PANI/ LLDPE samples, illustrating the lack of chemical interaction between the individual composite components as well as their stability during blending at 150 ºC.

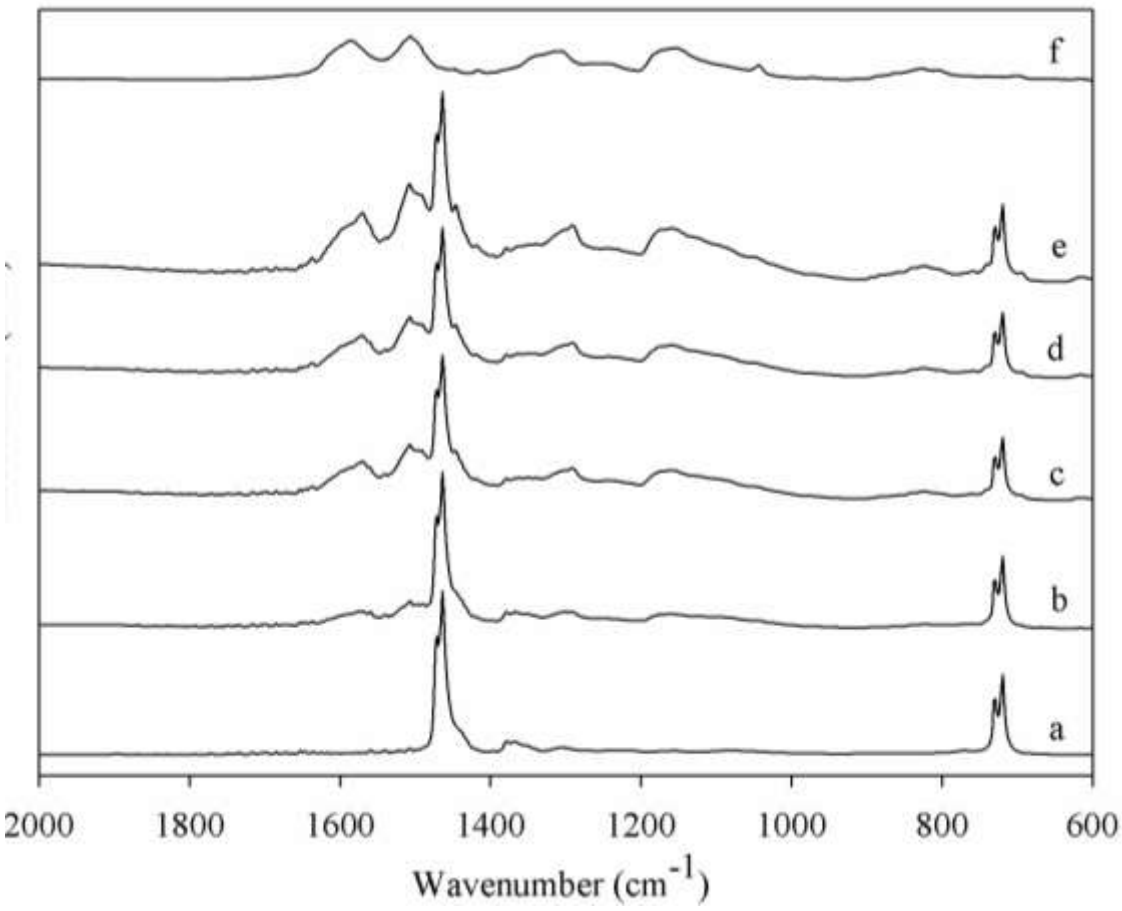

Figure 5.3. FTIR spectra of a) LLDPE, b) PEPA5, c) PEPA10,

d) PEPA15, e) PEPA20 and f) NR-PANI.

5.3.2.2 XPS

The presence of NR-PANI in the composite samples was confirmed further by XPS studies. XPS is a powerful technique for the determination of atomic concentrations at the sample surface and for the acquisition of chemical bonding information [311]. The elemental compositions for carbon and nitrogen in the samples determined from XPS wide scans are

provided in Table 5.1. The spectra of all of the composite samples showed the presence of nitrogen, indicating NR-PANI was present at least at the surface of the films. These NR-PANI segments would be available for the scavenging of free radicals in the first instance. Nitrogen was not detected on the surface LLDPE as its chemical structure consists of only carbon and hydrogen. The N/C ratio of the samples increased in the order LLDPE < PEPA5 < PEPA10 < PEPA15 < PEPA20, consistent with the composite formulations. Typical deconvoluted carbon 1s spectra of LLDPE and PEPA20 are shown in Figure 5.4. The carbon 1s spectra of LLDPE contained a symmetric C-C peak at 284.6 eV indicating the presence of only one valence state for carbon which corresponded to C_xH_y functionalities such as $–CH_3$ and $–CH_2$ [311]. An additional peak at about 285 eV was fitted in the carbon 1s spectra of the composite samples. This peak was attributed to C-N groups of NR-PANI [190]. Thus, the XPS studies indicated the existence of NR-PANI and LLDPE components in the composites, as evidenced by morphological and FTIR studies.

Table 5.1. XPS data of LLDPE and NR-PANI/ LLDPE composites.

Sample	N (atm. %)	C (atm. %)	N/C (x 10^{-3})
LLDPE	0	100	0
PEPA5	0.9	99.1	0.9
PEPA10	1.7	98.3	1.7
PEPA15	2.2	97.8	2.2
PEPA20	2.8	97.2	2.9

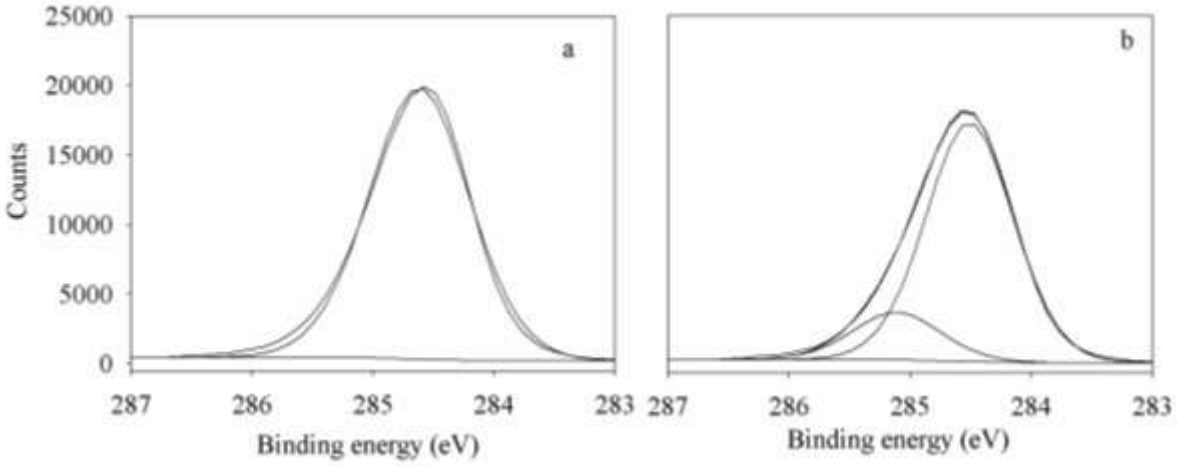

Figure 5.4. Deconvoluted C 1s spectra of a) LLDPE and b) PEPA20.

5.3.2.3 ESR

ESR spectroscopy has been used to characterize the spin concentrations and interactions of the electronic spins of pure PANI [278] as well as of PANI as composite components [199]. The LLDPE sample did not present any ESR signal as shown in Figure 5, a phenomena observed previously by Chipara *et. al*. (2003) [199]. However, the NR-PANI/ LLDPE samples exhibited a symmetrical, single narrow line spectrum. A typical spectrum of PEPA20 sample is shown in Figure 5.5. While Chipara *et. al*. (2003) have reported a single narrow line spectra of PE/ PANI composites located close to g = 2.0 [199], Nand *et. al*. (2011) have reported the location of the ESR spectrum of PANI in the range g = 2.0033 to 2.0038 [278]. The ESR spectrum of the composite samples, in the current study, were located at g = 2.0030 as shown in Table 5.2. The resonance spectra thus show the presence of

unpaired electronic spins in the composite samples, which can be attributed to the polarons within the NR-PANI structure [278].

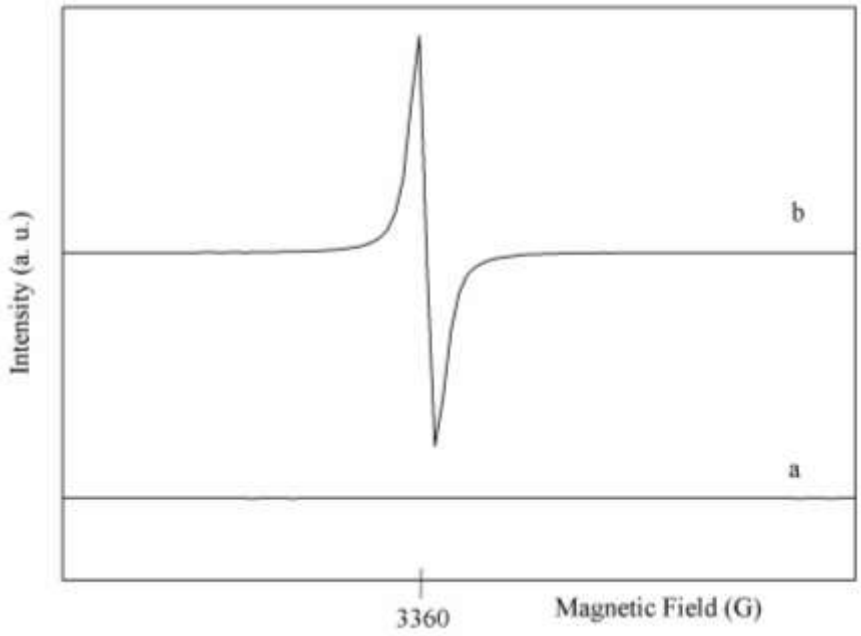

Figure 5.5. ESR spectra of a) LLDPE and b) PEPA20.

The peak to peak resonance line width (ΔH_{pp}) and spin concentrations, calculated using Equation 5.1, are presented in Table 5.2.

$$N_{sample} = \frac{I_{sample}}{I_{CuSO_4}} \times \frac{\left(n_{CuSO_4} \times N_A\right)}{m_{sample}} \qquad \text{(Eq. 5.1)}$$

where N_{sample} is the spin concentration of the composite sample (spins g^{-1}), n_{CuSO_4} is the moles of copper sulfate, N_A is the Avogadro constant, I_{sample} and I_{CuSO_4} are the areas under the integrated ESR signals of the composite sample and copper sulfate respectively, and m_{sample} is the mass of the composite sample (g). The ΔH_{pp} values decreased as the fraction of NR-PANI increased in the composites, showing an enhancement of exchange interactions, due to the decrease in the average distance between uncoupled electronic spins, also indicating good homogeneity of the composite materials at the submicron level [199]. NR-PANI is believed to be the contributor of the spins in the composites and so the spin concentrations also increased as the fraction of NR-PANI in the composites was raised. The theoretical concentration of the spins in the composites were predicted using the spin concentration of pure NR-PANI, reported earlier to be 3.53 x 10^{19} spins g^{-1} [278]. The slight discrepancy between the predicted and measured spin concentrations may be due NR-PANI undergoing redox transitions at the moderately high temperature experienced during blending [278].

Table 5.2. ESR *g* factor, ΔH_{pp} and spin concentration of NR-PANI/ LLDPE composites.

Sample	*g* factor	ΔH_{pp} (G)	Predicted [spin] (x 10^{18} spins g^{-1})	Measured [spin] (x 10^{18} spins g^{-1})
PEPA5	2.0030	2.93	1.8	2.4
PEPA10	2.0030	2.88	3.5	4.4
PEPA15	2.0030	2.86	5.3	4.8
PEPA20	2.0030	2.82	7.1	8.2

5.3.3 Electrical conductivity

The electrical conductivity of LLDPE, PEPA5, PEPA10, PEPA15 and PEPA20 were 2.29 x 10^{-15}, 3.38 x 10^{-15}, 6.94 x 10^{-15}, 1.19 x 10^{-14} and 1.93 x 10^{-14} S cm^{-1} respectively. The conductivity of the NR-PANI has been earlier reported to be 2.3 x 10^{-3} S cm^{-1} [258]. The conductivity of the composites increased with the addition of NR-PANI and is consistent with the decrease in ΔH_{pp} values of the composite samples. This indicates good dispersion and formation of a partially conducting network of NR-PANI in the LLDPE matrix. Similar observations were made in earlier studies when HCl doped PANI was incorporated in a PE matrix [199, 312]. Moreover, a percolation threshold of 20% PANI was observed for the highly conductive HCl doped PANI. The current study was limited to composites with 20 % loading of NR-PANI, not doped by any added acids and of a low conductivity, and no percolation threshold behaviour was observed.

5.3.4 Crystallinity and melting behaviour

The changes in the crystallinity of LLDPE, upon addition of NR-PANI, were studied by XRD measurements. The XRD patterns of LLDPE, NR-PANI/ LLDPE composites and pure NR-PANI are shown in Figure 5.6. LLDPE showed typical crystalline peaks at 2θ = 22º, 24º and 36º. Badr *et al*. (2000) have also observed three crystalline peaks in the region 2θ = 15 - 40º for a low density PE sample [313]. Pure NR-PANI exhibited peaks at about 2θ = 6.5º, 19º and 26º. The peak at 2θ = 6.5º is characteristic of an interlayer repeat distance of alkyl spacers between parallel planes of stacked PANI backbones [204]. The NR-PANI/ LLDPE composites showed characteristic peaks of LLDPE together with the 2θ = 6.5º NR-

PANI peak. While the intensity of the peak at 2θ = 6.5º increased with NR-PANI loading in the composite samples, the intensities of all of the other peaks decreased, signifying a lowering in LLDPE crystallinity upon blending with NR-PANI. The presence of the 2θ = 6.5º peak in the composite samples showed that NR-PANI had maintained its microstructure upon blending with LLDPE.

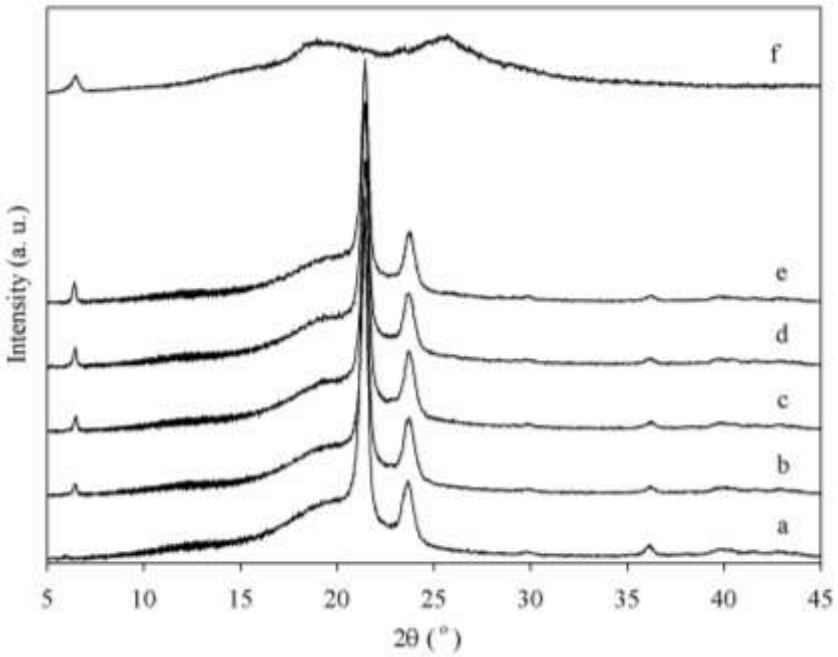

Figure 5.6. XRD patterns of a) LLDPE, b) PEPA5, c) PEPA10, d) PEPA15, e) PEPA20 and f) NR-PANI.

DSC measurements were also undertaken to investigate the changes in crystallinity of LLDPE upon blending with NR-PANI. The DSC thermograms of pure LLDPE and the NR-PANI/ LLDPE composite samples, given in Figure 5.7, were similar to the thermogram of

LLDPE reported by Liu and Harrison (1994) [314]. LLDPE is known to be a complex material. The polymer chains are usually linear but have a significant number of branches introduced using co-monomers such as but-1-ene and oct-1-ene [315]. Therefore, the broad endothermic curve of LLDPE, as shown in Figure 5.7, is attributable to its broad and multimodal chemical composition distribution [314]. The samples exhibited two melting peaks, at about 118 ºC and 121 ºC, overlapping with each other. However, blending with NR-PANI did not affect the LLDPE melting temperature.

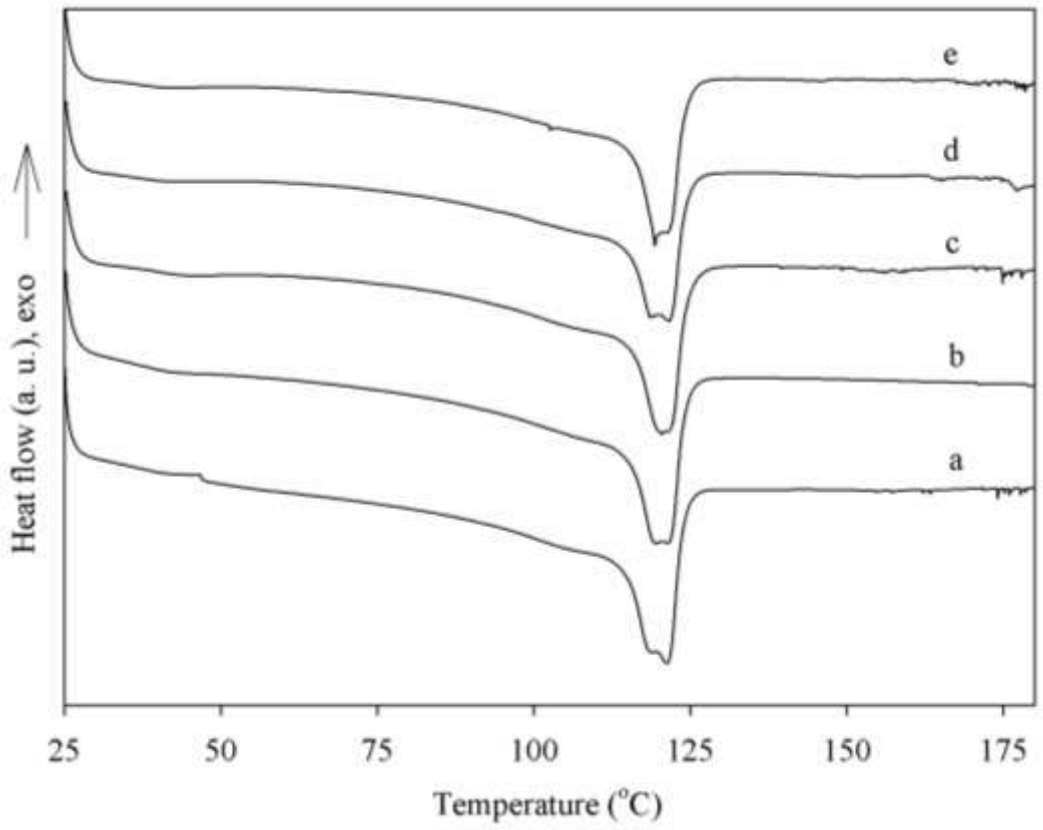

Figure 5.7. DSC thermograms of a) LLDPE, b) PEPA5,

c) PEPA10, d) PEPA15 and e) PEPA20.

The enthalpy of melting (ΔH_m) values of LLDPE, PEPA5, PEPA10, PEPA15 and PEPA20 were 117.9, 103.2, 95.0, 86.2 and 77.2 J g^{-1} respectively. Their corresponding degree of LLDPE crystallinity (X_c), calculated using Equation 5.2, were 40.2, 37.1, 36.0, 34.6 and 32.9 % respectively.

$$Xc(\%) = \frac{\Delta H_m}{w\Delta H_m^o} \times 100 \qquad \text{(Eq. 5.2)}$$

where w is the weight fraction of LLDPE in the composite and ΔH^o_m is the enthalpy of melting of 100 % crystalline PE, taken to be 293 Jg^{-1} [315]. The degree of crystallinity of LLDPE decreased upon blending with NR-PANI. The NR-PANI particles would have occupied spaces between the LLDPE chains and prevented them from attaining an ordered arrangement, thus resulting in lower crystallinity. In a previous report, the decrease in the degree of crystallinity of low density PE upon blending with camphorsulfonic acid-doped PANI was also observed [198].

5.3.5 Mechanical properties

The tensile strength, Young's modulus and elongation at break values of LLDPE as well as the LLDPE/NR-PANI samples are given Table 5.3. LLDPE exhibited a higher tensile strength and elongation at break than the NR-PANI/ LLDPE composite samples. The tensile strength and elongation at break decreased while the Young's modulus increased as the NR-PANI fraction in the composites increased. Similar observations on the mechanical properties

of PE/ HCl doped PANI composites have been made by Chipara *et al*. (2003) [199]. Overall, blending LLDPE with NR-PANI yielded materials with higher stiffness and a lower tensile strength. However, the LLDPE/NR-PANI composites still exhibited appreciable mechanical properties not very different from LLDPE itself. The tensile strength and elongation at break of LLDPE decreased by only 29 % and 36 % respectively, while the Young's modulus increased by 38 % upon incorporation of 20 % NR-PANI. A more severe decline in the mechanical properties has been reported when PANI was blended, even at lower loading, with other thermoplastics, such as PET [203, 316].

Table 5.3. Tensile strength, Young's modulus and elongation at break of LLDPE and NR-PANI/ LLDPE composites.

Sample	Tensile strength (MPa)	Young's modulus (GPa)	Elongation at break (%)
LLDPE	28 ± 2	0.29 ± 0.01	787 ± 51
PEPA5	25 ± 0.4	0.32 ± 0.01	734 ± 58
PEPA10	24 ± 0.6	0.35 ± 0.01	649 ± 23
PEPA15	22 ± 1	0.36 ± 0.01	564 ± 64
PEPA20	20 ± 0.2	0.40 ± 0.01	500 ± 18

The increase in Young's modulus, upon incorporation of NR-PANI, could be attributed to the filler-like behaviour of NR-PANI particles as was the case when PE was blended with starch in another study [304]. NR-PANI particles occupied spaces between the

LLDPE chains and thus increased its rigidity. The decrease in the tensile strength and elongation at break could be ascribed to the immiscibility, characterized by a lack of interfacial adhesion, between LLDPE and NR-PANI [199, 312]. Due to their differences in polarity, no effective interaction was achieved between NR-PANI and LLDPE. This resulted in a lack of interfacial adhesion between the components and was also evident in the ESEM micrographs. In the PANI/ PE composites, the PE chains are able to slip along the polyaniline particles due to poor adhesion. This exerts increased stress on the PANI particles, which have poor mechanical properties and low elasticity, leading to microcracks and polymer failure [199].

5.3.6 Free radical scavenging activity

The free radical scavenging capacity, used as a measure of antioxidant activity, of the LLDPE and NR-PANI/ LLDPE composites are presented in Figure 5.8. The free radical scavenging capacity of the samples increased with a greater fraction of NR-PANI in the composites. Saikia *et al*. (2010) have made similar observations with starch/ PANI composites where higher free radical scavenging, also measured using the DPPH assay, was achieved with increased PANI fraction in the composites [182]. Similar, observations have been made with regards to NR-PANI/ PET composites [316]. The NR-PANI/ PET composites were limited to a maximum of 3 % NR-PANI loading due to adverse effects on the mechanical properties of the composites upon greater NR-PANI loading. The free radical scavenging capacity of the NR-PANI/ PET composite containing 3 % NR-PANI was 2.78

nmol cm^{-2} [316], which was 17 times lower than the free radical scavenging capacity of PEPA20.

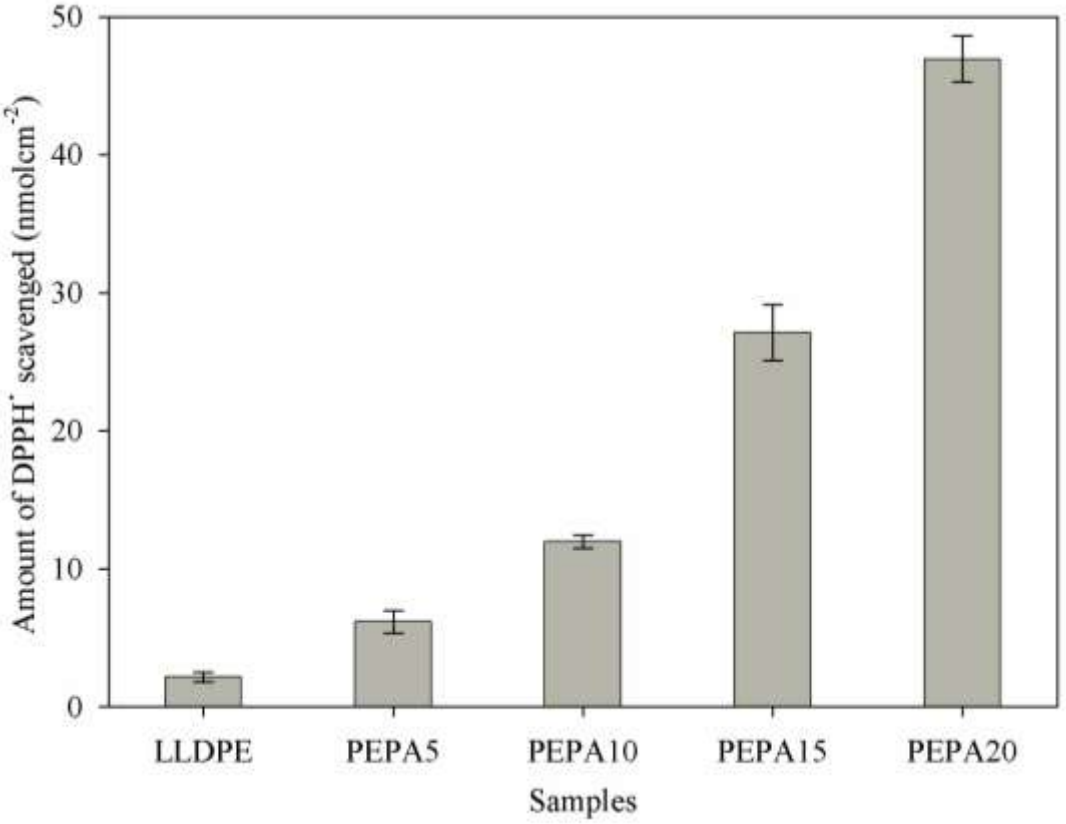

Figure 5.8. Free radical scavenging activity of LLDPE and NR-PANI/ LLDPE composites.

The free radical scavenging capacity of LLDPE itself was 2.16 nmol cm^{-2}. This is attributed to trivial amounts of antioxidants already present in the commercial LLDPE sample employed in this study. PE is normally compounded with antioxidants such as butylated hydroxytoluene (BHT) to reduce thermal degradation during processing [303]. However, these added antioxidants are not considered active packaging materials as they are not sufficient to prevent the oxidation of foodstuffs [45]. The free radical scavenging

capacity of a pristine NR-PANI sample was 3.50 μmol mg^{-1} , and when thermally treated at 150 ºC it decreased to 3.29 μmol mg^{-1} [278, 317]. The theoretical maximum free radical scavenging capacity of the NR-PANI/ LLDPE composites, based on the free radical scavenging capacity of NR-PANI treated at 150 ºC, the weight of the samples and NR-PANI content of the composites, would be 5.4, 9.8, 11.8 and 21.3 μmol cm^{-2} for PEPA5, PEPA10, PEPA15 and PEPA20 respectively. The observed free radical scavenging capacity of the composite samples, presented in Figure 5.8, were much less than the theoretical estimations and correspond to 0.1 to 0.2 % of the total NR-PANI loaded in the composites being available for DPPH radical scavenging. This result indicated that free radical scavenging activity is primarily a surface phenomenon. Most of the active polymer was confined within the bulk of the host polymer and only the polymer segments available at the surface participated in the scavenging of the free radicals.

NR-PANI reduces DPPH radicals by donating hydrogen atoms, while the NR-PANI segments are in turn oxidized to the pernigraniline form when in contact with DPPH radicals [258]. Therefore, a higher free radical scavenging capacity was achieved by having a higher concentration of NR-PANI particles exposed to the DPPH test solution. XPS analysis revealed increasing amount of nitrogen on the composite surfaces as the fraction of NR-PANI was increased. Consequently, higher radical scavenging activity was observed with an increased loading of NR-PANI in the composites. The free radical scavenging capacity of LLDPE increased by 2.8, 5.5, 12.5 and 21.7 times by incorporating 5, 10, 15 and 20 % NR-PANI respectively. This geometric type increase in the free radical scavenging capacity may

be due to greater accessibility of NR-PANI, by the DPPH free radicals as the NR-PANI fraction in the composites increased.

5.4 Conclusions

NR-PANI/ LLDPE composites, with 5, 10, 15 and 20 wt% NR-PANI, loading were prepared by melt processing. Electron microscopy revealed an even distribution of NR-PANI particles in the LLDPE matrix. The presence of distinct phase boundaries indicated lack of interfacial adhesion between the two components. Higher loading led to coalescence of NR-PANI and the size of NR-PANI particles dispersed in the LLDPE matrix increased. The electrical conductivities of the composites increased with a higher NR-PANI loading, also suggesting good dispersion and the formation of a conducting network of NR-PANI in the LLDPE matrix. FTIR spectra of the composites showed bands due to both NR-PANI and LLDPE. While the polymers had not undergone any noticeable degradation during blending, they had not interacted chemically as no additional bands were observed in the FTIR spectra. XPS analysis revealed an increasing amount of NR-PANI on the composite surfaces with higher loading, while the crystallinity of LLDPE decreased upon blending with NR-PANI. Blending with NR-PANI, also decreased the tensile strength and elongation at break of LLDPE, due to insufficient interfacial adhesion between NR-PANI and LLDPE, while the Young's modulus of the composites increased with NR-PANI loading, indicating a filler-like behaviour of NR-PANI. However, the NR-PANI/ LLDPE composites still exhibited excellent mechanical properties. The composites exhibited an increase in free radical

scavenging capacity, a measure of antioxidant activity, with an increase in NR-PANI loading, showing that they could be potentially used for antioxidant packaging applications.

CHAPTER SIX

Evaluation of Extruded LLDPE/ PANI Composites for Active Packaging Applications

This chapter has been submitted for publication as:

Nand A.V., Swift S., Uy B., Kilmartin P.A. Evaluation of extruded low polyethylene/ polyaniline blends for active packaging applications. *Journal of Food Engineering.* In press.

6.1 Introduction

Packaging is an integral part of the food sector. It has helped globalize the food industry by providing food preservation and protection systems so that long distance transfers of food stuffs can be facilitated [3]. Socio-economic demands for hygienic, safer and cost effective packaging materials have brought about considerable developments in the area of packaging. One innovation that is attracting increased attention is active food packaging systems. Active food packaging systems consist of active agents such as antioxidants or antimicrobials, either contained in sachets, functionalized on the surface or incorporated directly in the packaging matrices [6, 7, 38, 42, 45, 318 - 320]. These systems have the capability to interact dynamically with the products or their immediate environment to enhance product shelf life, beyond simply providing an inert barrier to external elements [321]. While the presence of antioxidants helps lower the rate of rancidity leading to lipid oxidation and brown coloration, antimicrobial agents lessen food spoilage by pathogenic microorganisms [6, 19, 322].

Various active packaging systems, containing synthetic as well as natural additives, have been reported in the recent literature. Flat extruded ethylene vinyl alcohol copolymer films containing green tea extract [43, 44] or beta-cylcodextrins [323], which exhibit antioxidant properties, have been proposed for active packaging applications. PLA films containing α-tocopherol and BHT [40], LDPE films containing natural antioxidants derived from barley husk [41] and PET trays sprayed with citrus fruit extracts [39] have also shown antioxidant properties. Moreover, soy protein isolate coated PP/ PE films [24], thymol and carvacrol incorporated PP films [22], PE and PE/ PA composite films coated with sorbic acid

[20] and PP films activated with plasticized proteins [5] have exhibited antimicrobial properties. However, it would be useful to incorporate a single active material showing both antioxidant and antimicrobial properties, in food packaging matrices.

PANI, an intrinsically conducting polymer, is gaining recognition for its antimicrobial [324, 325] as well as free radical scavenging properties [79, 80, 258, 278]. Thus, incorporating PANI in polymer matrixes such as LDPE, one of the most widely used packaging materials in the food sector [326], has the potential to yield antioxidant as well as antimicrobial active packaging systems.

The objective of the current study was to evaluate melt processed NR-PANI/ LLDPE composites, with both antioxidant and antimicrobial properties, for active packaging applications. The spectroscopic characterization, thermal and mechanical properties, microscopy and DPPH radical scavenging capacity of the composites have been reported chapter five. The results of biocompatibility, antimicrobial, ORAC, NR-PANI leaching, oxygen permeability and accelerated aging of fish oil tests on the NR-PANI/ LLDPE composites are presented here. Incorporating NR-PANI in a LLDPE matrix improved its oxygen barrier properties and introduced antioxidant as well as antimicrobial capabilities. Moreover, the NR-PANI/ LLDPE composites were biocompatible, making them suitable for food packaging applications.

6.2 Experimental

6.2.1 Materials

Fluorescein sodium salt, sodium thiosulphate, potassium iodide, chloroform, acetic acid, 6-hydroxy-2,5,7,8-tetramethylchroman-2-carboxylic acid (trolox), phosphate buffered saline (PBS), phosphate buffer tablets, resazurin sodium salt and Tween 80, purchased from Sigma-Aldrich, were used as received. For mammalian cell culture experiments using murine fibroblast cell line L929 (ATCC CCL-1), Dulbecco's Modified Eagle Medium (DMEM), 0.4 % Trypan blue solution and foetal calf serum (FCS) were obtained from Life Technologies. Cell culture was performed in 24-well tissue culture plates (TCP) (Nunc) and fluorescence readings were taken in black 96-well plates (Perkin Elmer). 25 % Glutaraldehyde was obtained from Scharlau. For bacterial culture of *Staphylococcus aureus* ATCC 6838, Difco tryptic soy broth (TSB) and Difco trypticase soy agar (TSA) were purchased from Fort Richard (Auckland). 2,2´-azobis-2-methylpropionamidine dihydrochloride (AAPH) was purchased from Merck. Ropufa fish oil was supplied by Invita Ltd (New Zealand). LLDPE resin (FC21HN) having a melt flow index of 1.0 g $(10\ min)^{-1}$ and 0.918 g cm^{-3} density was obtained from TCL Hunt Ltd (New Zealand). Details of other chemicals used are given in section 2.2.1.

6.2.2 PANI synthesis

NR-PANI, consisting of micro/ nanorods and flake-like structures, and G-PANI, having a granular morphology were synthesized as described in section 2.2.2.

6.2.3 Film preparation

NR-PANI/ LLDPE films, with 5, 10, 15 and 20 % loading of NR-PANI, designated as PEPA5, PEPA10, PEPA15 and PEPA20 respectively, was prepared as described section 5.2.3.

6.2.4 Leaching studies

4 x 4 cm^2 pieces of the film samples were immersed in 20 mL of Milli-Q water with occasional stirring. 5 mL aliquots were removed after 2, 7, 14 and 21 days and replaced with 5 mL fresh Milli-Q water. UV spectra of the leachates were obtained using a Shimadzu UV-1700 UV-visible spectrophotometer. 10 mg NR-PANI and G-PANI were dispersed in 10 mL water for 2 days and the spectra of the filtrates were obtained for comparison.

6.2.5 Oxygen transmission rate (OTR) measurement

50 cm^2 film samples were tested using a Mocon Ox-Tran 2/10 oxygen permeability system. The OTR was determined at 23 ± 0.2 °C and 2.5 % relative humidity with 100 % oxygen as the permeate. The samples were conditioned in the instrument for 3 hours before commencing the measurements. All samples were analyzed at least in duplicate.

6.2.6 Biocompability test

157 mm^2 LLDPE and NR-PAN/ LLDPE film disks were placed in petri dishes and sterilized under UV for 30 min. The film samples were then transferred to a 24-well tissue culture plate (TCP) containing 2 mL agar solution made in water. The agar was allowed to

set to anchor the film samples at the bottom of the wells. 1 mL aliquots of DMEM supplemented with 10 % heat activated FCS, containing 1 x 10^5 cell/ mL L929 mammalian cells, were placed in each well containing the film samples. Trypan blue exclusion was used to enumerate live cells. Test controls without any film samples were also set up. Cell adhesion and proliferation was measured using a resazurin fluorescence assay, which is used to quantify viable cells at various stages of proliferation [327]. The cells were incubated at 37 °C in 5 % CO_2 in air for 24 h, after which the DMEM was replaced with 1 mL of 500 µM resazurin solution in DMEM and incubated for 4 h. The supernatant was collected and centrifuged at 1600 rpm for 5 min at room temperature to pellet any cells. 100 µL of the centrifuged supernatant was aliquoted in triplicate into a 96 well black microtitre plate and the fluorescence value was recorded at 530 nm excitation and 590 nm emission using a Perkin Elmer Enspire 2300 Multilabel Reader. The cultures on sample films in the 24 well plates were washed once with DMEM before fresh DMEM supplemented with 10 % FCS was added and returned to the incubator. The above procedure was repeated daily over the course of 4 days. After obtaining the fluorescence reading on the 4^{th} day, the cells were washed with PBS, fixed with 2.5 % glutaraldehyde in PBS and stored at 4 °C. The fixed cells were imaged using a FEI Quanta 200FE environmental electron scanning microscope (ESEM) at 2 °C, after washing away the glutaraldehyde with Milli-Q water. At least three trials of each sample were undertaken.

6.2.7 Antimicrobial activity

Antimicrobial effects of the films was analysed using the JIS Z 2801:2000 assay. Film samples cut into 50 x 50 mm^2 and 40 x 40 mm^2 pieces were sterilized by soaking in ethanol for 1 min, after which the samples were aseptically transferred to sterile petri dishes and left to air dry in a class II biosafety cabinet. An overnight TSB culture of *S. aureus* ATCC 6838 was diluted into PBS to 1 x 10^7 CFU/ mL and 100 µL, containing 1 x 10^6 CFU, was dispensed on the surface of the dry 50 x 50 mm^2 film samples and covered with the 40 x 40 mm^2 film samples. The 40 x 40 mm^2 sample was pressed down to spread the cell suspension evenly over the 50 x 50 mm^2 piece, ensuring that no air bubbles were trapped between the film samples. The samples were incubated in a humid environment at 37 °C for 24 hours under static conditions. The samples were then aseptically transferred into stomacher bags and 10 mL of TSB containing 1 % (v/v) Tween 80 was added. The bags were homogenised twice for 30 s with a 1 min break between the two sessions using a stomacher to resuspend the bacteria in the TSB. Pour plates of 0.9 mL homogenate plus 19 mL molten TSA cooled to 55 °C and 9 mL homogenate plus 9 mL molten TSA were made. Homogenate dilutions (1:200, 1:2000 and 1:20000) were made in PBS and plated to TSA. Agar plates were incubated at 37 °C for 24 h, after which the agar plates were examined for colony growth and CFU enumerate. At least three trials of each sample were performed.

6.2.8 ORAC assay

A 4.20 x 10^{-6} M stock solution of fluorescein sodium salt was made using phosphate buffer (pH 7.4) and stored in the dark at 4 ºC, where it is stable for several weeks [328]. A

fresh 4.20 x 10^{-8} M working solution was prepared daily by diluting the stock solution with phosphate buffer. A 1.55 x 10^{-5} M AAPH solution was made in phosphate buffer on the day of use and kept on ice. LLDPE and NR-PANI/ LLDPE sample discs measuring 157 mm^2 were placed in a 24 well plate. 1.9 mL fluorescein sodium salt working solution was added to each well containing the samples, followed by the addition of 100 µL AAPH solution. The solutions were mixed manually for 5 seconds and the fluorescence measurements were started immediately using a Perkin Elmer Walac 1420 Victor^3 multilable counter operating with a 485 nm excitation and 535 nm emission wavelength. The fluorescence values were recorded at 2 min intervals for 198 min at 37 ºC. A blank, without any film samples, was also set up and fluorescence values recorded as for the film samples. The fluorescence readings of the solutions containing the film samples were corrected for auto fluorescence by the samples before any calculations were performed. The fluorescence values of 100 µL trolox standards (12.5, 50, 100 and 200 µM) were also recorded after addition to 1.9 mL fluorescein sodium salt solution followed by 100 µL of AAPH. The final trolox concentrations were 0.6, 2.4, 4.8 and 9.5 µM. A blank with additional 100 µL phosphate buffer in place of trolox was run with the standards. All samples were analysed in triplicate.

6.2.9 Accelerated aging of oil

157 mm^2 LLDPE and NR-PANI/ LLDPE film disks were immersed in 10 mL Ropufa fish oil having a peroxide value (*PV*) of 6 meq peroxides/ kg oil and incubated at 60 °C. A control, without any film samples, was also setup. The *PV* of the oil samples was determined after 3, 6 and 9 days of incubation.

Approximately 3 g of the fish oil was weighed in a conical flask and 30 mL of chloroform/ acetic acid (2:3) mixture by volume was added to it. The contents were stirred until all of the fish oil dissolved in the chloroform/ acetic acid mixture. 0.5 mL of saturated potassium iodide solution, prepared by dissolving 20 g of potassium iodide in 12 mL Milli-Q water, was added to the flask. The contents of the flask were stirred occasionally and allowed to interact for 1 min. The hydroperoxides, generated through lipid oxidation during the accelerated aging of oil, produced iodine upon reaction with potassium iodide as follows:

$$ROOH + 2H^+ + 2I^- \rightarrow I_2 + ROH + H_2O$$

$$ROOR + 2H^+ + 2I^- \rightarrow I_2 + 2ROH$$

$$I_2 + 2S_2O_3^{2-} \rightarrow S_4O_6^{2-} + 2I^-$$

30 mL of Milli-Q water was added to the flask and the liberated iodine was immediately titrated with 0.05 N sodium thiosulphate solution using 0.5 mL of 1 % starch solution as an indicator. A blank, without any oil sample, was also run. The *PV* of the oil sample exposed to LLDPE and NR-PANI/ LLDPE composite samples and the control were determined using Equation 6.1.

$$PV\,(\text{meq peroxides/kg oil}) = \frac{(S-B)\times N\times 1000}{m} \qquad \text{(Eq. 6.1)}$$

where *S* is the volume of titrant used in the titration of the sample, *B* is the volume of titrant used in the titration of a blank without any oil sample, *N* is the normality of the sodium thiosulphate titrant (0.05N) and *m* is the weight of the oil sample (g).

6.3 Results and Discussions

6.3.1 Leachibility of NR-PANI

The leachibility of NR-PANI from the NR-PANI/ LLDPE composites in Milli-Q water, mimicking an aqueous food simulant [44], was monitored by UV-visible spectroscopy. UV-vis spectra of filtrates of NR-PANI and G-PANI suspensions in Milli-Q water, shown in Figure 6.1, were also recorded. The spectra of NR-PANI exhibited a peak at ca. 410 nm, which can be attributed to $n \rightarrow \pi^*$ transitions of the sp^2 nitrogen atoms [329] of phenazine-type oligomers. NR-PANI was synthesized via the "falling pH" route and phenazine-type structures form at the initial higher pH, and are then coated with more regular PANI as the pH of the synthesis media falls [258]. This was confirmed by the absence of the ca. 410 nm peak in the spectra of the filtrate of the G-PANI suspension as shown in Figure 6.1. G-PANI, synthesized at low pH, consists of only regular PANI chains, free of the phenazine type structures [258].

A representative set of spectra of the leachates of LLDPE after 2 days and PEPA20 film after 2, 7, 14 and 21 days are given in Figure 6.1. The spectra of the leachates from PEPA20 after 2 days had a slightly higher absorbance at ca. 410 nm compared to the LLDPE sample after 2 days. This may be due to leaching of trivial amounts of NR-PANI from the

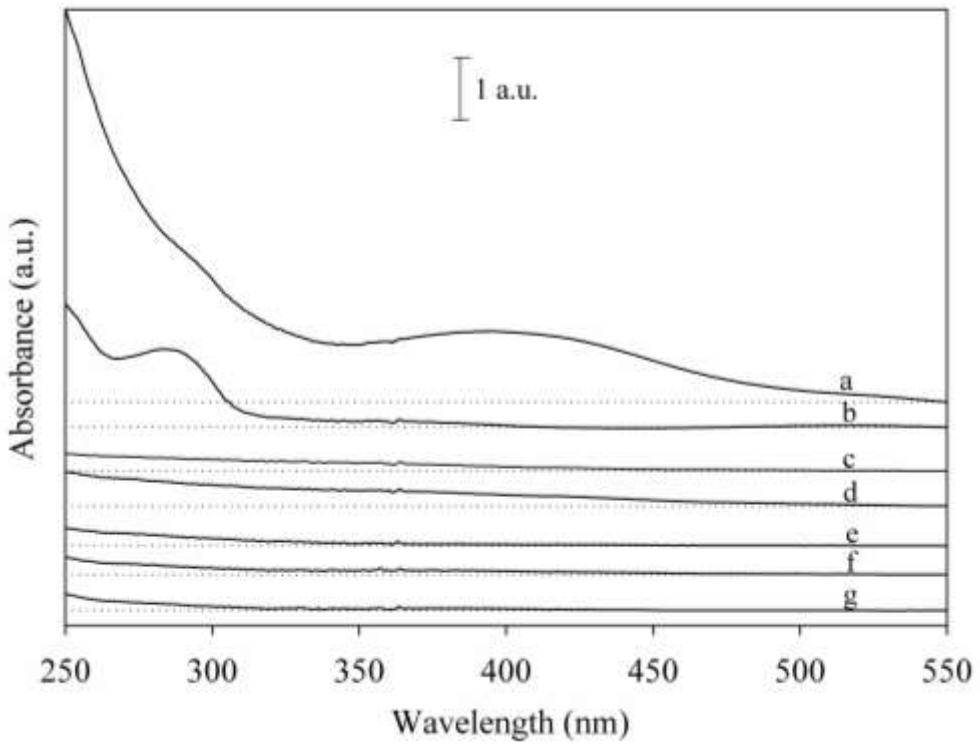

Figure 6.1. UV spectra of filtrates of a) NR-PANI after 2 days, b) G-PANI after 2 days, c) LLDPE after 2 days and PEPA20 after d) 2 days, e) 14 days and g) 21 days.

films, or may be due to a slightly greater degree of LLDPE components leaching from the composite films. A distinct peak at ca. 410 nm signifying the presence of NR-PANI, was absent in the spectra of the test media of all the composite samples, illustrating no significant leaching of NR-PANI from the composite films. Schwope *et al*. (1987), have observed the leachibility of low molecular weight active agents such as BHT and Irganox 1010 from LDPE packaging films [303]. However, NR-PANI, being a polymeric compound, has a much higher molecular weight than BHT and Irganox 1010 and the larger NR-PANI chains appear to be sufficiently trapped within the LLDPE matrix, and thus no significant leaching was

observed. Dispenza *et al*. (2012), have also observed that polyaniline nanoparticles, dispersed into a nanocomposite hydrogel, did not migrate out upon immersion in distilled water at 40 °C for 72 hours [194]. Active films having synthetic additives are losing their consumer appeal due to safety issues arising from the migration of the additives into the food products [3, 22, 40, 330]. However, polymeric additives, like NR-PANI, have considerable potential in the packaging industry as they are active materials but do not leach significantly from their host matrices.

6.3.2 Oxygen permeability

The oxygen permeability values of the samples were calculated using Equation 6.2.

$$P = \frac{\text{OTR}}{\Delta p} \times t \qquad \text{(Eq. 6.2)}$$

where P is the oxygen permeability (cm^3.mm/ m^2.day.atm), OTR is the oxygen transmission rate (cm^3/ m^2.day) and Δp is the partial pressure (atm) difference across the film barrier and t is the film thickness (mm).

Oxygen permeability results of the LLDPE and NR-PANI/ LLDPE films are presented in Figure 6.2. The oxygen permeability of LLDPE was 102.2 ± 0.7 cm^3.mm/ m^2.day.atm. This value was comparable to the results of Shields *et al*. (2008), where the oxygen permeability of LLDPE was determined to be ca. 110 ml.mm/ m^2.day.atm [305]. The incorporation of 5, 10, 15 and 20 wt % NR-PANI in the LLDPE matix resulted in a 6.2, 18.2,

21.9 and 32.2 % lowering of the oxygen permeability of LLDPE respectively. Permeation studies on PANI membranes have shown that they have relatively low oxygen permeability [331]. It is hypothesised that when incorporated into LLDPE, the NR-PANI particles have the potential to increase the tortuosity in the diffusive path of oxygen through the matrix. Permeability is lessened when length of the path that the penetrating gas travels through a material is increased [305]. Therefore, the oxygen barrier property of LLDPE was improved through the incorporation of NR-PANI. Similarly, Walker *et al*. (2007), have also shown an improvement in the barrier properties of PE, where the oxygen permeability was reduced after incorporation of starch [304].

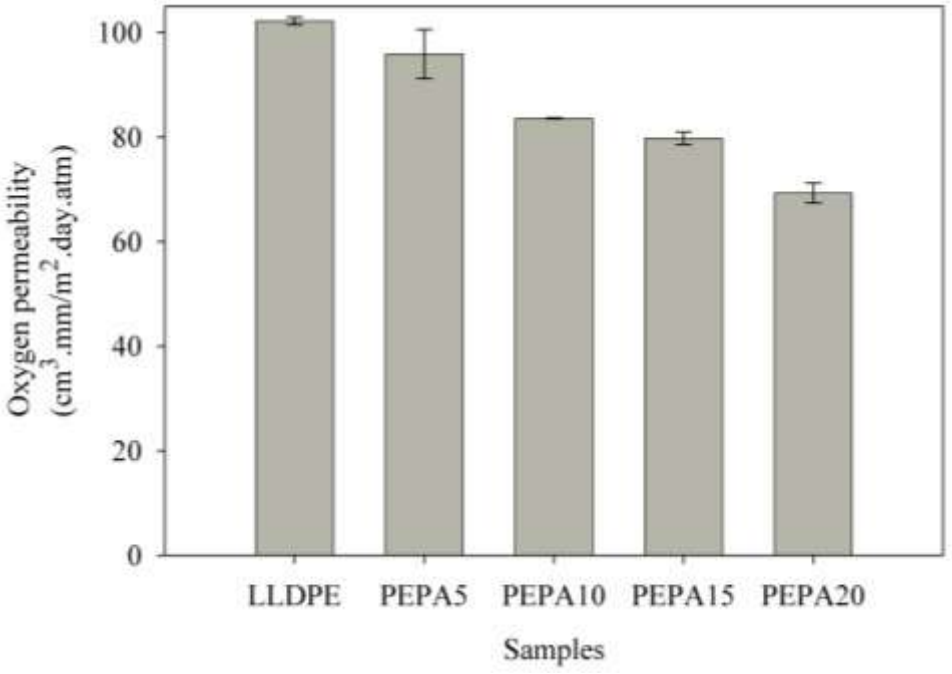

Figure 6.2. Oxygen permeability of LLDPE and NR-PANI/ LLDPE films.

6.3.3 Biocompatibility

To establish that LLDPE and NR-PANI/ LLDPE films can provide a surface able to support the growth of mammalian cells, L929 cells were seeded into the wells of TCP containing the film samples. Empty wells were inoculated as controls. It is hypothesized that there would be no reduction in L929 cell growth on LLDPE films containing NR-PANI if these were biocompatible. Growth was measured daily, for four days, as fluorescence produced following incubation with resazurin (Figure 6.3). The measurements from three independent experiments with three replicates each time showed no inhibition of growth when NR-PANI is blended with LLDPE. The NR-PANI/ LLDPE films, in fact, had a higher growth compared to the LLDPE sample, possibly due to the increased attachment arising from an increased positive charge conferred by NR-PANI chains on the film surface.

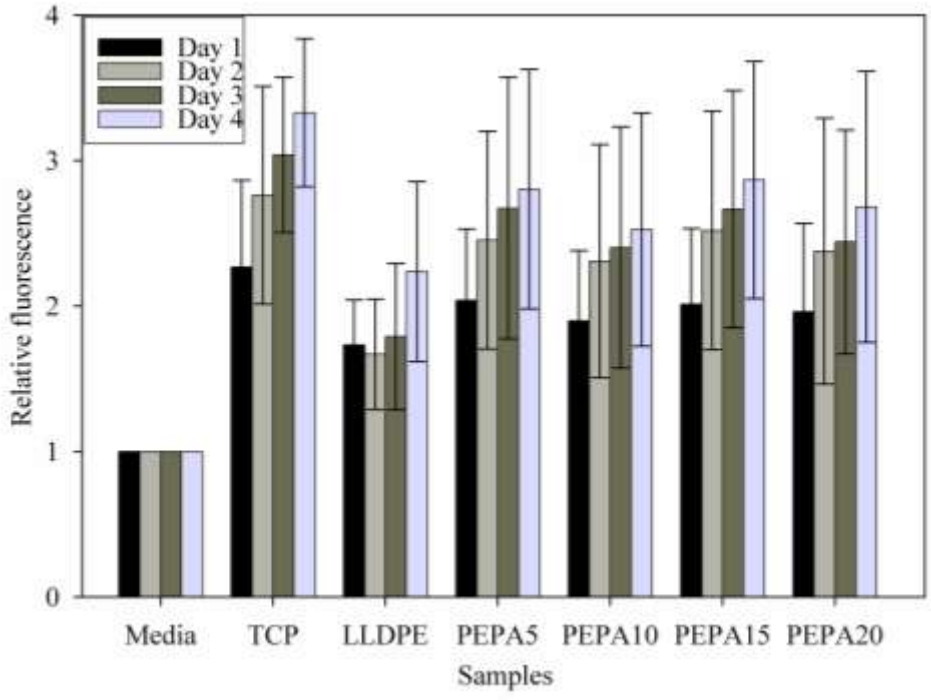

Figure 6.3. L929 mammalian cell viability on LLDPE and NR-PANI/ LLDPE composites.

The cell density on the NR-PANI/ LLDPE composites as well as the LLDPE samples increased over the four days, demonstrating that the film surfaces were conducive to cell proliferation. The ESEM images, given in Figure 6.4, also demonstrated that the cells were able to adhere and proliferate on the film samples, thus substantiating the biocompatibility of LLDPE and NR-PANI/ LLDPE composites. In the composite samples, NR-PANI did not negate the biocompatibility of LLDPE, its host polymer. This phenomenon has been previously witnessed when PANI nanoparticles were incorporated in poly (vinyl alcohol) hydrogels [194]. However, the polystyrene TCP exhibited higher viable cell density than all of the test samples. This could be attributed to its superior cell attachment properties.

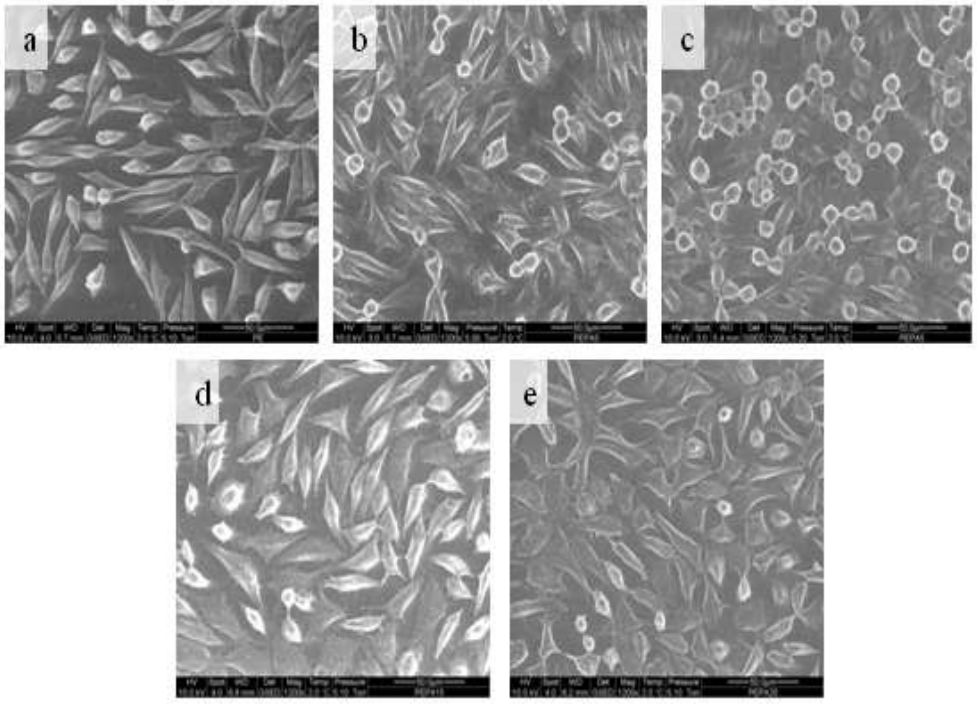

Figure 6.4. ESEM images of L929 mammalian cell proliferation on a) LLDPE, b) PEPA5, c) PEPA10, d) PEPA15 and e) PEPA20.

6.3.4 Antimicrobial efficacy

To establish that biocompatible LLDPE films containing NR-PANI also exhibited antimicrobial properties, 1 x 10^6 CFU *S. aureus* cells were incubated for 24 hours between matching films of LLDPE or NR-PANI/ LLDPE. Films of NR-PANI showed at least 10^6 fold reduction in viable *S. aureus* (Figure 6.5), whereas no reduction was seen for the pure LLDPE films. Representative pour plates showing the results of the antimicrobial tests on the film samples are shown in Figure 6.6. The LLDPE test petri dish shows innumerable *S. aureus* colonies where as the NR-PANI/ LLDPE test petri dishes do not.

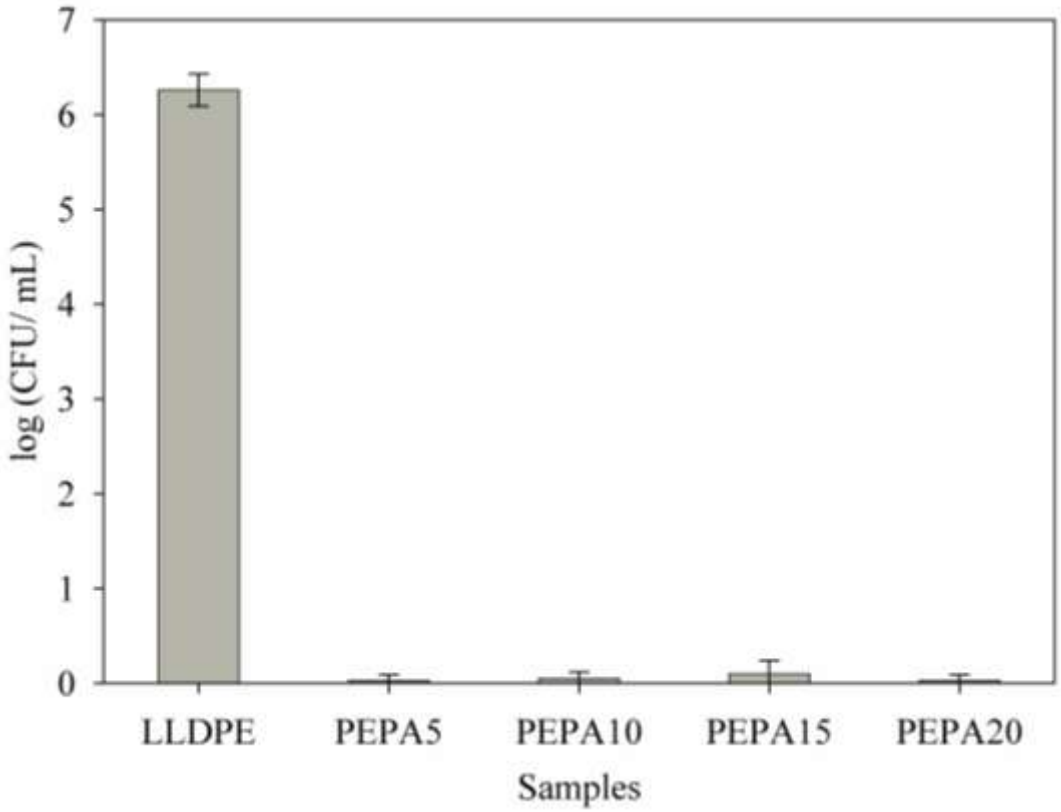

Figure 6.5. Antimicrobial activity against *S. aureus*.

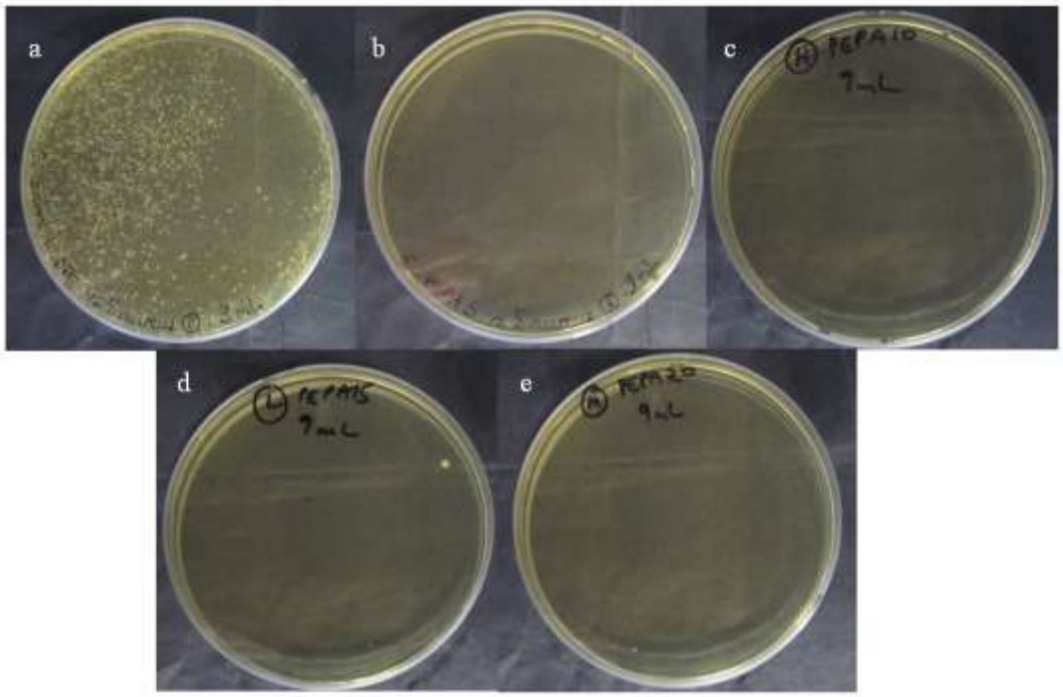

Figure 6.6. Antimicrobial test results of a) LLDPE, b) PEPA5, c) PEPA10, d) PEPA15 and e) PEPA20.

Earlier studies have shown that PANI possesses antimicrobial qualities [324, 325]; therefore, the antimicrobial properties of the composite films are due to the presence of NR-PANI. Although the mechanism of antimicrobial action is not fully resolved, the bacterial cell walls may collapse due to the electrostatic adherence between NR-PANI and the bacteria, leading to leakage of intracellular fluids and consequently death of the bacteria [325]. Further studies have indicated that the mechanism of killing may be more complex, and involve metabolic dysregulation and oxidative stress [324]

6.3.5 Antioxidant properties

NR-PANI is known to have an excellent DPPH radical scavenging capacity [258], and when incorporated in PET or LLDPE matrices, the composites also exhibited free radical scavenging characteristics [316, 332]. The DPPH radical scavenging assay uses a stable model free radical to assess the radical scavenging abilities of samples [333]. However, the ORAC assay is considered to be the most useful tool to estimate the "total antioxidant activity" of a sample [334]. The ORAC assay was used to express the "total antioxidant activity" of LLDPE and NR-PANI/ LLDPE composites through monitoring of the oxidation of fluorescein, used as a fluorescence probe, into nonfluorescent products by the peroxy radicals generated in the analysis mixture. The relative fluorescence versus time curves of the LLDPE and NR-PANI/ LLDPE composite samples are given in Figure 6.7. The areas under the curves (*AUC*) were calculated using Equation 6.3.

$$AUC = \left(0.5 + \frac{f_2}{f_0} + \frac{f_4}{f_0} + \frac{f_6}{f_0} + ... + \frac{f_n}{f_0} + ... + \frac{f_{198}}{f_0} \right) \times \Delta t \qquad \text{(Eq. 6.3)}$$

where f_0 is the initial fluorescence reading, f_n is the fluorescence reading at time *n* and *t* is the cycle time (2 min). The *Net AUC* was calculated using Equation 6.4.

$$Net\ AUC = AUC_{sample} - AUC_{blank} \qquad \text{(Eq. 6.4)}$$

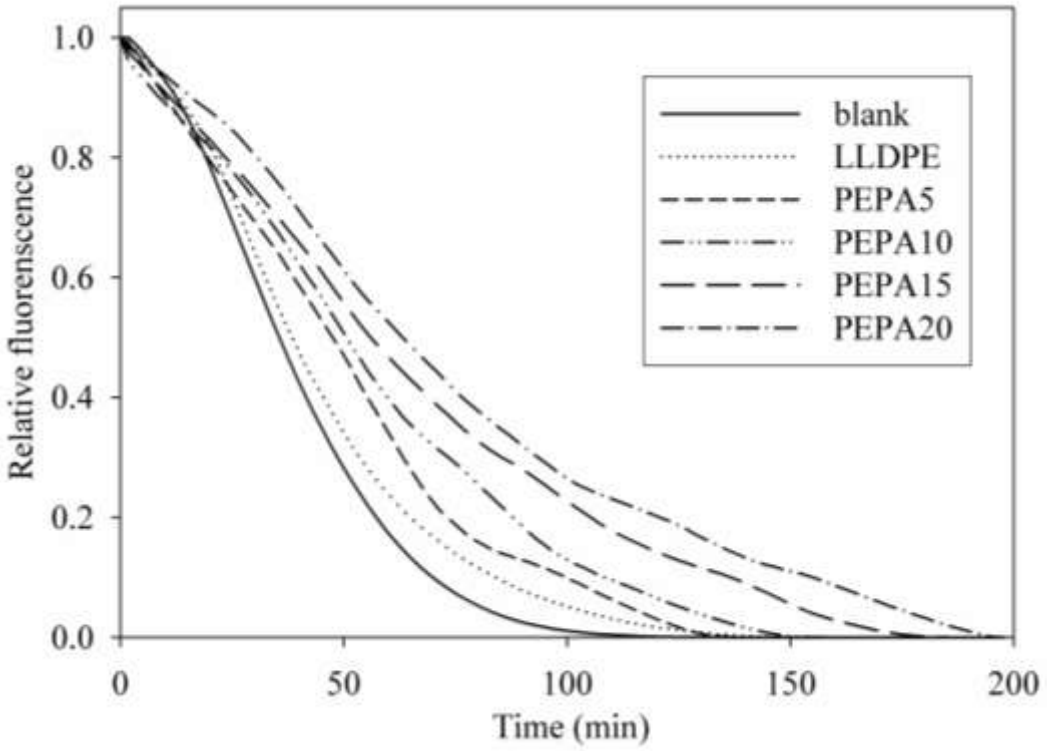

Figure 6.7. Fluorescence decay curves of fluorscein in the presence of LLDPE and NR-PANI/ LLDPE composites.

The ORAC assay has been applied mostly to liquid samples such as milk, wine and food extracts [328, 335, 336, 337]. Recently, it was applied to organic extracts of essential oil/ PP active packaging films [338]. An adaptation of methods employed by other researchers [328, 337] was used to approximate the relative ORAC values of the polymeric LLDPE and NR-PANI/ LLDPE samples in the current study. The trolox concentration (*C*, $\mu molL^{-1}$) corresponding to the *Net AUC* of the sample was calculated using the linear regression equation of the trolox calibration plot (Equation 6.5). The final results were converted to trolox equivalents using Equation 6.6.

$$Net\ AUC = 0.322\ C - 0.528 \qquad \text{(Eq. 6.5)}$$

$$\text{Relative ORAC value (trolox equivalent, } \mu\text{molm}^{-2}) = \left(\frac{C \times V}{A} \right) \qquad \text{(Eq. 6.6)}$$

where V is the volume of analysis mixture (1 x 10^{-4} L) and A is the area of the sample (1.57 x 10^{-4} m^2). The *AUC*, *Net AUC* and relative ORAC values of LLDPE and NR-PANI/ LLDPE composites are given in Table 6.1.

Table 6.1. *AUC*, *Net AUC* and relative ORAC values of LLDPE and NR-PANI/ LLDPE composites.

Sample	*AUC*	*Net AUC*	Relative ORAC value (trolox equivalents, μmolm^{-2})
LLDPE	42.84 ± 1.61	5.77 ± 2.16	12.5 ± 3.2
PEPA5	48.68 ± 2.32	11.61 ± 2.32	24.1 ± 4.6
PEPA10	52.62 ± 3.11	20.05 ± 3.11	40.8 ± 6.1
PEPA15	65.77 ± 0.32	28.70 ± 0.32	57.8 ± 0.6
PEPA20	71.70 ± 3.95	35.70 ± 1.51	71.7 ± 2.9

The *AUC*, *Net AUC* and consequently the relative ORAC values of the samples increased with higher loading of NR-PANI in the composites. This translates into higher

antioxidant activity as the amount of NR-PANI in the composites increased. Saenz *et al*. (2003), observed that an increase in the *Net AUC* reflects a greater activity of the antioxidants to prevent potential peroxy radical damage [336]. The NR-PANI chains in the film samples scavenged the peroxy radicals by reducing them to neutral species. In the process, NR-PANI was oxidized, as shown in Scheme 6.1. Therefore, there were fewer radicals left to interact with fluorescein, the fluorescence probe, resulting in a prolonged decay of its fluorescence. Davalos *et al*. (2003), have also observed a retarded decay of the fluorescence curve in the presence of antioxidants [328]. The relative fluorescence versus time curves of the samples, Figure 6.7, clearly shows a slower decline in the fluorescence values as the amount of NR-PANI in the samples increased, hence resulting in higher *Net AUC* values. However, an interesting observation was that even in the presence of a pure LLDPE sample, the fluorescence decay was slower than a blank without any samples. This could be attributed to the presence of trivial amounts of antioxidants in the LLDPE sample employed in this study, as LDPE is normally compounded with antioxidants to reduce thermal degradation during processing [303]. A 5, 10, 15 and 20 % loading of NR-PANI resulted in 93, 226, 362 and 474 % increase, respectively, in the relative ORAC values (trolox equivalent), reflecting an increase in the antioxidant activity of NR-PANI/ LLDPE composites as the amount of incorporated NR-PANI increased.

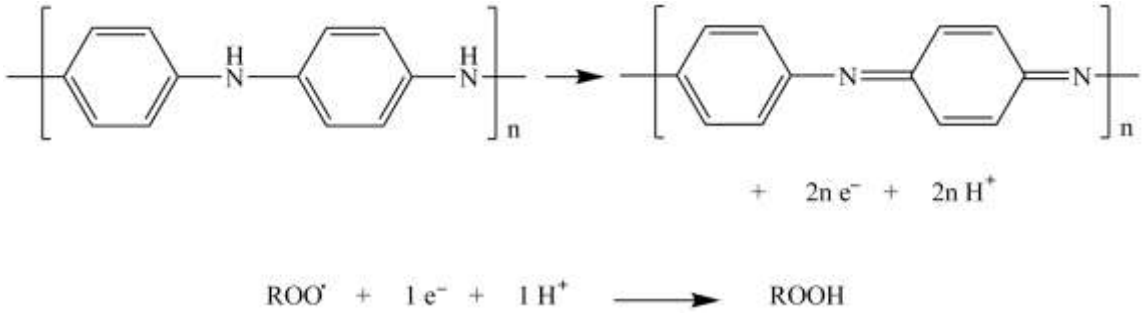

Scheme 6.1. Neutralization of peroxy radicals by NR-PANI.

6.3.6 Accelerated aging of Ropufa fish oil

Polyunsaturated fats, such as Ropufa fish oil, are prone to lipid oxidation where the non-conjugated double bonds are converted to conjugated double and triple bonds [41, 339]. The degree of lipid oxidation can be assessed by quantifying either the primary or secondary products of the oxidation reaction. Peroxide values (*PV*), a quantification of the peroxides which are the primary oxidation products, have been utilized most often for this purpose [41]. Ropufa fish oil samples were subjected to accelerated aging at 60 °C, in the presence and absence of the LLDPE or NR-PANI/ LLDPE films.

The Ropufa fish oil control samples without any test films showed an increase in *PV* values, indicating oxidation of the lipids, over the 9 day period. However, a decrease in the *PV* value of the oil sample was observed after 9 days. This was attributed to the lower availability of the substrate and decomposition of the peroxide molecules [41]. Hence, tests on the oxidation of Ropufa fish oil were limited to 9 days.

Table 6.2. *PV* of Ropufa fish oil in the presence of LLDPE and NR-PANI/ LLDPE films.

Samples	*PV* of Ropufa oil (meq peroxides/ kg oil) after		
	3 days	6 day	9 days
Control	44.2 ± 0.3	91.9 ± 2.2	122 ± 2.2
LLDPE	36.2 ± 0.8	72.1 ± 1.1	94.4 ± 1.9
PEPA5	26.7 ± 2.0	40.2 ± 1.6	69.4 ± 1.0
PEPA10	16.8 ± 1.5	27.0 ± 1.4	56.9 ± 0.3
PEPA15	12.4 ± 1.1	18.5 ± 1.3	45.6 ± 0.7
PEPA20	7.5 ± 0.1	12.6 ± 1.2	38.3 ± 0.7

The *PV* of Ropufa fish oil, given in Table 6.2, also increased in the presence of all the film samples over the 9 days. However, a lower increase, compared to the test controls, was observed in the presence of the NR-PANI/ LLDPE films. The magnitude of the increase in *PV* values on all analysis days were in the order: LLDPE > PEPA5 > PEPA10 > PEPA15 > PEPA20. Lower *PV* values were observed as the concentration of NR-PANI in the films became higher. For instance, on the 9^{th} day, the *PV* of LLDPE, PEPA5, PEPA10, PEPA15, PEPA20 were 23, 43, 53, 63 and 69 % lower, respectively, than the control sample. LLDPE, without any NR-PANI, also exhibited a slight suppression in the *PV* values, which could be due to its trivial amounts of antioxidants, incorporated as processing aids. The NR-PANI/ LLDPE composites, thus, demonstrated their antioxidant capability by slowing the oxidation of Ropufa fish oil. Lipid oxidation is a chain reaction through the formation of free radicals [45]. Therefore, the antioxidant capacity of the composite films is attributed to the free

radical scavenging property of NR-PANI, which helped terminate oxidation at an early stage and lessened build up of new radicals in the oxidation process. Nerin *et al*. (2006) have also shown that antioxidants could be effectively utilized to prevent the radical initiated oxidation process [340].

6.4 Conclusions

Incorporating NR-PANI into LLDPE improved the properties of the host polymer, as needed for active packaging applications. The NR-PANI particles increased the tortousity in the diffusive path of oxygen through the matrix, resulting in a lower oxygen permeability. NR-PANI was trapped within the LLDPE matrix and the composites did not show significant leaching of NR-PANI in Milli-Q water, even at a 20 % loading. The NR-PANI/ LLDPE composites were also biocompatible to mammalian cells, signifying their safety when in contact with food stuffs. Incorporation of NR-PANI enhanced the antioxidant capability of LLDPE and introduced antimicrobial efficacy. The oxidation of Ropufa fish oil was delayed in the presence of the NR-PANI/ LLDPE composites. Higher protection from oxidation was observed with an increased loading of NR-PANI in the composite films. Therefore, the NR-PANI/ LLDPE composites represent novel materials, with both antioxidant and antimicrobial properties, available for use in active packaging applications.

CHAPTER SEVEN

Conclusions

7.1 General Conclusions

The central aim of this study was to demonstrate the relevance of PANI, a solid antioxidant, in the development of active packaging materials. Most of the current applications of PANI are based mainly on its ability to conduct electricity. However, the outcomes of this study have the potential to add new dimensions to the applications of PANI. The free radical scavenging property of PANI can be successfully utilized to maintain the quality and extend the shelf – life of food products using PANI based packaging materials. During the course of this study, the factors affecting free radical scavenging capacity of PANI were studied before PANI was compositeed with PET and LLDPE to yield active packaging materials.

The effects of conductivity, surface area and oxidation level on the free radical scavenging capacity of PANI were investigated on four different samples. NR-PANI was synthesized by oxidizing aniline using APS via the "falling pH" route; while G-PANI was prepared by oxidizing aniline using APS in the presence of HCl. NR-PANI and G-PANI

were further dedoped using ammonium hydroxide to yield NR-PANIdd and G-PANIdd respectively. G-PANI, being HCl doped, had a higher electrical conductivity than the NR-PANI sample. The NR-PANI sample consisted of nano/ micro – rods and flakes and G-PANI had a granular morphology. Dedoping did not affect the morphology of either NR-PANI or G-PANI.

Interestingly, the granular G-PANI sample had a higher BET surface area than the nano/ micro – rod NR-PANI sample. The BET surface area of the samples was in the order: G-PANIdd > G-PANI > NR-PANIdd > NR-PANI. Dedoping increased the BET surface area of the as prepared PANI samples, indicating an increase in the free volume upon removal of dopants. The level of oxidation of the PANI samples, determined through the analysis of N 1s core level XPS spectra, was in the order: G-PANIdd > NR-PANIdd > G-PANI > NR-PANI. The oxidation level of both NR-PANI and G-PANI increased upon treatment with ammonium hydroxide. NR-PANI exhibited the highest DPPH radical scavenging capacity, followed by G-PANI and NR-PANI having similar activities while G-PANIdd showed the lowest DPPH radical scavenging capacity. The free radical scavenging capacity of PANI was thus independent of conductivity and surface area but heavily dependent on the oxidation level of the sample. A lower oxidation level resulted in a higher DPPH radical scavenging capacity across the samples. NR-PANI, being the more reduced sample, would be the ideal choice for antioxidant applications.

Thermal processing is the industrially favored method for large scale processing of polymers. Therefore, the thermal stability and the effect of elevated temperatures on the free radical scavenging capacity of the PANIs were examined. The as–prepared NR-PANI, NR-

PANIdd, G-PANI and G-PANIdd were thermally stable, in air, up to 300, 340, 250 and 350 °C respectively. Thermal degradation of both NR-PANI and G-PANI followed first order kinetics at higher temperatures. The PANI samples were further treated isothermally at 100, 125, 150, 175, 200, 250 and 300 °C for 30 minutes in air. Thermal treatment did not have a pronounced effect on the morphology of the PANIs. NR-PANI and NR-PANIdd retained a nano/ micro – rod and flake like morphology while G-PANI and G-PANIdd retained their granular morphologies up to 300 °C.

The PANI samples became amorphous upon thermal treatment. Conductivity of both NR-PANI and G-PANI increased upon thermal treatment at 100 °C but decreased after being subjected to higher temperatures. The initial increase was attributed to loss of moisture from the polymer samples while the decrease in conductivity was attributed to loss of ordered arrangement of PANI chains upon thermal treatment. The *Q/B* ratios of the PANIs, determined from the corresponding FTIR spectra, initially decreased upon thermal treatment up to 175 °C for NR-PANI and NR-PANIdd; and 200 °C for G-PANI and G-PANIdd. However, the *Q/B* ratios increased after treatment at higher temperatures. The spin concentrations of the PANIs, determined by ESR, increased after treatment up to 175 °C for NR-PANI and G-PANI, 150 °C for NR-PANIdd and 250 °C for G-PANIdd; but decreased after treatment at higher temperatures. The spectroscopic measurements indicated that the PANIs underwent crosslinking at lower temperatures, followed by oxidation at higher temperatures.

NR-PANI and NR-PANIdd showed a slight decrease in DPPH free radical scavenging capacity upon thermal treatment up to 175 ºC and a rapid decrease after treatment

at higher temperatures. G-PANI and G-PANIdd also exhibited a slight decrease in DPPH free radical scavenging capacity upon thermal treatment up to 200 ºC and a rapid decrease thereafter. The rapid decrease in the DPPH radical scavenging capacity of the PANIs was attributed to the oxidation of the polymer chains. Furthermore, the free radical scavenging capacity of the PANIs was not related to the spin concentrations of the polymers.

NR-PANI/ PET blends were prepared by dispersing NR-PANI, having a high free radical scavenging capacity, in the melt of PET at 265 °C. The composites had 1, 2 and 3 wt% loading of NR-PANI. Optical microscopy revealed an even distribution of NR-PANI particles in the PET matrix. The electrical conductivity of the composite films increased with higher NR-PANI loading. The presence of NR-PANI on the surface of the composite films was confirmed by XPS. The MFI values of the composites increased as the amount of NR-PANI increased, indicating easier flow of the melt with higher NR-PANI composition. The MFI analysis thus suggested a lowering of the PET molecular weight. This was attributed to the hydrolysis of the PET chains at the high processing temperature, aided by the occluded moisture and acidic dopants of NR-PANI. The hydrolysis of PET chains were further confirmed by the increasing O/C ratios, deduced from the XPS spectra of the samples, with higher loading of NR-PANI in the composites.

The crystallinity of PET increased with increasing amount of NR-PANI in the composites. Lower molecular weight chains, resulting from the hydrolysis of PET, upon incorporation of NR-PANI, realigned easily leading to higher PET crystallinity. Incorporation of NR-PANI in the PET matrix had a detrimental impact on the mechanical properties of PET. The tensile strength and elongation at break decreased while the Young's

modulus of PET increased with higher loading of NR-PANI. However, the composites exhibited free radical scavenging capabilities when tested using the DPPH assay. The DPPH radical scavenging capacity of PETPA1, PETPA2 and PETPA3 films were 1.1, 1.7 and 2.8 $nmolcm^{-2}$ respectively. The DPPH radical scavenging capacity of the composites increased with increasing amount of NR-PANI in the composites. NR-PANI/ PET composites can be potentially utilized for antioxidant active packaging applications; however, their mechanical properties need to be improved if higher NR-PANI loading is to be considered.

NR-PANI/ LLDPE composites were also fabricated by dispersing NR-PANI in the melt of LLDPE. The blending was done at 150 °C with 5, 10, 15 and 20 wt% loading of NR-PANI in the composites. ESEM images revealed an even dispersion of NR-PANI in the LLDPE matrix with coalescence of the NR-PANI particles at higher loading. The increase in the electrical conductivity of LLDPE upon addition of NR-PANI also indicated good dispersion of the additive. Phase boundaries between NR-PANI and LLDPE were also visible in the ESEM images, suggesting absence of sufficient interfacial adhesion due to the difference in the polarity of the two polymer components. FTIR and XPS results also confirmed the lack of chemical interactions between NR-PANI and LLDPE upon blending. However, the NR-PANI/ LLDPE composite films had good mechanical properties. The composite films also exhibited excellent DPPH radical scavenging capacity, which increased with higher loading of NR-PANI. The DPPH radical scavenging capacity of PEPA5, PEPA10, PEPA15 and PEPA20 were 6.1, 11.9, 27.1 and 46.9 $nmolcm^{-2}$ respectively. The NR-PANI/ LLDPE composites exhibited superior free radical scavenging properties than the NR-PANI/ PET composites.

Incorporation of NR-PANI in the LLDPE matrix resulted in composites with improved oxygen barrier properties compared to LLDPE. Moreover, NR-PANI did not leach out significantly from the composite films when the leaching tests were undertaken in water. The composite films were biocompatible with the films supporting the growth of L929 mammalian cells. Addition of NR-PANI also introduced antimicrobial properties in the LLDPE matrix. The composite films exhibited antimicrobial efficacy against *S. aureus* even at 5 % loading of NR-PANI. The antioxidant properties of the composite films were further investigated using the ORAC assay. The fluorescence decay of fluorescein, employed as the fluorescence probe, was successfully retarded by incorporating NR-PANI in LLDPE. Similarly, the oxidation of Ropufa fish oil was delayed in the presence of NR-PANI/ LLDPE films. The antioxidant activity of NR-PANI/ LLDPE films increased with higher loading of NR-PANI.

NR-PANI was successfully utilized to improve the oxygen barrier and antioxidant properties of LLDPE. While the NR-PANI/ LLDPE composites were biocompatible, they also exhibited antimicrobial efficacy. Additionally, the NR-PANI/ LLDPE composites had good mechanical properties and NR-PANI did not leach out of the composite films. The NR-PANI/ LLDPE composites represent a novel material with potential active food packaging applications.

7.2 Recommendations for Future Work

Composites of NR-PANI and PET or LLDPE have exhibited free radical scavenging capability, thus demonstrating the enormous scope for the utilization of NR-PANI, as a solid

antioxidant, in the development of active packaging materials. This study was limited to the development and characterization of NR-PANI/ PET and NR-PANI/ LLDPE composites for active food packaging applications. However, various research projects can be undertaken in the future to compliment or extend the studies reported in this thesis.

The effect of different dopant ions, on the free radical scavenging capacity of PANI, needs to be studied in detail. Organic dopants such as DBSA, CSA and *p*TSA have been often utilized in the synthesis of PANI, resulting in different morphologies. The dopants may also affect the oxidation level of PANI, leading to varying free radical capacities of the PANIs.

Melt blending the organic acid doped PANIs with thermoplastics like PET, PE or PP would be a worthwhile exercise. Functionalized thermoplastics such as metallocene PE can also be used as compatibilizers for composites [198]. The interaction between the dopant groups of PANI and functionalized thermoplastics can result in improved mechanical properties of the composites. However, this needs to be further investigated.

Another area of future research would be improving the technique of melt processing the PANI/ thermoplastic composites. The composites employed in this study were prepared by extrusion. However, extruding a powder (PANI) with thermoplastic pellets needs to be carefully executed so that the powder is evenly dispersed in the thermoplastic melt. This is a time consuming exercise and would need to be improved if composites are to be prepared on a commercial scale. Using a PANI additive masterbatch pellets, instead of the PANI powder, can help overcome this problem.

Moreover, from an applications point of view, packaging containers can be fabricated

from the PANI/ thermoplastic composites and the quality of food products packaged in these containers monitored over long periods of time. Studying the chemical characteristics as well as physical parameters, such as the colour and taste of the packaged food products, will indicate the effectiveness of the PANI/ thermoplastic containers as active packaging materials. Additional, leaching studies of the composites in different media as well as the leachibility tests on thermally treated NR-PANI could be done.

Finally, research projects can also be undertaken to chemically graft PANI on the surface of various thermoplastics. PANI available on the surface of the substrates is utilized, in the first instance, for the free radical scavenging activity. Therefore, grafting PANI on the thermoplastic surfaces has the potential to elevate their free radical scavenging capacity.

REFERENCES

1. Brody A.L., Bugusu B., Han J.H., Sand C.K., McHugh T.H. (2008) Innovative food packaging solutions. *Journal of Food Science* 73: R107-R116.
2. Marsh K., Bugusu B. (2007) Food packaging: roles, materials and environment issues. *Journal of Food Science* 72: R39-R35.
3. Lim, L-T. (2011) Active and intelligent packaging materials. In: Moo-Young, Butler, M., Webb, C., Moreira, A., Grodzinski, B., Cui, Z.F., Agathos, S. (Eds.) *Comprehension Biotechnology*, vol. 4, 2nd ed., Elsevier, Amsterdam, Netherlands, pp. 629-644.
4. Silvestre C., Duraccio D., Cimmino S. (2011) Food packaging based on polymer nanomaterials. *Progress in Polymer Science* 36: 1766-1782.
5. Lee J-W., Son S-M., Hong S-I. (2008) Characterization of protein-coated polypropylene films as a novel composite structure for active food packaging application. *Journal of Food Engineering* 86: 484-493.
6. Kerry J.P., O'Grady M.N., Hogan S.A. (2006) Past, current and potential utilization of active and intelligent packaging systems for meat and muscle-based products: a review. *Meat Science* 74: 113-130.
7. Restuccia D., Spizziri U.G., Parisi O.I., Cirillo G., Curio M., Iemma F., Puoci F., Vinci G., Picci N. (2010) New EU regulation aspects and global market of active and intelligent packaging for food industry applications. *Food Control* 21: 1425-1435.
8. Brody A.L. (2001) What's active in active packaging. *Food Technology* 55: 104-106.
9. Floros J.D., Dock L.L., Han J.H. (1997) Active packaging technologies and

applications. *Food Cosmetics and Drug Packaging* 20: 10-17.

10. Ozdemir M., Floros J.D. (2004) Active food packaging technologies. *Critical Reviews in Food Science and Nutrition* 44: 185-193.
11. Smith J.P., Ramaswamy H.S., Simpson B.K. (1990) Developments in food packaging technology. Part II Storage aspects. *Trends in Food Science and Technology* 1: 111-118.
12. Byun Y., Darby D., Cookey K., Dawson P., Whiteside S. (2011) Development of oxygen scavenging system containing a natural free radical scavenger and a transition metal. *Food Chemistry* 124: 615-619.
13. Byun Y., Bae H.J., Whiteside S. (2012) Active warm-water fish gelatin film containing oxygen scavenging system. *Food Hydrocolloids* 27: 250-255.
14. Byun Y., Whiteside S. (2012) Ascorbyl palmitate-β-cyclodextrin inclusion complex as an oxygen scavenging microparticle. *Carbohydrate Polymers* 87: 2114-2119.
15. Anthierens T., Ragaert P., Verbrugghe S., Ouchchen A., Geest B.G.D., Noseda B., Mertens J., Beladjal L., Cuyper D.D., Dierickx W., Prez F.D., Devlieghere F. (2011) Use of endosperm-forming bacteria as an active oxygen scavenger in plastic packaging metarials. *Innovative Food Science and Emerging Technologies* 12: 594-599.
16. Vermeiren L., Devlighere F., van Beest M., de Kruijf N., Debevere J. (1999) Developments in the active packaging of foods. *Trends in Food Science and Technology* 10: 77-86.
17. Han J.H. (2000) Antimicrobial food packaging. *Food Technology* 54: 55-65.

18. Suppakul P., Miltz J., Sonneveld K., Bigger S.W. (2003) Active packaging technologies with an emphasis on antimicrobial packaging and its applications. *Journal of Food Science* 68: 408-420.
19. Quintavalla S., Vicini L. (2002) Antimicrobial food packaging in meat industry. *Meat Science* 62: 373-380.
20. Hauser C., Wunderlich J. (2011) Antimicrobial packaging films with a sorbic acid based coating. *Procedia Food Science* 1: 197-202.
21. Suppakul P., Sonneveld K., Bigger S. W., Miltz J. (2011) Diffusion of linalool and methychaviol from polyethylene based antimicrobial packaging films. *LWT – Food Science and Technology* 44: 1888-1893.
22. Ramos M., Jimenez A., Peltzer M., Garrigos M.C. (2012) Characterization and antimicrobial activity studies of polypropylene films with carvacrol and thymol for active packaging. *Journal of Food Engineering* 109: 513-519.
23. Nobile M.A.D., Conte A., Buonocore G.G., Incoronato A.L., Massaro A., Panza O. (2009) Active packaging by extrusion processing of recyclable and biodegradable polymers. *Journal of Food Engineering* 93: 1-6.
24. Gamage G.R., Park H-J., Kim K.M. (2009) Effectiveness of antimicrobial coated oriented polypropylene/polyethylene films in sprout packaging. *Food Research International* 42: 832-839.
25. Tankhiwale R., Bajpai S.K. (2012) Preparation, characterization and applications of ZnO-nanoparticles coated polyethylene films for food packaging. *Colloids and Surfaces B: Biointerfaces* 90: 16-20.

26. Labuza T.P., Breene W.M. (1989) Applications of "active packaging" for improvement of shelf-life and nutritional quality of fresh and extended shelf-life foods. *Journal of Food Processing and Preservation* 13: 1-69.
27. Wessling C., Nielsen T., Leufven A., Jagerstad M. (1998) Mobility of α-tocopherol and BHT in LDPE in contact with fatty food stimulants. *Food Additives and Contaminants* 15: 709-715.
28. Granda-Restrepo D., Peralta E., Troncoso-Rojas R., Soto-Valdez H. (2009) Release of antioxidants from co-extruded active packaging developed for whole milk powder. *International Dairy Journal* 19: 481-488.
29. Gemili S., Yemenicioglu A., Altinkaya S.A. (2010) Development of antioxidant food packaging materials with controlled release properties. *Journal of Food Engineering* 96: 325-332.
30. Tovar L., Salafranca J., Sanchez C., Nerin C. (2005) Migration studies to assess the safety in use of a new antioxidant packaging. *Journal of Agricultural and Food Chemistry* 53: 5270-5275.
31. Pezo D., Salafranca J., Nerin C. (2008) Determination of the antioxidant capacity of active food packagings by in situ gas-phase hydroxyl radical generation and high-performance liquid chromatography-fluorescence detection. *Journal of Chromatography A* 1178: 126-133.
32. Bentayeb K., Rubio C., Batlle R., Nerin C. (2007) Direct determination of carnosic acid in a new active packaging based on natural extract of rosemary. *Analytical and Bioanalytical Chemistry* 389: 1989-1996.

33. Peltzer M., Wagner J., Jimenez A. (2009) Migration study of carvacrol as a natural antioxidant in high density polyethylene for active packaging. *Food Additives and Contaminants A* 26: 938-946.

34. Nerin C., Tovar L., Djenane D., Camo J., Salafranca J., Beltran J.A., Roncales P. (2006) Stabilization of beef meat by a new active packaging containing natural antioxidants. *Journal of Agricultural and Food Chemistry* 54: 7840-7846.

35. Granda-Restrepo D.M., Soto-Valdez H., Peralta E., Troncoso-Rojas R., Vallejo-Cordoba B., Gamez-Meza N., Graciano-Verdugo A.Z. (2009) Migration of α-tocopherol from an active multilayer film into whole milk powder. *Food Research International* 42: 1396-1402.

36. Pereira de Abreu D.A.P., Losada P.P., Maroto J., Cruz J.M. Evaluation of effectiveness of a new active packaging film containing natural antioxidants (from barley husk) that retard lipid damage in frozen Atlantic salmon (*Salmo salar L*.). *Food Research International* 43: 1277-1282.

37. Lopez de Dicastillo C., Alonso J.M., Catala r., Gavara R., Hernandez-Munoz P. (2010) Improving the antioxidant protection of packaged food by incorporating natural flavonoids into ethylene-vinyl alcohol copolymer (EVOH) films. *Journal of Agricultural and Food Chemistry* 58: 10958-10964.

38. Camo J., Beltran J.A., Roncales P. (2008) Extension of the display life of lamb with an antioxidant active packaging. *Meat Science* 80: 1086-1091.

39. Contini C., Katsikogianni M.G., O'Neill F.T., O'Sullivan M., Dowling D.P., Monahan F.J. (2011) Development of active packaging containing natural

antioxidants. *Procedia Food Science* 1: 224-228.

40. Byun Y., Kim Y.T., Whiteside S. (2010) Characterization of an antioxidant polylactic acid (PLA) film prepared with α-tocopherol, BHT and polyethylene glycol using film cast extruder. *Journal of Food Engineering* 100: 239-244.
41. Pereira de Abreu D.A., Losada P.P., Maroto J., Cruz J.M. (2011) Natural antioxidant active packaging film and its effect on lipid damage in frozen blue shark (*Prionace glauca*). *Innovative Food Science and Emerging Technologies* 12: 50-55.
42. Bolumar T., Andersen M.L., Orlien V. (2011) Antioxidant active packaging for chicken meat processed by high pressure treatment. *Food Chemistry* 129: 1406-1412.
43. Lopez de Dicastillo C., Nerin C., Alfaro P., Catala R., Gavara R., Hernandez-Munoz P. (2011) Development of new antioxidant active packaging films based on ethylene vinyl alcohol copolymer (EVOH) and green tea extract. *Journal of Agricultural and Food Chemistry* 59: 7832-7840.
44. Lopez de Dicastillo C., Gomez-Estaca J., Catala R., Gavara R., Hermandez-Munoz P. (2012) Active antioxidant packaging films: development and effect on lipid stability of brined sardines. *Food Chemistry* 131: 1376-1384.
45. Nerin C. (2010) Antioxidant active food packaging and antioxidant edible films. In: Decker E.A., Elias R.J., McClements D.J. (Eds.) *Oxidation in Foods and Beverages and Antioxidant Applications, vol. 2 – Management in Different Industry Sectors*, 1st edition, Woodhead Publishing, Cambridge, United Kingdom, pp. 496-515.
46. Kubow S. (1992) Routes of formation and toxic consequences of lipid oxidation products in foods. *Free Radical Biology and Medicine* 12: 63-81.

47. Muik B., Lendl B., Molina-Diaz A., Ayora-Canada M.J. (2005) Direct monitoring of lipid oxidation in edible oils by fourier transform raman spectroscopy. *Chemistry and Physics of Lipids* 134: 175-182.
48. Lagurre M., Lecomte J., Villeneuve P. (2007) Evaluation of the ability of antioxidant to counteract lipid oxidation: existing methods, new trends and challenges. *Progress in Lipid Research* 46: 244-282.
49. Faustman C., Sun Q., Mancini R., Suman S.P. (2010) Myoglobin and lipid oxidation interactions: mechanistic bases and control. *Meat Science* 86: 86-94.
50. Finley J.W., Given P. Jr. (1986) Technological necessity of antioxidants in the food industry. *Food and Chemical Toxicology* 24: 999-1006.
51. Sevanian A., Hochstein P. (1985) Mechanisms and consequences of lipid peroxidation in biological systems. *Annual Review of Nutrition* 5: 365-390.
52. Hseih R.J., Kinsella J.E. (1989) Oxidation of polyunsaturated fatty acids: mechanisms, products and inhibition with emphasis on fish. *Advances in Food and Nutrition Research* 33: 233-341.
53. Frankel E.N. (1980) Lipid oxidation. *Progress in Lipid Research* 19: 1-22.
54. Frankel E.N. (1984) Lipid oxidation: mechanisms, products and biological significance. *Journal of the American Oil Chemists' Society* 61: 1908-1917.
55. Gordon M.H. (1990) The mechanism of antioxidant action *in vitro*. In: Hudson B.J.F. (Ed.) *Food Antioxidants*, Elsevier, Amsterdam, Netherlands, pp. 1-18.
56. Nawar W.W. (1984) Chemical changes in lipids produced by thermal processing. *Journal of Chemical Education* 61: 299-302.

57. Halliwell B., Aeschbach R., Loliger J., Aruomo O.I. (1998) The characterization of antioxidants. *Food and Chemical Toxicology* 33: 601-617.

58. Zujovic Z.D., Gizdavic-Nikolaidis M., Kilmartin P.A., Travas-Sejdic J., Cooney R.P., Bowmaker G.A. (2005) Solid state magnetic resonance studies of polyaniline as a radical scavenger. *Applied Magnetic Resonance* 28: 123-126.

59. Kuczkowski J.A., Gillick J.G. (1984) Polymer-bound antioxidants. *Rubber Chemistry and Technology* 57: 621-651.

60. Yang C.Y., Reghu M., Heeger A.J., Cao Y. (1996) Thermal stability of polyaniline networks in conducting polymer composites. *Synthetic Metals* 79: 27-32.

61. Yue J., Epstein A.J., Zhong Z., Gallangher P.K. (1991) Thermal stability of polyanilines. *Synthetic Metals* 41-43: 765-768.

62. Wei Y., Hsueh K.F. (1989) Thermal analysis of chemically synthesized polyaniline and effects of thermal aging on conductivity. *Journal of Polymer Science: Part A: Polymer Chemistry* 27: 4351-4363.

63. Holze R. (2011) Co-polymers – a refined way to tailor intrinsically conducting polymers. *Electrochimica Acta* 56: 10479-10492.

64. MacDiarmid A.G. (2001) Synthetic metals: a novel role for organic polymers. *Angewandte Chemie International Edition* 40: 2581-2590.

65. Svirskis D., Travas-Sejdic J., Rodgers A., Garg S. (2010) Electronically controlled drug delivery based on intrinsically conducting polymers. *Journal of Controlled Release* 146: 6-15.

66. Unsworth J., Lunn B.A., Innis P.C., Jin Z., Kaynak A., Booth N.G. (1992) Technical

review: conducting polymer electronics. *Journal of Intelligent Material Systems and Structures* 3: 380-395.

67. Fincher Jr C.R., Peebles D.L., Heeger A.J., Druy M.A., Matsumura Y., MacDiarmid A.G., Shirakawa H., Ikeda S. (1978) Anisotropic optical properties of pure and doped polyacetylene. *Solid State Communications* 27: 489-494.
68. Liu X., Gao K., Li Y., Fu J., Wei J., Xie S. (2007) Polaron formation dynamics in conducting polymers. *Synthetic Metals* 157: 380-385.
69. Kim D.Y., Lee J.Y., Lee C.Y., Kang E.T., Tan K.L. (1995) Difference in doping behavior between polypyrrole films and powders. *Synthetic Metals* 72: 243-248.
70. Luthra V., Singh R., Gupta S.K., Mansingh A. (2008) Mechanism of dc conduction in polyaniline doped with sulfuric acid. *Current Applied Physics* 3: 219-222.
71. Ansari M.O., Mohammad F. (2011) Thermal stability, electrical conductivity and ammonia sensing studies on *p*-toluenesulfonic acid doped polyaniline: titanium dioxide (*p*TSA/Pani:TiO_2) nanocomposites. *Sensors and Actuators B: Chemical* 157: 122-129.
72. Cui B., Qiu H., Fang K., Fang C. (2007) Effect of vacuum annealing on characteristics of the DBSA-doped polyaniline pellets. *Synthetic Metals* 157: 11-16.
73. MacDiarmid A.G., Epstein A.J. (1994) The concept of secondary doping as applied to polyanilne. *Synthetic Metals* 65: 103-116.
74. Pud A., Ogurtsov N., Korzhenko A., Shapoval G. (2003) Some aspects of preparation methods and properties of polyaniline blends and composites with organic polymers. *Progress in Polymer Science* 28: 1701-1753.

75. Cao Y., Smith P., Heeger A.J. (1992) Counter-ion processibility of conducting polyblends of polyaniline in bulk polymers. *Synthetic Metals* 48: 91-97.

76. Pud A.A. (1994) Stability and degradation of conducting polymers in electrochemical systems. *Synthetic Metals* 66: 1-18.

77. Min G. (1999) Conducting polymers and their applications in the film industry – polyaniline/ polyimide blended films. *Synthetic Metals* 102: 1163-1166.

78. Ismail M.N., Ibrahim M.S., Abd El-Ghaffar M.A. (1998) Polyaniline as an antioxidant and antirad in SBR vulcanizates. *Polymer Degradation and Stability* 62: 337-341.

79. Hsu C.F., Basle C., Travas-Sejdic J.. Kilmartin P. (2011) $ABTS^{\bullet+}$ scavenging activity of polypyrrole, polyaniline and poly(3,4-ethylenedioxythiophene). *Polymer International* 60: 69-77.

80. Hsu C. F., Zhang L., Peng H., Travas-Sejdic J., Kilmartin P.A. (2008) Scavenging of DPPH free radicals by polypyrrole powders of varying levels of overoxidation and or/ reduction. *Synthetic Metals* 158: 946-952.

81. Gizdavic-Nikolaidis M., Travas-Sejdic J., Kilmartin P.A., Bowmaker G.A., Cooney R.P. (2004) Evaluation of antioxidant activity of aniline and polyaniline. *Current Applied Physics* 4: 343-346.

82. Wang J., Zhu L.H., Li J., Tang H.Q. (2007) Antioxidant activity polyaniline nanofibers. *Chinese Chemical Letters* 18: 1005-1008.

83. Banerjee S., Saikia J.P., Kumar A., Kumar B.K. (2010) Antioxidant activity and haemolysis prevention efficiency of polyaniline nanofibers. *Nanotechnology* 21: 1-8.

84. Zujovic Z.D., Gizdavic-Nikolaidis M.R., Kilmartin P.A., Idriss H., Senanayake S.D., Bowmaker G.A. (2006) Solid-state NMR study of ^{15}N labeled polyaniline upon reaction with DPPH. *Polymer* 47: 1166-1171.

85. Hsu C.F., Peng H., Zhang L., Travas-Sejdic J., Kilmartin P.A. (2009) Structural changes in polyaniline upon reaction with DPPH$^{\bullet}$. *e-Journal of Surface Science and Nanotechnology* 7: 269-272.

86. Hsu C.F., Zhang L., Peng H., Travas-Sejdic J., Kilmartin P.A. (2008) Free radical scavenging properties of polypyrrole and poly(3,4-ethylenedioxythiophene). *Current Applied Physics* 8: 316-319.

87. Parsa A., Ghani S.A. (2009) The improvement of free-radical scavenging capacity of the phosphate medium. *Electrochimica Acta* 54: 2856-2860.

88. Gizdavic-Nikolaidis M., Travas-Sejdic J., Bowmaker G.A., Cooney R.P., Kilmartin P.A. (2004) Conducting polymers as free radical scavengers. *Synthetic Metals* 140: 225-232.

89. Gizdavic-Nikolaidis M.R., Stanisavljev D.R., Easteal A.J., Zujovic Z.D. (2010) Microwave assisted synthesis of functionalized polyaniline nanostructures with advanced antioxidant properties. *The Journal of Physical Chemistry C* 114: 18790-18796.

90. Palaniappan S., John A. (2008) Polyaniline materials by emulsion polymerization pathway. *Progress in Polymer Science* 33: 732-758.

91. Laslau C., Zujovic Z., Travas-Sejdic J. (2010) Theories of polyaniline nanostructure self-assembly: towards an expanded, comprehensive multi-layer theory (MLT).

Progress in Polymer Science 35: 1403-1419.

92. Stejskal J., Sapurina I., Trchova M. (2010) Polyaniline nanostructures and the role of aniline oligomers in their formation. *Progress in Polymer Science* 35: 1420-1481.
93. Lange U., Roznyztovskaya N.V., Mirsky V.M. (2008) Conducting polymers in chemical sensors and arrays. *Analytica Chimica Acta* 614: 1-26.
94. Xia Y., Wiesinger J.M., MacDiarmid A.G., Epstein A.J. (1995) Camphorsulfonic acid fully doped polyaniline emeraldine salt: conformations in different solvents studied by an ultraviolet/ visible/ near-infrared spectroscopic method. *Chemistry of Materials* 7: 443- 445.
95. Stejskal J., Kratochvil P., Jenkins A.D. (1995) Polyaniline: forms and formation. *Collections of Czechoslovak Chemical Communications* 60: 1747-1755.
96. Stejskal J., Kratochvil P., Jenkins A.D. (1996) The formation of polyaniline and the nature of its structures. *Polymer* 37: 367-369.
97. Bhadra S., Khastgir D., Singha N.K., Lee J.H. (2009) Progress in preparation, processing and applications of polyaniline. *Progress in Polymer Science* 34: 783-810.
98. Zhang D., Wang Y. (2006) Synthesis and applications of one-dimensional nano-structured polyaniline: an overview. *Materials Science and Engineering B* 134: 9-19.
99. Ansari R., Keivani M.B. (2006) Polyaniline conducting electroactive polymers: thermal and environmental stability studies. *E-Journal of Chemistry* 3: 202-217.
100. Cao Y., Li S., Xue Z., Guo D. (1986) Spectroscopic amd electrical characterization of some aniline oligomers and polyaniline. *Synthetic Metals* 16: 305-317.

101. Kuwabata S., Martin C.R. (1994) Investigation of the gas-transport properties of polyaniline. *Journal of Membrane Science* 91: 1-12.

102. Huang J., Kaner R.B. (2004) A general chemical route to polyaniline nanofibers. *Journal of American Chemical Society* 126: 851-855.

103. Adams P.N., Laughlin P.J., Monkman A.P. (1996) Synthesis of high molecular weight polyaniline at low temperatures. *Synthetic Metals* 76: 157-160.

104. Rao P.S., Sathyanarayana D.N. (2004) Electron spin resonance spectroscopy and electrical conductivity studies on some polyaniline salts and their bases. *Indian Journal of Chemistry A* 43A: 1377-1384.

105. Kang Y.S., Lee H.J., Namgoong J., Jung B., Lee H. (1999) Decrease in electrical conductivity upon oxygen exposure in polyanilines doped with HCl. *Polymer* 40: 2209-2213.

106. Laslau C., Zujovic Z.D., Zhang L., Bowmaker G.A., Travas-Sejdic J. (2009) Morphological evolution of self-assembled polyaniline nanostructures obtained by pH-stat chemical oxidation. *Chemistry of Materials* 21: 954-962.

107. Trchova M., Stejskal J. (2011) Polyaniline: the infrared spectroscopy of conducting polymer nanotubes (IUPAC technical report). *Pure and Applied Chemistry* 83: 1803-1817.

108. Krinichnyi V.I., Roth H-K., Hinrichsen G., Lux F., Luders K. (2002) EPR and charge transfer in H_2SO_4 doped polyaniline. *Physical Review B* 65: 1552059(1-14).

109. Palaniappan S., Sydulu S.B., Prasanna T.L., Srinivas P. (2011) High- temperature oxidation of aniline to highly ordered polyaniline-sulfate salt with a nanofiber

morphology and its use as electrode materials in symmetric supercapacitors. *Journal of Applied Polymer Science* 120: 780-788.

110. Prokes J., Stejskal J. (2004) Polyaniline prepared in the presence of various acids. 2. Thermal stability and conductivity. *Polymer Degradation and Stability* 86: 187-195.

111. Blaha M., Riesova M., Zednik J., Anzlovar A., Zigon M., Vohlidal J. Polyaniline synthesis with iron (III) chloride – hydrogen peroxide catalyst system: reaction course and polymer structure study. *Synthetic Metals* 161: 1217-1225.

112. Prasannan A., Truong T.L.B., Hong P-D., Somanathan N., Shown I., Imae Y. (2011) Synthesis and characterization of "hairy urchin" – like polyaniline by using β-cyclodextrin as a template. *Langmuir* 27: 766-773.

113. Zhang H., Li Y., Wang X., Li J., Wang F. (2011) A facile route to hollow microspherical polyaniline. *Polymer* 52: 4246-4252.

114. Menardo C., Nechtschein M., Rousseau A., Travers J.P. (1988) Investigation on the structure of polyaniline: 13C NMR and titration studies. *Synthetic Metals* 25: 311-322.

115. Trchova M., Sedenkova I., Tobolkova E., Stejskal J. (2004) FTIR spectroscopic and conductivity study of the thermal degradation of polyaniline films. *Polymer Degradation and Stability* 86: 179-185.

116. Sedenkova I., Trchova M., Stejskal J. (2008) Thermal degradation of polyaniline films prepared in solutions of strong and weak acids and in water – FTIR and Raman spectroscopic studies. *Polymer Degradation and Stability* 93: 2147-2157.

117. Crowley K., Morrin A., Hernandez A., O'Malley E., Whitten P.G., Wallace G.G.,

Smyth M. R., Killard A. (2008) Fabrication of an ammonia gas sensor using inkjet-printed polyaniline nanoparticles. *Talanta* 77: 710-717.

118. Cao Y., Smith P., Heeger A.J. (1993) Counter-ion induced processibility of conducting polyaniline. *Synthetic Metals* 55-57: 3514-3519.

119. Krinichnyi V.I., Roth H-K., Schrodner M., Wessling B. (2006) EPR study of polyaniline highly doped by *p*-toluenesulfonic acid. *Polymer* 47: 7460-7468.

120. Trchova M., Konyushenko E.N., Stejskal J., Kovarova J., Ciric-Marjanovic G. (2009) The conversion of polyaniline nanotubes to nitrogrn-containing carbon nanotubes and their comparison with multi-walled carbon nanotubes. *Polymer Degradation and Stabiltiy* 94: 929-938.

121. Hopkins A.R., Lipeles R.A., Hwang S-J. (2008) Morphology characterization of polyaniline nano- and microstructures. *Synthetic Metals* 158: 594-601.

122. Genies E.M., Lapkowski M. (1987) Spectroelectrochemical evidence for an intermediate in electropolymerization of aniline. *Journal of Electroanalytical Chemistry and Interfacial Electrochemistry* 236: 189-197.

123. Genies E.M., Lapkowski M. (1987) Electrochemical in situ epr evidence of two polaron – bipolaron states in aniline. *Journal of Electroanalytical Chemistry and Interfacial Electrochemistry* 236: 199-208.

124. Mohilner D.M., Adams R.N., Argersinger W.J. (1962) Investigation of the kinetics and mechanism of the anodic oxidation of aniline in aqueous sulfuric acid solution at a platinum electrode. *Journal of American Chemical Society* 84: 3618-3622.

125. Wei Y., Tang X., Sun Y. (1989) A study of the mechanism of aniline

polymerization. *Journal of Polymer Science: Part A: Polymer Chemistry* 27: 2385-2396.

126. Stejskal J., Gilbert R.G. (2002) Polyaniline preparation of a conducting polymer (IUPAC technical report). *Pure and Applied Chemistry* 74: 857-867.

127. Prokes J., Trchova M., Hlavata D., Stejskal J. (2002) Conductivity ageing in temperature – cycled polyaniline. *Polymer Degradation and Stability* 78: 393-401.

128. Trchova M., Matejka P., Brodinova J., Kalendova A., Prokes J., Stejskal J. (2006) Structural and conductivity changes during the pyrolysis of polyaniline base. *Polymer Degradation and Stability* 91: 114-121.

129. Sedenkova I., Prokes J., Trchova M., Stejskal J. (2008) Conformational transition in polyaniline films – spectroscopic and conductivity studies of ageing. *Polymer Degradation and Stability* 93: 428-435.

130. Milton A.J., Monkman A.P. (1993) A comparative study of polyaniline films using thermal analyses and IR spectroscopy. *Journal of Physics D: Applied Physics* 26: 1468-1474.

131. Kang Y., Kim S.K., Lee C. (2004) Doping of polyaniline by thermal acid – base exchange reaction. *Materials Science and Engineering C* 24: 39-41.

132. Rozlivkova Z., Trchova M., Exnerova M., Stejskal J. (2011) The carbonization of granular polyaniline to produce nitrogen – containing carbon. *Synthetic Metals* 161: 1122-1129.

133. Rimbu G.A., Iordoc M., Vasilescu-Mirea R., Stamatin I., Iordache I., Zaharescu T. (2008) Polyaniline rod – like structure as self – electrocatalyst for hydrogen

oxidation reactions. *Optoelectronics and Advanced Materials – Rapid Communications* 2: 876-880.

134. Schuhman W., Lammert R., Uhe B., Schmidt H.L. (1990) Polypyrrole, a new possibility for covalent binding of oxidoreductases to electrode surfaces as a base for stable biosensors. *Sensors and Actuators B: Chemical* 1: 537-541.

135. Ramanavicius A., Ramanaviciene A., Malinauskas A. (2006) Electrochemical sensors based on conducting polymer – polypyrrole. *Electrochimica Acta* 51: 6025-6037.

136. Weng S., Lin Z., Chen L., Zhou J. (2010) Electrochemical synthesis and optical properties of helical polyaniline fibers. *Electrochimica Acta* 55: 2727-2733.

137. Dmitrieva E., Harima Y., Dunsch L. (2009) Influence of phenazine structure on polaron formation in polyaniline: in situ electron spin resonance – ultraviolet/ visible – near infrared spectroelectrochemical study. *Journal of Physical Chemistry B* 113: 16131-16141.

138. Bhadra S., Singha N.K., Khastgir D. (2007) Electrochemical synthesis of polyaniline and its comparison with chemically synthesized polyaniline. *Journal of Applied Polymer Science* 104: 1900-1904.

139. Giz M.J., de Albuquerque S.L.M., Torresi R.M. (2000) AFM morphological study of electropolymerized polyaniline films modified by surfactant and large anions. *Electrochemistry Communications* 2: 377-381.

140. Genies E.M., Syed A.A., Tsintavis C. (1985) Electrochemical study of polyaniline in aqueous and organic medium. Redox and kinetic properties. *Molecular Crystals and*

Liquid Crystals 121: 181-186.

141. Diaz A.F., Logan J.A. (1980) Electroactive polyaniline fibers. *Journal of Electroanalytical Chemistry and Interfacial Electrochemistry* 111: 111-114.

142. Nekrasov A.A., Ivanov V.F., Gribkova O.L., Vannikov A.V. (1996) Electrochemical and chemical synthesis of polyaniline on the surface of vacuum deposited polyaniline films. *Journal of Electroanalytical Chemistry* 412: 133-137.

143. Bhadra S., Singha N.K., Khastgir D. (2007) Dual functionality of PTSA as electrolyte and dopant in the electrochemical synthesis of polyaniline, and its effect on electrical properties. *Polymer International* 56: 919-927.

144. Cruz G.J., Morales J., Castillo-Ortega M.M., Olayo R. (1997) Synthesis of polyaniline films by plasma polymerization. *Synthetic Metals* 88: 213-218.

145. Takeda S. (1999) A new type of CO_2 sensor built up with plasma polymerized polyaniline thin film. *Thin Solid Films* 343-344: 313-316.

146. De Barros R.A., de Azevedo W.M., de Aguiar F.M. (2003) Photo – induced polymerization of polyaniline. *Materials Characterzation* 50: 131-134.

147. Jing X.L., Wang Y.Y., Wu D., She L., Guo Y. (2006) Polyaniline nanofibers prepared with ultrasonic irradiation. *Journal of Polymer Science Part A: Polymer Chemistry* 44: 1014-1019.

148. Jing X., Wang Y.Y., Wu D., Qiang J.P. (2007) Sonochemical synthesis of polyaniline nanofibers. *Ultrasonics Sonochemistry* 14: 75-80.

149. Jin Z., Su Y., Duan Y. (2001) A novel method for polyaniline synthesis with the immobilized horseradish peroxide enzyme. *Synthetic Metals* 122: 237-242.

150. Roman P., Cruz-Silva R., Vazquez-Duhalt R. (2012) Peroxidase – mediated synthesis of water – soluble fully sulfonated polyaniline. *Synthetic Metals* 162: 794-799.

151. Stejskal J., Sapurina I. (2005) Polyaniline: thin films and colloidal dispersions. *Pure and Applied Chemistry* 77: 815-826.

152. Sapurina I., Stejskal J. (2009) Ternary composites of multi – wall carbon nanotubes, polyaniline, and noble – metal nanoparticles for potential applications in electrocatalysis. *Chemical Papers* 63: 579-585.

153. Laslau C., Zujovic Z.D., Travas-Sejdic J. (2009) Polyaniline "nanotube" self – assembly: the stage of granular agglomeration on nanorod templates. *Macromolecular Rapid Communications* 30: 1663-1668.

154. Chiou N-R., Epstein A.J. (2005) A simple approach to control the growth of polyaniline nanofibers. *Synthetic Metals* 153: 69-72.

155. Chiou N-R. Epstein A.J. (2005) Polyaniline nanofibers prepared by dilute polymerization. *Advanced Materials* 17: 1679-1683.

156. Wu J.H., Tang Q.W., Li Q.H., Lin J.M. (2008) Self – assembly growth of oriented polyaniline arrays: a morphology and structure study. *Polymer* 49: 5262-5267.

157. Xia H.B., Narayanan J., Cheng D.M., Xiao C.Y., Liu X.Y., Chan H.S.O. (2005) Formation of ordered arrays of oriented polyaniline nanoparticle nanorods. *Journal of Physical Chemistry B* 109: 12677-12684.

158. Wang Y. Tran H.D., Kaner R.B. (2009) Template – free growth of aligned bundles of conducting polymer nanowires. *Journal of Physical Chemistry C* 113: 10346-

10349.

159. Konyushenko E.N., Stejskal J., Sedenkova I., Trchova M., Sapurina I., Cieslar M., Prokes J. (2006) Polyaniline nanotubes: conditions of formation. *Polymer International* 55: 31-39.

160. Stejskal J., Sapurina I., Trchova M., Konyushenko E.N., Holler P. (2006) The genesis of polyaniline nanotubes. *Polymer* 47: 8253-8262.

161. Stejskal J., Sapurina I., Trchova M., Konyushenko E.N. (2008) Oxidation of aniline: polyaniline granules, nanotubes and oligoaniline microspheres. *Macromolecules* 41: 3530-3536.

162. Huang H.F., Lin C.W. (2009) Exploration of the formation mechanism of polyaniline nanotubesand nanofibers through a template – free method. *Synthetic Metals* 159: 1824-1830.

163. Huang Y.F., Lin C.W. (2009) Introduction of methanol in the formation of polyaniline nanotubes in acid – free aqueous solution through a self – curling process. *Polymer* 50: 775-782.

164. Wang X., Liu N., Yan X., Zhang W.J., Wei Y. (2005) Alkali – guided synthesis of polyaniline hollow microspheres. *Chemistry Letters* 34: 42-43.

165. Jin E., Wang X., Liu N., Zhang W.J. (2007) Self – assembled microspheres of glucose – containing polyaniline by alkali – guided method. *Materials Letters* 61: 4959-4962.

166. Huang K., Meng X-H., Wan MX. (2006) Polyaniline microspheres constructed with their own self – assembled nanofibers. *Journal of Applied Polymer Science* 100:

3050-3054.

167. Zhang L.J., Wan M.X., Wei Y. (2006) Hollow polyaniline microspheres with conductive and fluorescencent function. *Macromolecular Rapid Communications* 27: 888-893.

168. Rezaei S.J.T., Bide Y., Nabid M.R. (2011) A new approach for the synthesis of polyaniline microstructures with a unique tetragonal star – like morphology. *Synthetic Metals* 161: 1414-1419.

169. Zhu Y., Li J., Wan M., Jiang L. (2008) 3D – boxlike polyaniline microstructures with super – hydrophobic and high – crystalline properties. *Polymer* 49: 3419-3423.

170. Yu X., Fan H., Wang H., Zhao N., Zhang X., Xu J. (2011) Self – assembly hierarchical micro/ nanostructures of leaf – like polyaniline with 1D nanorods on 2D foliage surface. *Materials Letters* 65: 2724-2727.

171. Yu X., Fan H., Wang H., Zhao N., Zhang X., Xu J. (2011) Self – assembly of flower – like polyaniline – polyvinyl alcohol multidimensional architectures from 2D petals. *Materials Letters* 65: 2812-2815.

172. Gao Y., Kang Z-H., Li X., Cui X-J., Gong J. (2011) Vapour phase synthesis of crystalline polyaniline with dendritic morphology. *CrystEngComm* 13: 3370-3372.

173. Trchova M., Sedenkova I., Konyushenko E.N., Stejskal J., Holler P., Ciric-Marjanovic G. (2006) Evolution of polyaniline nanotubes: the oxidation of aniline in water. *Journal of Physical Chemistry B* 110: 9461-9468.

174. Wessling B. (1998) Dispersion as the link between basic research and commercial applications of conducting polymers (polyaniline). *Synthetic Metals* 93: 143-154.

175. Wang Y.Y., Jing X.L. (2004) Preparation of an epoxy/ polyaniline composite coating and its passivation effect on cold rolled steel. *Polymer Journal* 36: 374-379.

176. Wang Y.Y., Jing X.L. (2005) Intrinsically conducting polymers for electromagnetic interference shielding. *Polymers for Advanced Technologies* 16: 344-351.

177. Fatyeyeva K., Pud A.A., Bardeau J-F., Tabellout M. (2011) Structure – property relationship in aliphatic polyamide/ polyaniline surface layered composites. *Materials Chemistry and Physics* 130: 760-768.

178. Dhawan S.K., Kumar D., Ram M.K., Chandra S., Trivedi D.C. (1997) Application of conducting polyaniline as sensor material for ammonia. *Sensors and Actuators B: Chemical* 40: 99-103.

179. Lu W., Smela E., Adams P., Zuccarello G., Mattes B.R. (2004) Development of solid– in- hollow electrochemical linear actuators using highly conductive polyaniline. *Chemistry of Materials* 16: 1615-1621.

180. Gizdavic-Nikolaidis M., Travas-Sejdic J., Bowmaker G.A., Cooney R.P., Thompson C., Kilmartin P.A. (2004) The antioxidant activity of conducting polymers in biomedical applications. *Current Applied Physics* 4: 347-350.

181. Kilmartin P.A. (2010) Antioxidant plastics based upon conducting polymers. *Chemistry in New Zealand* 74: 101-105.

182. Saikia J.P., Banerjee S., Konwar B.K., Kumar A. (2010) Biocompatible novel starch/ polyaniline composites: characterization, anti-cytotoxicity and antioxidant activity. *Colloids and Surfaces B: Biointerfaces* 81: 158-164.

183. Buettner G.R. (1993) The pecking order of free radicals and antioxidants: lipid

peroxidation, α-tocopherol and ascorbate. *Archives of Biochemistry and Biophysics* 300: 535-543.

184. Danilewicz J.C. (2011) Mecanism of autoxidation of polyphenols and participation of sulfite in wine. *American Journal of Enology and Viticulture* 62: 319-328.

185. Humpolicek P., Kasparkova V., Saha P., Stejskal J. (2012) Biocompatibility of polyaniline. *Synthetic Metals* 162: 722-727.

186. Bidez P.R., Li S.X., MacDiarmid A.G., Venancio E.C., Wei Y., Lelkes P.I. (2006) Polyaniline, an electroactive polymer, supports adhesion and proliferation of cardiac myoblasts. *Journal of Biomaterials Science: Polymer Edition* 17: 199-212.

187. Wang H.J., Li L.W., Li D.F., Wang J.Y. (2008) Characterization of nanostructure and cell compabtility of polyaniline films with different dopant acids. *Journal of Physical Chemistry B* 112: 2671-2677.

188. Liu S., Wang J., Zhang D., Zhang P., Ou J., Liu B., Yang S. (2010) Investigation on cell biocompatible behaviors of polyaniline film fabricated electroless surface polymerization. *Applied Surface Science* 256: 3427-3431.

189. Kumar A., Banerjee ., Saikia J.P., Konwar B.K. (2010) Swift heavy ion irradiation induced enhancement in the antioxidant activity and biocompatibility of polyaniline nanofibers. *Nanotechnology* 21: 1-8.

190. Kamalesh S., Tan P., Wang J., Lee T., Kang E-T., Wang C-H. (2000) Biocompatibility of electroactive polymers in tissues. *Journal of Biomedical Research* 52: 467-478.

191. Dispenza C., Leone M., Presti C.L., Librizzi F., Spadaro G., Vetri V. (2006) Optical

properties of biocompatible polyaniline nano-composites. *Journal of Non-Crystalline Solids* 352: 3855-3840.

192. Prabhakar P.K., Raj S., Anuradha P.R., Sawant S.N., Doble M. (2011) Biocompatibility studies on polyaniline and polyaniline – silver nanoparticle coated polyurethane composite. *Colloids and Surfaces B: Biointerfaces* 86: 146-153.

193. Kim H-S., Hobbs H.L., Wang L., Rutten M.J., Wamser C.C. (2009) Biocompatible composites of polyaniline nanofibers and collagen. *Synthetic Metals* 159: 1313-1318.

194. Dispenza C., Sabatino M-A., Niconov A., Chmielewska D., Spadaro G. (2012) E-beam crosslinked, biocompatible functional hydrogels incorporating polyaniline nanoparticles. *Radiation Physics and Chemistry* 81: 1456-1459.

195. Pandey S.S., Gerard M., Sharma A.L., Malhotra B.D. (2000) Thermal analysis of chemically synthesized polyemeraldine base. *Journal of Applied Polymer Science* 75: 149-155.

196. Ikkalaa O.T., Laakso J., Vakiparta K., Virtanen E., Ruohonen H., Jarvinen H., Taka T., Passiniemi P., Osterholm J-E. (1995) Counter - ion induced processibility of polyaniline: conducting melt processible polymer blends. *Synthetic Metals* 69: 97-100.

197. Yang J.P., Rannou P., Planes J., Pron A., Nechtschein M. (1998) Preparation of low density polyethylene – based polyaniline conducting polymer composites with low percolation threshold via extrusion. *Synthetic Metals* 93: 169-173.

198. Annala M., Lofgren B. (2006) compatibilization of conductive polyethylene/ polyaniline blends. *Macromolecular Materials and Engineering* 291: 848-857.

199. Chipara M., Hui D., Notingher P.V., Chipara M.D., Lau K.T., Sankar J., Panaitescu D. (2003) On polyethylene – polyaniline composites. *Composites Part B: Engineering* 34: 637-645.

200. Paul R.K., Pillai C.K.S. (2000) Melt/ solution processable conducting polyaniline with novel sulfonic acid dopants and its thermoplastic blends. *Synthetic Metals* 114: 27-35.

201. Shacklette L.W., Han C.C., Luly M.H. (1993) Polyaniline blends in thermoplastics. *Synthetic Metals* (1993) 3532-3537.

202. Zilberman M., Titelman G.I., Siegmann A., Haba Y., Narkis M., Alperstein D. (1997) Conductive blends of thermally dodecylbenzene sulfonic acid doped polyaniline with thermoplastic polymers. *Journal of Applied Polymer Science* 66: 243-253.

203. Mitzakoff S., Paoli M-A. D. (1999) Blends of polyaniline and engineering plastics. *European Polymer Journal* 35: 1791-1798.

204. Morgan H., Foot P.J.S., Brooks N.W. (2001) The effects of composition and processing variables on the properties of thermoplastic polyaniline blends and composites. *Journal of Materials Science* 36: 5369-5377.

205. Krinichnyi V.I., Tokarev S.V., Roth H-K., Schrodner M., Wessling B. (2006) EPR study of charge transfer in polyaniline highly doped by *p*-toluenesulfonic acid. *Synthetic Metals* 156: 1368-1377.

206. Zhang Q-H., Wang X-H., Chen D-J., Jing X-B. (2004) Electrically conductive, melt – processed ternary blends of polyaniline/ dodecylbenzene sulfonic acid, ethylene/

vinyl acetate, and low – density polyethylene. *Journal of polymer Science: Part B: Polymer Physics* 42: 3750-3758.

207. Ray S., Easteal A.J., Cooney R.P., Edmonds N.R. (2009) Structure and properties of melt – processed PVDF/ PMMA/ polyaniline blends. *Materials Chemistry and Physics* 113: 829-838.

208. Kahol P.K., Pinto N.J. (2004) An EPR investigation of electrospun polyaniline – polyethylene oxide blends. *Synthetic Metals* 140: 269-272.

209. Guimaraes I.S., Hidalgo A.A., Cunha H.N., Santos L.M., Santos J.A.V., Junior J.R.S. (2012) thermal and morphological characterization of conducting polyaniline/ polystyrene blends. *Synthetic Metals* 162: 705-709.

210. Ebrahim S., Kashyout A-H., Soliman M. (2009) Ac and Dc conductivities of polyaniline/ poly vinyl formal blend films. *Current Applied Physics* 9: 448-454.

211. Jousseaume V., Morsli M., Bonnet A., Lefrant S. (1998) X-ray photoelectron spectroscopy of conducting polyaniline and polyaniline – polystyrene blends. *Journal of Applied Polymer Science* 67: 1209-1214.

212. Goh S.H., Chan H.S.O., Ong C.H. (1996) Miscibility of polyaniline/ poly(vinyl acetate) blends. *Polymer* 37: 2675-2679.

213. Banerjee P. Mandal B.M. (1995) Blends of HCl – doped polyaniline nanoparticles and poly (vinyl chloride) with extremely low percolation threshold – a morphology study. *Synthetic Metals* 74: 257-261.

214. Kutanis S., Karakisla M., Akbulut U., Sacak M. (2007) The conductive polyaniline/ poly(ethylene terephthalate) composite fabrics. *Composites Part A: Applied Science*

and Manufacturing 38: 609-614.

215. Hirase R., Hasegawa M., Shirai M. (2003) Conductive fibers based on poly(ethylene terephthalate) – polyaniline composites manufactured by electrochemical polymerization. *Journal of Applied Polymer Science* 87: 1073-1078.

216. Kim B., Koncar V., Dufour C. (2006) Polyaniline – coated PET conductive yarms: study of electrical, mechanical, and electro – mechanical properties. *Journal of Applied Polymer Science* 101: 1252-1256.

217. Fryczkowski R., Rom M., Fryczkowska B. (2005) Polyester fibers finished with polyaniline. *Fibres and Textiles in Eastern Europe* 13: 141-143.

218. Korzhenko A.A., Tabellout M., Emery J.R., Pud A.A., Rogalsky S., Shapoval G.S. (1998) dielectric relaxation properties of poly(ethylene terephthalate) – polyaniline composite films. *Synthetic Metals* 98: 157-160.

219. Zhang H., Li C. (1991) Chemical synthesis of transparent and conducting polyaniline – poly(ethylene terephthalate) composite films. *Synthetic Metals* 44: 143-146.

220. Pud A.A., Rogalsky S.P., Shapoval G.S., Korzhenko A.A. (1999) The polyaniline/ poly(ethylene terephthalate) composite. 1. Peculiarities of the matrix aniline redox polymerization. *Synthetic Metals* 99: 175-179.

221. Tabellout M., Fatyeyeva K., Baillif P-Y., Bardeau J-F., Pud A.A. (2005) the influence of the polymer matrix on the dielectric and electrical properties of conductive polymer composites based on polyaniline. *Journal of Non – Crystalline Solids* 351: 2835-2841.

222. Pud A.A., Tabellout M., Kassiba A., Korzhenko A.A., Rogalsky S.P., Shapoval G.S.,

Houze F., Schneegans O., Emery J.R. (2001) the poly(ethylene terephthalate)/ polyaniline composite: AFM, DRS and EPR investigations of some doping effects. *Journal of Materials Science* 36: 3355-3363.

223. Goswami S., Mitra M.K., Chattopadhyay K.K. (2009) Enhanced field emission from polyaniline nano – porous thin films on PET substrate. *Synthetic Metals* 159: 2430-2436.

224. Zhou H., Shi Z., Lu Y. (2010) Conducting polyaniline/ poly(tetrafluoroethylene) composite films with tunable surface morphology and hydrophilicity. *Synthetic Metals* 160: 1925-1930.

225. Elyashevich G.K., Sidorovich A.V., Smirnov M.A., Kuryndin I.S., Bobrova N.V., Trchova M., Stejskal J. (2006) Thermal and structural stability of composite systems based on polyaniline deposited on porous polyethylene films. *Polymer Degradation and Stability* 91: 2786-2792.

226. Elyashevich G.K., Terlemezyan L., Kuryndin I.S., Lavrentyev V.K., Mokreva P., Rosova E.Y., Sazanov Y.N. (2001) Thermochemical and deformational stability of microporous polyethylene films with polyaniline layer. *Thermochimica Acta* 374: 23-30.

227. Caramori S.S., Fernandes K.F. (2008) The use of poly(ethylene terephthalate) – polyaniline composite for trypsin immobilization. *Materials Science and Engineering C* 28: 1159-1163.

228. Wang J., liu X., Choi H-S., Kim J-H. (2008) Conducting polymer films fabricated by oxidative graft copolymerization of aniline on poly(acrylic acid) grafted

poly(ethylene terehthalate) surfaces. *Journal of Physical Chemistry B* 112: 14829-14835.

229. Chen Y., Kang E.T., Neoh K.G., Tan K.L. (2000) Covalent immobilization of invertase onto the surface modified polyaniline from graft copolymerization with acrylic acid. *European Polymer Journal* 36: 2095-2103.

230. Kang E.T., Neoh K.G., Pun M.Y., Tan K.L., Loh F.C. (1995) Charge transfer interactions between polyaniline and surface functionlized polymer substrates. *Synthetic Metals* 69: 105-108.

231. Zhong W., Yang Y., Yang W. (2005) Oxidative graft – polymerization of aniline on the surface of poly(propylene) – graft – polyacrylic acid films. *Thin Solid Films* 479: 24-30.

232. Ji L.Y., Kang E.T., Neoh K.G. (2002) Oxidative graft polymerization of aniline on PTFE films modified by surface hydroxylation and silanization. *Langmuir* 18: 9035-9040.

233. Li G., Zhang C., Peng H. (2008) Facile synthesis of self – assembled polyaniline nanodisks. *Macromolecular Rapid Communications* 29: 63-67.

234. Golczak S., Kanciurzewska A., Fahlman M., Langer K., Langer J.J. (2008) Comparative XPS surface study of polyaniline thin films. *Solid State Ionics* 179: 2234-2239.

235. Jang J. (2006) Conducting polymer nanomaterials and their applications. *Advances in Polymer Science* 199: 189-260.

236. Wiznerowicz F. (1994) Conducting polymers instead of carbon black. *Wire* 44: 102-

108.

237. Zhang L., Zujovic Z.D., Peng H., Bowmaker G.A., Kilmartin P.A., Travas-Sejdic J. (2008) Structural characteristics of polyaniline nanotubes synthesized from different buffer solutions. *Macromolecules* 41: 8877-8884.

238. Zujovic Z.D., Laslau C., Bowmaker G.A., Kilmartin P.A., Webber A.L., Brown S.P., Travas-Sejdic J. (2010) Role of aniline oligomeric nanosheets in the formation of polyaniline nanotubes. *Macromolecules* 43: 662-670.

239. Zhang L., Peng H., Zujovic Z.D., Kilmartin P.A., Travas-Sejdic J. (2007) Characterization of polyaniline nanotubes formed in the presence of amino acids. *Macromolecular Chemistry and Physics* 208: 1210-1217.

240. Li X., Li N., Dai N., Wang G. (2009) Large – area fibrous network of polyaniline formed on the surface of diatomite. *Applied Surface Science* 255: 8276-8280.

241. Chowdhury A., Saleh F.S., Rahman M.R., Rahim A. (2008) Influence of pH on the specific surface area of polyaniline matrices. *Journal of Applied Polymer Science* 109: 1764-1771.

242. Huang J., Kaner R.B. (2006) The instrinsic nanofibrillar morphology of polyaniline. *Chemical Comunications* 4: 367-376.

243. He L. (2005) Preparation of polyaniline microspheres with nanostructured surfaces by a solid – stabilized emulsion. *Material Letters* 59: 2133-2136.

244. Losito L., Malitesta C., Bari I.D., Calvano C.D. (2005) X - ray photoelectron spectroscopy characterization of poly(2,3-diaminophenazine) films electrosynthesized of platinum. *Thin Solid Films* 473: 104-113.

245. Bhadra S., Khastgir D. (2008) Extrinsic and intrinsic structural changes during heat treatment of polyaniline. *Polymer Degradation and Stability* 93: 1094-1099.

246. Kumar S.N., Gaillard F., Bouyssoux G. (1990) High – resolution XPS studies of electrochemically synthesized conducting polyaniline films. *Synthetic Metals* 36: 111-127.

247. Tan K.L., Tan B.T.G., Kang E.T., Neoh K.G. (1989) X – ray photoelectron spectroscopy studies of the chemical structure of polyaniline. *Physical Reviews B* 39: 8070-8073.

248. Laska J., Pron A., Zagorska M., Lapkowski S., Lefrant S. (1995) Thermally processable conducting polyaniline. *Synthetic Metals* 69: 113-115.

249. Kulkarni V.G., Campbell L.D., Mathew W.R. (1989) Thermal stability of polyaniline. *Synthetic Metals* 30: 321-325.

250. Chandrakanthi N., Careem M.A. (2000) Thermal stability of polyaniline. *Polymer Bulletin* 44: 101-108.

251. Babazadeh M. (2007) A direct one – pot method for synthesis of polyaniline doped with dodecyl benzene sulfonic acid in aqueous medium and study of its thermal properties. *Iranian Polymer Journal* 16: 389-96.

252. Nascimento G.M.D., Silva C.H.B., Temperini M.L.A. (2008) Spectroscopic characterization of the structural changes of polyaniline nanofibers after heating. *Polymer Degradation and Stability* 93: 291-297.

253. Palaniappan S., Narayana B.H. (1994) Temperature effects on conducting polyaniline salts: thermal and spectral studies. *Journal of Polymer Science: Part A*

Polymer Chemistry 32: 2431-2436.

254. Ding L., Wang X., Gregory R.V. (1999) Thermal properties of chemically synthesized polyaniline (EB). *Synthetic Metals* 104: 73-78.

255. Mathew R., Mattes B.R., Espe M.P. (2002) A solid state NMR characterization of cross - linked polyaniline powder. *Synthetic Metals* 131: 141-147.

256. Amano K., Ishikawa H., Kobayashi A., SatohnM., Hasegawa E. (1994) Thermal stability of chemically synthesized polyaniline. *Synthetic Metals* 62: 299-232.

257. Pereira de Silva J.E., de Faria D.L.A., Cordoba de Torresi S.I., Temperini M.L.A. (2000) Influence of thermal treatment on doped polyaniline studied by resonance raman spectroscopy. *Macromolecules* 33: 3077-3083.

258. Nand A.V., Ray S., Easteal A.J., Waterhouse G.I.N., Gizdavic-Nikolaidis M., Cooney R.P., Travas-Sejdic J., Kilmartin P.A. (2011) Factors affecting the radical scavenging activity of polyaniline. *Synthetic Metals* 161: 1232-1237.

259. Mentus S., Ciric-Marjanovic G., Miroslava T., Stejskal J. (2009) Conducting carbonized polyaniline nanotubes. *Nanotechnology* 20: 245601.

260. Conklin J.A., Huang S.C., Huang S.M., Wen T., Kaner R.B. (1995) Thermal properties of polyaniline and poly(aniline-co-o-ethylaniline). *Macromolecules* 28: 6522-6527.

261. Furukawa Y., Ueda F., Hyodo Y., Harada I., Nakajima T., Kawagoe T. (1988) Vibrational spectra and structure of polyaniline. *Macromolecules* 21: 1297-1305.

262. Bhat N.V., Seshadri D.T., Phadke R.S. (2002) Simultaneous polymerization and crystallization of aniline. *Synthetic Metals* 130: 185-192.

263. Scherr E.M., MacDiarmid A.G., Manohar S.K., Masters J.G., Sun Y. Tang X., Druy M.A., Glatkowski P.J., Cajipe V.B., Fischer J.E., Cromack K.R., Jozefowicz M.E., Ginder J.M., McCall R.P., Epstein A.J. (1991) Polyaniline: oriented films anf fibers. *Synthetic Metals* 41: 735-738.

264. Iida M., Asaji T., Inque M., Grijalva H., Inque M.B., Nakamura D. (1991) Electron spin resonance study of intrinsic paramagnetism of soluble polyaniline perchlorates. *Bulletin of the Chemical Society of Japan* 64: 1509-1513.

265. Boyle A., Penneau J.F., Genies E., Riekel C. (1992) The effect of heating on polyaniline powders studied by real – time synchrotron radiation diffraction, mass spectroscopy and thermal analysis. *Journal of Polymer Science: Part B Polymer Physics* 30: 265-274.

266. Lu X., Tan C.Y., Tan J., Xu J., He C. (2003) Thermal degradation of electrical conductivity of polyacrylic acid doped polyaniline: effect of molecular weight of dopants. *Synthetic Metals* 138: 429-440.

267. Babazedeh M. (2009) Aqueous dispersions of DBSA – doped polyaniline: one - pot preparation, characterization and properties study. *Journal of Applied Polymer Science* 113: 3980-3984.

268. Kim S., Chen I.J. (1998) Annealing effect on the electrochemical property of polyaniline complexed with various acids. *Synthetic Metals* 97: 127-133.

269. Hota P.R., Parida R.K, Das S.C. (2009) XRD and thermal chracateristic studies of conducting polymers. *Journal of Reinforced Plastics and Composites* 28: 265-278.

270. Palaniappan S. (1997) Conductivity and spectral studies on heat treated poly(aniline-

co-2-chloroaniline) salts. *European Polymer Journal* 33: 1735-1739.

271. Hu S.Y., Prattipatu V., Mehta S., Schiraldi D.A., Hiltner A. Baer E. (2005) Improving gas barrier of PET by blending with aromatic polyamides. *Polymer* 46: 2685-2698.

272. Goddard J.M., Hotchkiss J.H. (2007) Polymer surface modification for the attachment of bioactive compounds. *Progress in Polymer Science* 32: 698-725.

273. Junkar I., Vesei A., Cvelbar U., Mozetic M., Strnad S. (2010) Influence of oxygen and nitrogen plasma treatment on polyethylene terephathalate (PET) polymers. *Vacuum* 84: 83-85.

274. Shukla S.R., Harad A.M. (2006) Aminolysis of polyethylene terephthalate waste. *Polymer Degradation and Stability* 91: 1850-1854.

275. Kit K.M., Schultz J.M., Gohil R.M. (1995) Morphology and barrier properties of oriented blends of poly(ethylene terephthalate) and poly(ethylene-2,6-naphthalate) with poly(ethylene-co-vinyl alcohol). *Polymer Engineering and Science* 35: 680-692.

276. Motta O., Di M.L., Incarnato L., Acierno D. (1996) Transport and mechanical properties of PET/ Rodrun 3000 blown films. *Polymer* 37: 2373-2377.

277. Martins C.R., Paoli M.A-D. (2005) Antistatic thermoplastic blend of polyaniline and polystyrene prepared in a double – screw extruder. *European Polymer Journal* 41: 2867-2873.

278. Nand A.V., Ray S., Gizdavic-Nikolaidis M., Travas-Sejdic J., Kilmartin P.A. (2011) The effects of thermal treatment on the antioxidant activity of polyaniline. *Polymer*

Degradation and Stability 96: 2159-2166.

279. Pesetskii S.S., Jurkowski B., Filimono O.V., Koval V.N., Golubovich V.V. (2011) PET/ PC blends: effect of chain extender and impact strength modifier on their structure and properties. *Journal of Applied Polymer Science* 119: 225-234.

280. Seo K.J., Cloyd J.D. (1991) Kinetics of hydrolysis and thermal degradation of polyester melts. *Journal of Applied Polymer Science* 42: 845-850.

281. Sanmon C., Yarwood J., Everall N. (2000) An FTIR study of the effect of hydrolytic degradation on the structure of thin PET films. *Polymer Degradation and Stability* 67: 149-158.

282. Girja B.G., Sailaja R.R.N., Madras G. (2005) Thermal degradation and mechanical properties of PET blends. *Polymer Degradation and Stability* 90: 147-153.

283. Pirzadeh E., Zadhoush A., Haghighat M. (2007) Hydrolytic and thermal degradation of PET fibers and PET granule: the effects of crystallization, temperature and humidity. *Journal of Applied Polymer Science* 106: 1544-1549.

284. Ozen I., Bozoklu G., Dalgicdir C., Yucel O., Unsal E., Cakamk M., Menceloglu Y.Z. (2010) Improvement in gas permeability of biaxially oriented PET films blended with high barrier polymers: the role of chemistry and processing conditions. *European Polymer Journal* 46: 226-237.

285. Zhu Z., Kelley M.J. (2005) IR spectroscopic investigation of the effect of deep UV irradiation on PET films. *Polymer* 46: 8883-8891.

286. Urbanova M., Subrt J., Galikova A., Pola J. (2006) IR laser ablative degradation of poly(ethylene terephthalate): formation of insoluble films with differently bonded

C=O groups. *Polymer Degradation and Stability* 91: 2318-2323.

287. Liang C.Y., Krimm S. (1959) Infrared spectra of high polymers: Part IX. Polyethylene terephthalate. *Journal of Molecular Spectroscopy* 3: 554-574.

288. Woo E.M., Jang F.H. (1999) Phase structural and miscibility in blend of poly(4-methyl styrene) with poly(cyclohexyl methacrylate). *Polymer* 40: 3803-3808.

289. Louette P., Bodino F., Pireaux J.J. (2005) Poly(ethylene terephthalate) (PET) XPS reference core level and energy loss spectra. *Surface Science Spectra* 12: 1-5.

290. Ramao W., Franco M.F., Corilo Y.E., Eberlin M.N., Spinace M.A.S., Paoli M. A-D. (2009) Poly(ethylene terephthalate) thermo-mechanical and thermo-oxidative degradation mechanisms. *Polymer Degradation and Stability* 94: 1849-1859.

291. Montaudo G., Puglisi C., Samperi F. (1992) Primary thermal degradation mechanisms of PET and PBT. *Polymer Degradation and Stability* 42: 13-28.

292. Hosseini S.S., Taheri S., Zadhoush A., Mehrabani-Zeinabad A. (2007) Hydrolytic degradation of poly(ethylene terephthalate). *Journal of Applied Polymer Science* 103: 2304-2309.

293. Bartolotta A., Marco G.D., Farsaci F., Lanza M., Pieruccini M. (2003) DSC and DMTA study of annealed cold – drawn PET: a three phase model interpretation. *Polymer* 44: 5771-5777.

294. Bikiaris D., Prinos J., Botev M., Betchev C., Panayiotou C. (2004) Blends of polymers with similar glass transition temperatures: A DMTA and DSC study. *Journal of Applied Polymer Science* 93: 726-735.

295. Mourad A-H. I. (2010) Thermo – mechanical characteristics of thermally aged

polyethylene/ polypropylene blends. *Materials and Design* 31: 913-917.

296. Dilara P.A., Briassoulis D. (2000) Degradation and stabilization of low density polyethylene films used as greenhouse covering materials. *Journal of Agricultural Engineering Research* 76: 309-321.

297. Raghavan D., Torma A.E. (1992) DSC and FTIR characterization of biodegradation of polyethylene. *Polymer Engineering and Science* 32: 438-442.

298. Nowak B., Pajak J., Drozd-Brakowicz M., Rymartz G. (2011) Microorganisms participating in the biodegradation of modified polyethylene films in different soils under laboratory conditions. *International Biodeterioration and Biodegradation* 65: 757-767.

299. Devilliers C., Fayolle B., Laiarinandrasana L., Oberti S., Gaudichet-Maurin E. (2011) Kinetics of chlorine – induced polyethylene degradation in water pipes. *Polymer Degradation and Stability* 96: 1361-1368.

300. Causin V., Marega C., Carresi P., Schiavone S., Marigo A. (2006) A quantitative differentiation method for plastic bags by infrared spectroscopy, thickness measurement and diferential scanning calorimetry for tracing the source of illegal drugs. *Forensic Science International* 164: 148-154.

301. Shaber E.P. (1987) Vertical interpositional augmentation genioplasty with porous polyethylene. *International Journal of Oral Maxillofacial Surgery* 16: 678-681.

302. Lingaraj K., Morris H., Bartlett J. (2011) Polyethylene thickness in unicompartmental knee arthroplasty. *The Knee* 18: 165-167.

303. Schwope A.D., Till D.E., Ehntholt D.J., Sidman K.R., Whelan R.H., Schwartz P.S.,

Reid R.C. (1987) Migration of BHT and Irganox 1010 from low density polyethylene (LDPE) to foods and food – simulating liquids. *Food and Chemical Toxicology* 25: 317-326.

304. Walker A.M., Tao Y., Torkelson J.M. (2007) Polyethylene/ starch blends with enhanced oxygen barrier and mechanical properties: Effect of granule morphology damage by shear solid-state shear pulverization. *Polymer* 48: 1066-1074.
305. Shields R.J., Bhattacharyya D., Fakirov S. (2008) Oxygen permeability analysis of microfibril reinforced composites from PE/ PET blends. *Composites: Part A* 39: 940-949.
306. Dirim S.N., Ozden H.O., Bayindirli A., Esin A. (2004) Modification of water vapour transfer rate of low density polyethylene films for food packaging. *Journal of Food Engineering* 63: 9-13.
307. Labuza T.P. (1996) An introduction to active packaging for foods. *Food Technology* 50: 68-84.
308. Huittric J., Mederic P., Moan M., Jarrin J. (1998) Influence of composition and morphology on rheological properties of polyethylene/ polyamide blends. *Polymer* 39: 4849-4856.
309. Gulmine J.V., Janissek P.R., Heise H.M., Akcelrud L. (2002) Polyethylene characterization by FTIR. *Polymer Testing* 21: 557-563.
310. Bruni P., Conti C., Corvi A., Rocchi M., Tosi G. (2002) Damaged polyethylene acetabular cups microscopy FT-IR and mechanical determinations. *Vibrational Spectroscopy* 29: 103-107.

311. Song J., Gunst U., Arlinghaus H.F., Vancso G.J. (2007) Flame treatment of low – density polyethylene: surface chemistry across the length scales. *Applied Surface Science* 253: 9489-9499.

312. Andreatta A., Smith P. (1993) Processing of conductive polyaniline – UHMW polyethylene blends from solutions in non – polar solvents. *Synthetic Metals* 55-57: 1017-1022.

313. Badr Y., Ali Z., Zahran A.H., Khafagy R.M. (2000) Characterization of gamma irradiated polyethylene films by DSC and X-ray diffraction techniques. *Polymer International* 49: 1555-1560.

314. Liu T.M., Harrison I.R. (1994) A DSC method of measuring short – chain branching distribution in linear low density polyethylene. *Thermochimica Acta* 233: 167-171.

315. Krupa I., Luyt A.S. (2001) Thermal and mechanical properties of extruded LLDPE/ wax blends. *Polymer Degradation and Stability* 73: 157-161.

316. Nand A.V., Ray S., Travas-Sejdic J., Kilmartin P.A. (2012) Characterization of polyethylene terephthalate/ polyaniline blends as potential antioxidant materials. *Materials Chemistry and Physics* 134: 443-450.

317. Nand A.V., Ray S., Easteal A.J., Gizdavic-Nikolaidis M., Cooney R.P., Travas-Sejdic J., Kilmartin P.A. (2012) Evaluation of polyaniline for packaging applications. *Materials Science Forum* 700: 236-239.

318. Colon M., Nerin C. (2012) Role of catechins in the antioxidant capacity of an active film containing green tea, green coffee, and grapefruit extracts. *Journal of Agricultural and Food Chemistry* 60: 9842-9849.

319. Lopez P., Sanchez C., Batlle R., Nerin C. (2007) Development of flexible antimicrobial films using essential oils as active agents. *Journal of Agricultural and Food Chemistry* 55: 8814-8824.

320. Gutierrez L., Sanchez C., Batlle R., Nerin C. (2009) New antimicrobial active package for bakery products. *Trends in Food Science and Technology* 20: 92-99.

321. Hutton T. (2003) *Food packaging: an introduction. Key topics in food science and technology*, No. 7, Campden and Chorleywood Food Research Association Group, Gloucestershire, United Kingdom, p. 108.

322. Perez-Perez C., Regalado-Gonzalez C., Rodriguez-Rodriguez C.A., Barbosa-Rodriguez J.R., Villasenor-Ortega F. (2006) Incorporation of antimicrobial agents in food packaging films and coatings. In: Guevara-Gonzalez R.G., Torres-Pacheco I. (Eds.) *Advances in agricultural and food biotechnology*. Research Signpost, Kerala, India, pp. 193-216.

323. Lopez de Dicastillo C., Catala R., Gavara R., Hernandez-Munoz P. (2011) Food applications of the active packaging EVOH films containing cyclodextrins for the preferential scavenging of undesirable compounds. *Journal of Food Engineering* 104: 380-386.

324. Gizdavic-Nikolaidis M.R., Bennett J.R., Swift S., Easteal A.J., Ambrose M. (2011) Broad spectrum antimicrobial activity of functionalized polyanilines. *Acta Biomaterialia* 7: 4204-4209.

325. Shi N., Guo X., Jing H., Gong J., Sun C., Yang K. (2006) Antimicrobial effect of the conducting polyaniline. *Journal of Materials Science and Technology* 22, 289-290.

326. Ornelas-Paz J.D.J., Zamudio-Flores P.B., Torres-Cisneros C.G., Holguin-Soto R., Ramos-Aguilar O.P., Ruiz-Cruz S., Guevara-Arauza J.C., Gonzalez-Aguilar G.A., Santana-Rodriguez V. (2012) The barrier properties and potential use of recycled – LDPE films as a packaging material to preserve the quality of Jalapeno peppers by modified atmospheres. *Scientia Horticulturae* 135: 210-218.

327. Magnani E., Bettini E. (2000) Resazurin detection of energy metabolism changes in serum – starved PC12 cells and of neuroprotective agent effect. *Brain Research Protocols* 5: 266-272.

328. Davalos A., Bartolome B., Suberviola J., Gomez-Cordoves C. (2003) ORAC – fluorescein as a model for evaluating antioxidant activity of wines. *Polish Journal of Food and Nutrition Sciences* 12/53: 133-136.

329. Valle M.A., Gacitua M.A., Borrego E.D., Zamora P.P., Diaz F.R>, Camarada M.B., Antilen M.P., Soto J.P. (2012) Electro-synthesis and characterization of aniline and *o*-anisidine oligomers. *International Journal of Electrochemical Science* 7: 2552-2565.

330. Nerin C., Tovar L., Salafranca J. (2008) Behaviour of a new antioxidant active film versus oxidizable model compounds. *Journal of Food Engineering* 84: 313-320.

331. Lee Y.M., Ha S.Y., Lee Y.K., Suh D.H., Hong S.Y. (1999) Gas separation through conductive polymer membranes. 2. Polyaniline membranes with high oxygen selectivity. *Industrial and Engineering Chemistry Research* 38: 1917-1924.

332. Nand A.V., Ray S., Travas-Sejdic J., Kilmartin P.A. (2012) Characterization of antioxidant low density polyethylene/ polyaniline blends prepared via extrusion. *Materials Chemistry and Physics* 135: 903-911.

333. Asghar Z., Masood Z. (2008) Evaluation of antioxidant properties of silymarin and its potential to inhibit peroxyl radicals *in vitro*. *Pakistan Journal of Pharmaceutical Sciences* 21: 249-254.

334. Price J.A., Sanny C.G., Shelvin D. (2006) Application of manual assessment of oxygen radical absorbance capacity (ORAC) for use in high throughput assay of "total" antioxidant activity of drugs and natural products. *Journal of Toxicological Methods* 54: 56-61.

335. Prior R.L., Hoang H., Gu L., Wu X., Bacchiocca M., Howard L., Hampsch-Woodill M., Huang D., Ou B., Jacob R. (2003) Assays for hydrophilic and lipophilic antioxidant capacity (oxygen radical absorbance capacity ($ORAC_{FL}$)) of plasma and other biological and food samples. *Journal of Agricultural and Food Chemistry* 51: 3273-3279.

336. Saenz A.T., Elisia I., Innis S.M., Friel J.K., Kitts D.D. (2009) Use of ORAC to assess antioxidant capacity of human milk. *Journal of Food Composition and Analysis* 22: 694-698.

337. Zulueta A., Esteve M.J., Frigola A. (2009) ORAC and TEAC assays comparison to measure the antioxidant capacity of food products. *Food Chemistry* 114: 310-316.

338. Bentayeb K., Vera P., Rubio C., Nerin C. (2009) An adaptation of the ORAC assay to the common laboratory equipment and subsequent application to antioxidant plastic films. *Analytical and Bioanalytical Chemistry* 394: 903-910.

339. Jacobsen C., Let M.B., Nielsen N.S., Meyer A.S. (2008) Antioxidant strategies for preventing oxidative flavor deterioration of food enriched with n-3 polyunsaturated

lipids: a comparative evaluation. *Trends in Food Science and Technology* 19: 76-93.

340. Pezo D., Salafranca J. Nerin C. (2006) Design of a method for generation of gas-phase hydroxyl radicals, and use of HPLC with fluorescence detection to assess the antioxidant capacity of natural essential oils. *Analytical and Bioanalytical Chemistry* 385: 1241-1246.